

# Supplementary material: Heat flow, morphology, pore fluids and hydrothermal circulation in a typical mid-Atlantic ridge flank near Oceanographer Fault-Zone

V. Le Gal<sup>b,d</sup>, F. Lucaleau<sup>a</sup>, M. Cannat<sup>a</sup>, J. Poort<sup>b</sup>, C. Monnin<sup>c</sup>,  
A. Battani<sup>d</sup>, F. Fontaine<sup>a</sup>, B. Goutorbe<sup>e</sup>, F. Rolandone<sup>b</sup>, C. Poitou<sup>a</sup>,  
M-M. Blanc-Valleron<sup>f</sup>, A. Piedade<sup>g</sup>, A. Hipólito<sup>h</sup>

<sup>a</sup>*Institut de Physique du Globe de Paris/Sorbonne Paris Cité, UMR CNRS 7154, 1 rue Jussieu, 75238, Paris cedex 05, France*

<sup>b</sup>*iSTeP, Université Pierre et Marie Curie, 4 place Jussieu, 75252, Paris cedex 05, France*

<sup>c</sup>*Geosciences Environnement Toulouse, 14 Avenue Edouard Belin, 31400, Toulouse, France*

<sup>d</sup>*Geosciences, IFP Energies nouvelles, 1-4 avenue de Bois-Préau, 92852 Rueil-Malmaison Cedex, France*

<sup>e</sup>*Universidade Federal Fluminense, Niterói, Brazil*

<sup>f</sup>*Museum National d'Histoire Naturelle, CP 48, 57 rue Cuvier, 75231 Paris cedex 05, France*

<sup>g</sup>*School of Earth and Ocean Sciences, Cardiff University, Main Building, Park Place, CF10 3AT Cardiff, United Kingdom*

<sup>h</sup>*Universidade dos Açores, Departamento de Geociências, Rua da Mãe de Deus, 9501-801 Ponta Delgada, Portugal*

---

## <sup>1</sup> 1. Oceanograflu survey

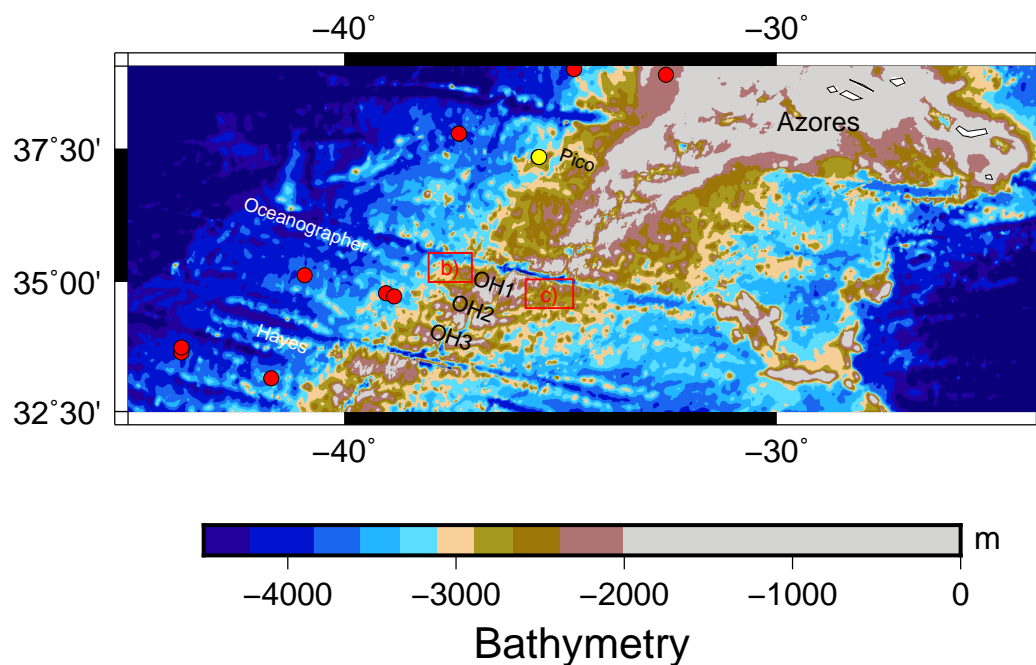
<sup>2</sup> The Oceanograflu survey is a marine geophysical cruise dedicated to the  
<sup>3</sup> study of hydrothermal processes on the flanks of a typical Mid-Atlantic  
<sup>4</sup> ridge segment (figure 1). Hydrothermal processes in the Atlantic are prob-  
<sup>5</sup> ably influenced by a rougher surface morphology than in faster spreading  
<sup>6</sup> ridges, where it was shown that the density of seamounts at the seafloor  
<sup>7</sup> governs the efficiency of heat removal (e.g. Lister, 1970, 1972; Davis et al.,  
<sup>8</sup> 1992, 1997; Fisher et al., 2003; Hutnak et al., 2006; Wheat and Fisher, 2008;  
<sup>9</sup> Fisher and Wheat, 2010). The Oceanographer-Hayes segment was therefore

10 chosen for its typical morphology of the Atlantic ocean and the existence of a  
11 previous geophysical study with multibeam bathymetry, seismic profiles, 3.5  
12 kHz echosounding, gravity and magnetism across the ridge (Cannat et al.,  
13 1999; Escartìn et al., 2001; Rabain et al., 2001).

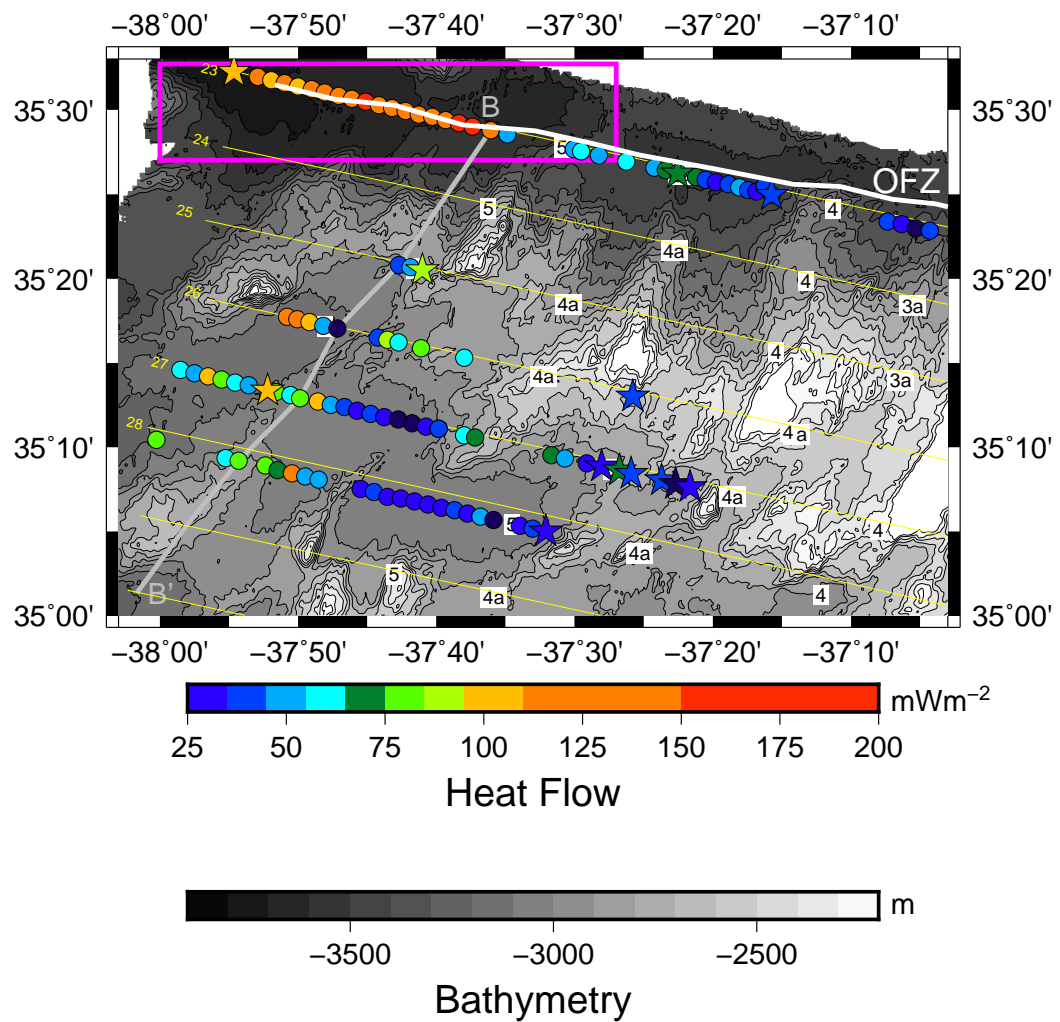
14 The survey was carried out from the fourth of June 2013 to the fifth of July  
15 2013 on the R/V “l’Atalante”. We got mostly heat flow measurements and  
16 cores, as other useful geophysical data were acquired before. We performed  
17 185 conventional heat flow measurements (178 successful) and 31 Küllenberg  
18 piston cores (30 successful).

19 We present in this supplementary material more details on the techniques  
20 and on the results.

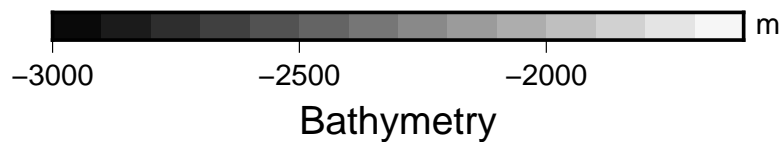
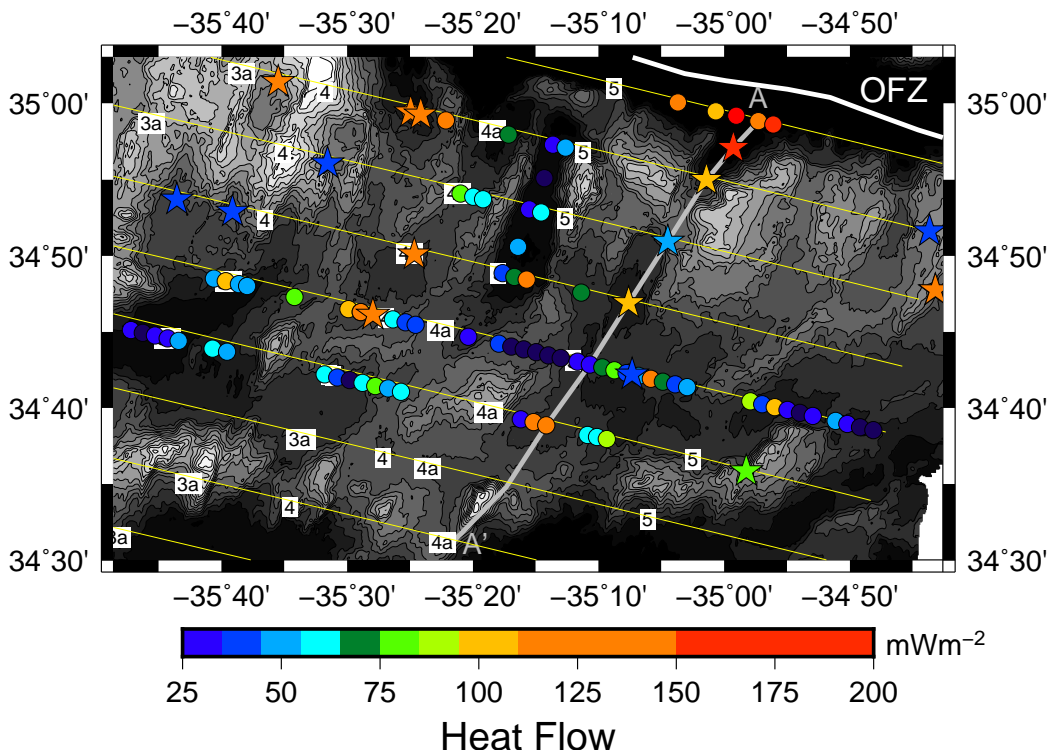
Figure 1: Distribution and magnitude of heat flow on bathymetric maps:Heat flow values  
are reported as circles for multi penetration probes and stars for measurements associated  
with Küllenberg cores; colours refer to the heat flow scale. The white line represents  
the morphological trace of OFZ and the yellow lines represent seismic profiles. Isochrons  
identified during the SudAçores survey (Rabain et al., 2001) are represented by a white  
box with the anomaly number: anomaly 3  $\simeq$  4.18 Ma, anomaly 3a  $\simeq$  5.89 Ma anomaly 4  
 $\simeq$  7.43 Ma, anomaly 4a  $\simeq$  8.69 Ma and anomaly 5  $\simeq$  9.74 Ma. Profiles AA’ and BB’ are  
reconstructed profiles shown in figure 12k.



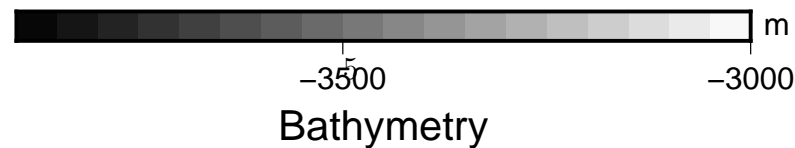
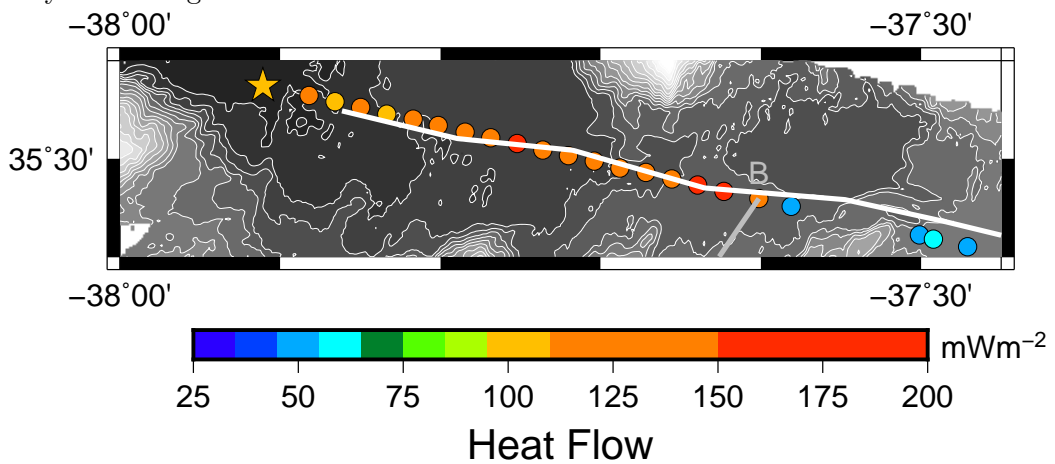
a: location of the study areas, Azores islands, holes from DSDP 82 (red circles) and DSDP 94 (yellow circle), and the three major fracture zones: Pico, Oceanographer and Hayes. Background corresponds to Gtopo30 bathymetry. The two red squares b) and c) correspond respectively to the western and eastern flanks of the studied ridge segment.



b: Distribution and magnitude of heat flow on the western flank of Oceanographer-Hayes OH1 segment



c: Distribution and magnitude of heat flow on the eastern flank of Oceanographer-Hayes OH1 segment



d: close up view of heat flow measurements near the Oceanographer Fracture Zone



a: Multipenetrator instrument after recuperation on the deck

b: THP autonomous temperature sensor attached to the core barrel

Figure 2: Heat flow measurements devices: sensors are arranged helically around the barrels.

## **2. Heat flow**

### **2.1. principles**

Marine heat flow involves measurements of the temperature gradient and thermal conductivity. As sea-bottom temperature is usually stable (Davis et al., 2003) for depths greater than 1000 m, short instruments ( $\sim$  5-10 m) are sufficient to determine thermal gradient. Thermal conductivity is measured in-situ with the POGO instrument or in laboratory: both use the needle-probe technique with constant heating.

We used two types of instruments (figure 2): a conventional Ewing-type instruments with seven outrigger thermistors (figure 2a) and a Küllenberg piston core equipped with autonomous thermal sensors (figure 2b).

The acquisition sequence includes two stages (figure 3) for the multipenetrator instrument and only the first one for Küllenberg instrument: (i)

<sup>34</sup> determination of temperature, (ii) determination of thermal conductivity.

<sup>35</sup> When the instrument penetrates in the sediment, the temperature of  
<sup>36</sup> sensors increases significantly because of the frictionnal heating (figure 3) and  
<sup>37</sup> then decreases progressively to equilibrium for infinite time after penetration.

<sup>38</sup> The equilibrium temperature can be extrapolated if temperature evolution  
<sup>39</sup> is recorded during at least 5-10 minutes. The temperature  $T(t)$  at any time  
<sup>40</sup> is given by (Bullard, 1954):

$$T(t) = T_\infty + T_{friction} \Phi(\alpha, \tau) \quad (1)$$

<sup>41</sup> where  $T_\infty$  is the equilibrium temperature,  $T_{friction}$  is the temperature anomaly  
<sup>42</sup> caused by friction and  $\Phi(\alpha, \tau)$  is a decay function following the peak temper-  
<sup>43</sup> ature.  $\alpha$  is a non dimensional parameter and  $\tau$  is the non dimensional time  
<sup>44</sup> constant of the probe:

$$\alpha = \frac{2\pi r^2 \rho C}{\mu} \quad (2)$$

<sup>45</sup>

$$\tau = \frac{\kappa t}{r^2} \quad (3)$$

<sup>46</sup> One can show that for time greater than 1 minute after the penetration, an  
<sup>47</sup> asymptotic solution is approached by:

$$\Phi(\alpha, \tau) = \frac{\mu}{4\pi\lambda t} \quad (4)$$

<sup>48</sup> where  $\mu$  is the heat capacity per unit length,  $r$  the probe radius,  $\lambda$  the thermal  
<sup>49</sup> conductivity and  $\kappa$  the thermal diffusivity of sediments. The equilibrium  
<sup>50</sup> temperature can be obtained from the intercept of a regression line made on

51 (T,1/t) couples with the time axis for infinite time, i.e. when 1/t tends to 0.  
 52 Thermal Conductivity is determined in the second stage of the acquisition  
 53 sequence (or measured on cores for Küllenberg probes) with a needle-probe  
 54 technique (Von Herzen and Maxwell, 1959). The thermistor is now heated  
 55 with a constant power ( $\sim 1$  W) during about 10 minutes, and the temperature  
 56 increases more importantly as the sediment conductivity is low (figure 3). In  
 57 the case of cores, the instrument is pulled up just after the first stage and the  
 58 thermal conductivity measured in the laboratory. The needle, which includes  
 59 a heating wire and a thermistor or a thermocouple, is inserted transversely  
 60 into the core (this provides the vertical component of thermal conductivity)  
 61 and heated at a constant power  $Q$ . The temperature increase of the probe  
 62 with the logarithm of time is proportional after some time delay to the inverse  
 63 of thermal conductivity:

$$\Delta T = \frac{Q}{4\lambda\pi} \ln(4\alpha t/Ba^2) \quad (5)$$

64 where  $t$  = time,  $Q$  = heat input per unit length per unit time,  $\lambda$  =  
 65 thermal conductivity of sediment sample,  $\alpha$  = thermal diffusivity of sediment  
 66 sample,  $a$  = probe radius and  $B$  = constant = 1.7811. This relationship is  
 67 valid only for large time  $t$  compared with  $a^2/\alpha$  and therefore, the interval of  
 68 measurement is important in estimating the thermal conductivity with this  
 69 method: the choice of the interval is usually done by searching the linear  
 70 domain in a plot of the temperature increase  $\Delta T$  as a function of  $\ln(t)$ .

71 One can notice from equation 4 that thermal conductivity could be also  
 72 inferred from the temperature evolution after the peak caused by frictional

73 heating, but as Q is not known, it can not be obtained directly but requires  
 74 inversion techniques (e.g. Lee and Von Herzen, 1994; Hartmann and Villinger,  
 75 2002) not used in the present survey.

76 *2.2. corrections*

77 *2.2.1. sedimentation*

78 As active sedimentation exists, part of the deep heat flow is expended  
 79 in warming cold sediment, which reduces surface heat flow subsequently.  
 80 Von Herzen and Uyeda (1963) reduced the problem of constant sedimentation  
 81 to a problem of heat conduction in a moving medium:

$$\frac{\partial^2 T}{\partial z^2} - \frac{U}{\kappa} \frac{\partial T}{\partial z} - \frac{1}{\kappa} \frac{\partial T}{\partial t} = -\frac{A_0}{K} \quad (6)$$

82 where K and  $\kappa$  are thermal conductivity and thermal diffusivity,  $A_0$  the rate  
 83 of heat generation per unit volume, U the rate of sedimentation. The initial  
 84 condition is  $T(z) = G z$ , where G is the unperturbed temperature gradient  
 85 and the upper boundary condition at  $z = 0$  is  $T = 0$ . If heat production is  
 86 neglected, the solution of equation 6 is (Von Herzen et al., 1974):

$$\frac{1}{G} \left( \frac{\partial T}{\partial z} \right)_{z=0} = (1 + 2\tau^2) \operatorname{erfc}(\tau) - \frac{2}{\sqrt{\pi}} \tau \exp(-\tau^2) \quad (7)$$

87 where  $\tau$  is a dimensionless parameter

$$\tau = \frac{U}{2} \left( \frac{t}{\kappa} \right)^{1/2} \quad (8)$$

88 However, this analytical solution does not include such important ef-

89 fects as variable sedimentation rates, compaction and its effect on thermal  
90 conductivity, or the thermal interaction with basement for high sedimenta-  
91 tion rates (Hutchison, 1985; Lucaleau and Le Douaran, 1985; Von Herzen  
92 et al., 1989; Harris et al., 2000). Numerical solutions can solve this prob-  
93 lem, and algorithms have been proposed by Hutchison (1985) and Lucaleau  
94 and Le Douaran (1985). Although the two algorithms use different strate-  
95 gies and hypothesis, both give very similar results (within 0.5% of heat flow  
96 anomaly, see table 1). Compaction is considered in both models as a function  
97 of porosity, which is assumed to decrease exponentially with depth. At the  
98 limit where surface porosity is equal to zero (no compaction), both models  
99 are in agreement with the analytical solution provided by Von Herzen et al.  
100 (1974). Sediment thickness has been picked as two-way travel time (TWT)  
101 on seismic profiles acquired during a previous survey (SUDACORES). The  
102 maximum TWT thickness reaches 0.45 s and assuming a velocity range of  
103 1850-2050 m/s, corresponds to a maximum of 830-920 m thick sediment  
104 cover. The heat flow correction due to sedimentation has been computed for  
105 the upper limit (2050 m/s) and for a constant rate during the period follow-  
106 ing accretion of the basement. Resulting sedimentation rates are therefore  
107 30-40 m/Ma for off-axis profiles and can reach a maximum of 85 m/Ma.  
108 These sedimentation rates are local rates and have obviously no significance  
109 on a regional scale. They can affect however the magnitude of heat flow by  
110 5% (with a maximum of 9%) when the compaction is included (assuming  
111 surface porosity = 0.6, compaction length scale= 1750 m and bulk surface  
112 conductivity =  $1 \text{ Wm}^{-1}\text{K}^{-1}$ ).

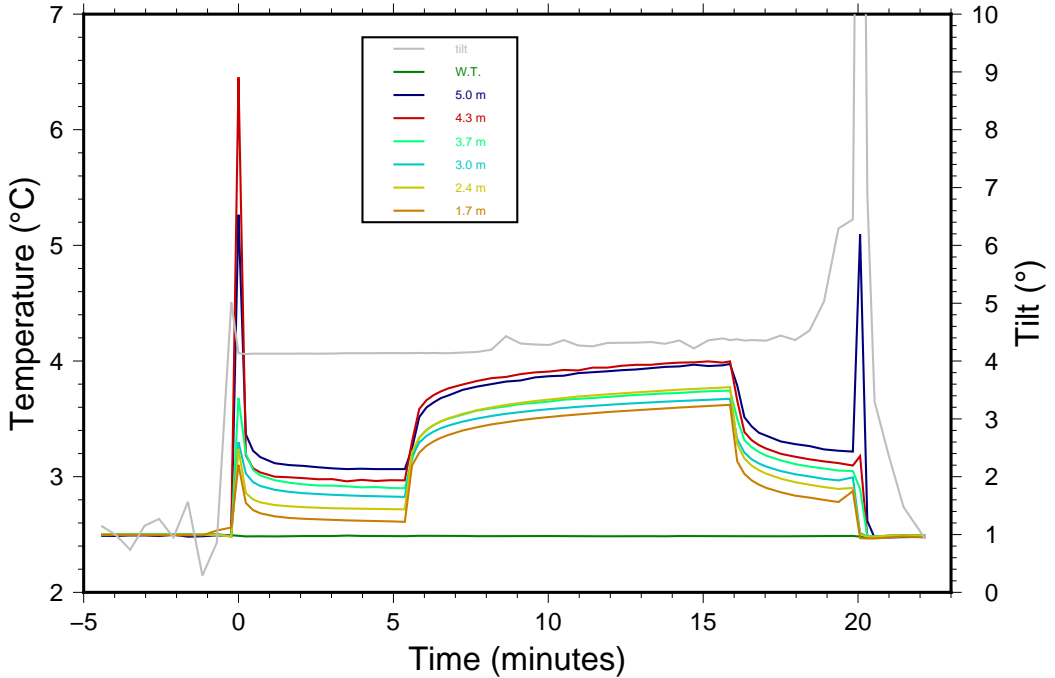


Figure 3: Heat flow acquisition sequence: this graph represents the evolution of temperature during a penetration of the POGO instrument into the sediment at  $t=0$ . For negative times, the instrument is still in the water and all sensors have the same temperature (about  $2.5^{\circ}\text{C}$ ). At  $t=0$ , the temperature increases suddenly; the magnitude of the peak depends on the strength of frictional heating and on the depth of each sensor: the red curve in the figure does not correspond to the deepest sensor, but the friction was probably more important than for the deepest sensor (blue curve). After the penetration, the temperature decrease is recorded for about 5 minutes to extrapolate equilibrium temperature and equilibrium temperature gradient, and then the sensors are heated with a constant power in order to get in-situ thermal conductivity. Increase of temperature depends on thermal conductivity, and again the red curve crosses the blue one because thermal conductivity of the deepest sensor is higher than that of the sensor just above. The temperature heating is recorded for about 10 minutes and then the power is shut down and the temperatures decrease. A new frictional peak is observed at 20 minutes when the instrument is pulled out from the sediment. The right vertical scale represents the tilt evolution during this acquisition sequence: the instrument is almost vertical in the water, gets an angle during penetration or pulling operations, and remains at about  $4^{\circ}$  during this measurement.

113    *2.2.2. topography and refraction*

114    Surface heat flow is perturbed by topographic variations across a thermal  
115    conductivity contrast (basalt/sediment, sediment/water). In order to correct  
116    heat flow for these two effects, we computed a stationnary 2D model along  
117    seismic lines with a uniform basal heat flow at 10 km and the observed  
118    geometry of basins (figure 4). A uniform surface temperature ( $T = 2.4^{\circ}\text{C}$ )  
119    was chosen and a contrast of  $0.5\text{-}1.0 \text{ Wm}^{-1}\text{K}^{-1}$  for the thermal conductivity  
120    across the sediment/basalt interface. Anomalies as large as  $\pm 100 \text{ mWm}^{-2}$   
121    can be observed locally, but as we have done measurement in basins, it usually  
122    ranges between  $\pm 10 \text{ mWm}^{-2}$ .

123    However, the 2D approximation could minimize the heat-refraction effect  
124    when measurements are very close to seamounts, but as we have no con-  
125    straints for a 3D model, the correction should be considered as a minimum  
126    value. We choose a constraint of  $0.5 \text{ Wm}^{-1}\text{K}^{-1}$  for the correction applied to  
127    Oceanograflu data, because a larger contrast of thermal conductivity obvi-  
128    ously tends to overestimate corrections for some data.

129    *2.2.3. heat flow results*

130    All temperature profiles and heat flow measurements are displayed along  
131    seismic profiles (figure 12) or as individual temperature/conductivity vs depth  
132    plots (figure 13). Two profiles perpendicular to the flowlines have been re-  
133    constructed and are shown in figure 12k. A synthesis of all data is presented  
134    as a table including site name, coordinates, water depth, etc. (table 2).

<sup>135</sup> *2.2.4. statistical distribution of data*

<sup>136</sup> Figure 5 shows an histogram of sedimentation and topography corrected  
<sup>137</sup> heat flow measurements on both flanks of the Oceanographer Hayes ridge.  
<sup>138</sup> The distribution of conductive values (derived from age of the sea floor and  
<sup>139</sup> Stein and Stein (1992) model) is shown on the same graph, and suggests that  
<sup>140</sup> heat flow, in average, is 40 % of this conductive value.

141    **3. Pore waters**

142    *3.1. protocol for pore water extraction*

143    Interstitial pore water extraction were done onboard. When the “Küllenberg”  
144    piston corer is back on the deck, the liner is marked and cut in 1.5 m long  
145    (these dimensions are imposed by the “Museum Nationale d’Histoire Na-  
146    turelle de Paris” core shack) core sections starting from the top. Then, the  
147    core sections were immediately transferred into the cold (8°C) laboratory,  
148    where interstitial waters were extracted with rhyzon© soil moisture sam-  
149    plers (Seeberg-Elverfeldt et al., 2005) (figure 7). Rhyzons consist of 2.5 x 50  
150    mm hydrophilic porous polymer that drive capillary sampling. Each Rhy-  
151    zon© is connected to a 10 to 30 ml pre-evacuated syringe for water recovery.  
152    On the first core meter, sampling was performed each 10 cm. The next  
153    sample was recovered at 130 cm, and from that Rhyzon© samplers were  
154    spaced with a resolution of 40 cm. Fluid extraction lasts between 1 and 6  
155    hours before sampled water is transferred into 12 mL vials and stored at low  
156    temperature (4°C).

157    *3.2. analytical method for pore water analyses*

158    Pore water samples were extracted from all cores, but only fourteen have  
159    been analysed for majors and minors constituents. One part of pore wa-  
160    ter analyses (cores: KT1, KT4, KT12, KT19, KT23) has been performed  
161    using ionic chromatography (Dionex ICS 2000® - anions: Cl-, SO42-) and  
162    ICP-OES (Horiba Jobin Yvon Ultima2® – cations: Ca2+, Mg2+, Na+,  
163    K+) at Toulouse laboratory (GET: Geosciences Environment Toulouse). The  
164    other part (cores: KT3, KT5, KT6, KT7, KT9, KT11, KT15, KT29, KT31)

165 has been completed at Ifremer-Brest in the LCGr (Laboratoire des Cycles  
166 Géochimiques et ressources) laboratory by ionic chromatography (Dionex  
167 AS 120<sup>®</sup>) for cations and anions. Pore water samples were diluted 500  
168 times (200 µL in 100 mL) in milliQ<sup>®</sup> water (ultra-pure water, resistivity  
169 of 18.2MΩ.cm). Calibrations were done with IAPSO standard and multi-  
170 element solution. All dilutions were weighed to correct the experimental  
171 uncertainties related to pipettes. Minor elements (Sr<sup>2+</sup>, Ba<sup>2+</sup>, B<sup>+</sup>, Mn<sup>2+</sup>,  
172 Li<sup>+</sup>) were analyzed using an High Resolution Inductively Coupled Plasma  
173 Mass Spectrometry (HR-ICP-MS Element 2 thermo scientific<sup>®</sup>) in UBO  
174 (Université de Bretagne Occidentale) laboratory. Samples and standards  
175 were prepared in clean room environments, where the atmosphere is filtered  
176 to limit the particular concentration. Hygrometry, pressure and temperature  
177 are precisely controlled in a clean room environment. Samples were diluted  
178 25 times (120 µl in 3 ml) in nitric acid at 2%. Standard NASS-5 and multi-  
179 elements solution (of Li, Sr, Mn, and Br) were used for calibrations. Each  
180 instruments have a precision of 2% in average.

#### 181 4. Morphology

182 In order to characterize the spatial dependence of topography, we use  
183 variograms, which can be defined by the following relation:

$$\gamma(l, \theta) = \frac{1}{2}E\left\{[Z(x, y) - (Z(x, y) + l(\theta))]^2\right\} \quad (9)$$

184 where  $\gamma(l, \theta)$  is the variogram, Z(x,y) the elevation at location (x,y),  $Z(x, y) +$   
185  $l(\theta)$  the elevation at a radial distance l in a direction  $\theta$  and  $E\{\}$  the mathe-

186 matic expectation.

187 The variogram is isotropic when the  $\gamma$  depends on the distance  $l$  only.

188 The main characteristics of variograms applied to the topographic surface  
189 were described by Roko et al. (1997). For  $l=0$  (nugget effect), the variogram  
190 represents the local relief and it should be close to zero for a sedimentary  
191 basin. If relief stabilizes at a given length scale, this value is called the sill,  
192 which characterizes the overall roughness of the area. The lag to sill is the  
193 range where relief is correlated to the length-scale and it may indicate some  
194 characteristic process of relief formation.

195 A comparison of isotropic and directional variograms is shown in figure  
196 8 for both flanks of the OH1 ridge segment. We used the GEBCO grid  
197 resolution in order to have a comparable resolution with other regions and  
198 also to speed up the calculation. It is clear that rugosity on the eastern flank  
199 of the ridge is much important than on the western flank. Rugosity is also  
200 higher on a direction parallel to the ridge axis (N12) than on a direction  
201 perpendicular to the ridge axis (N102).

202 We also compare seafloor and basement topographic roughness (Figure  
203 9).

204 Finally, we compare variograms in different areas (Figure 10) affected by  
205 hydrothermal circulations where detailed heat flow studies exist (Figure 11).  
206 The different characteristics (nugget effect, lag, sill) vary in the same way  
207 (e.g. larger values for OH1 than for Juan de Fuca).

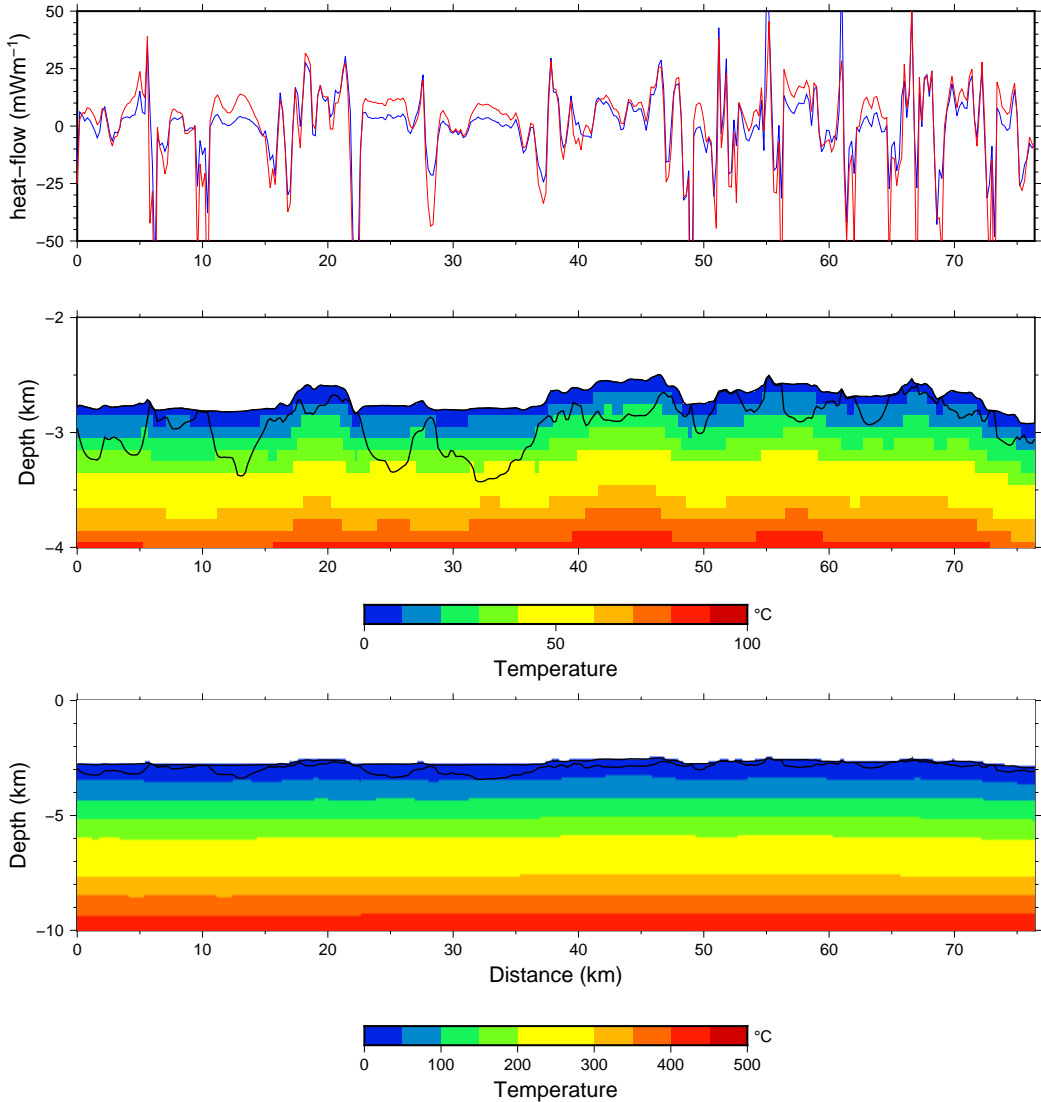


Figure 4: 2D model for profile 27E used to estimate topographic and refraction corrections. Lower panel represents the temperature field for stationary conditions, heat flow = 150  $\text{mW m}^{-2}$  at the bottom, 2.4°C at the sea-bottom and no heat flow through left and right vertical boundaries. Thermal conductivity is 2.5  $\text{W m}^{-1}\text{K}^{-1}$  in the basement, and 1.5 or 2.0  $\text{W m}^{-1}\text{K}^{-1}$  in the sediment. Middle panel is a close-up view of the lower panel. Upper panel is the heat flow anomaly (=correction) between calculated surface heat flow and bottom heat flow (150  $\text{mW m}^{-2}$ ). The red and blue curves correspond to a contrast of thermal conductivity of 1.0 and 0.5  $\text{W m}^{-1}\text{K}^{-1}$  respectively.

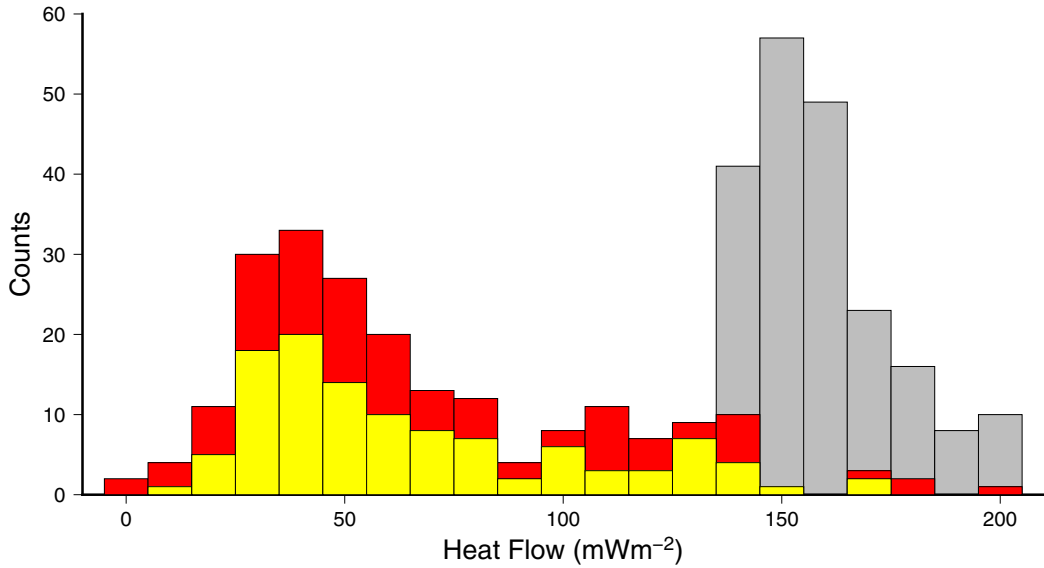


Figure 5: Histogram of Oceanograflu heat flow data. Gray colour corresponds to the Stein and Stein (1992) conductive model, yellow colour to the west flank and red colour to the east flank. Average values are respectively  $65.9 \pm 38.3 \text{ mWm}^{-2}$ ,  $67.7 \pm 44.0 \text{ mWm}^{-2}$  and  $158.4 \pm 16.3 \text{ mWm}^{-2}$  for the west flank, east flank and conductive values.

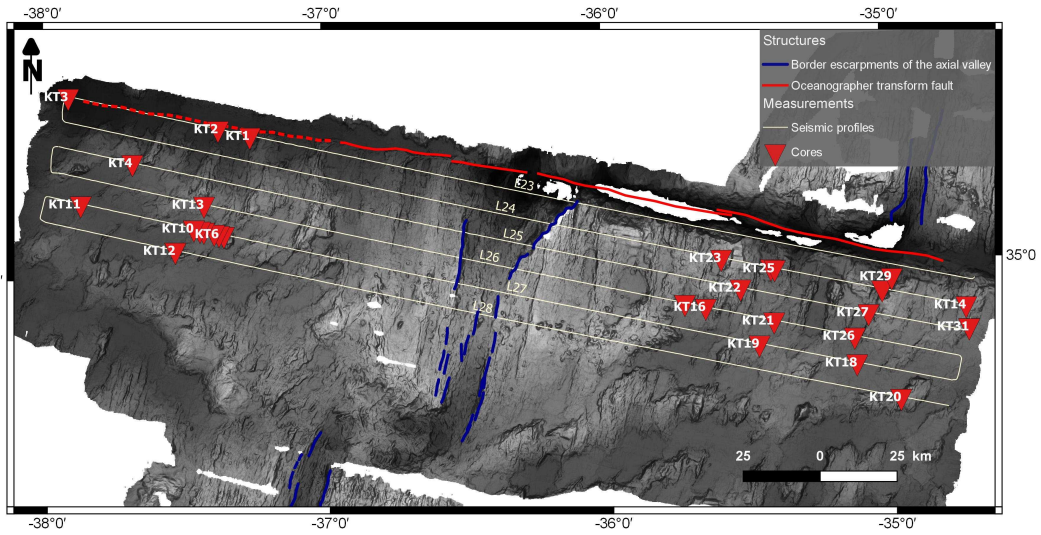


Figure 6: Location and id of Küllenberg cores



Figure 7: Rhyzon sampling on core KT2

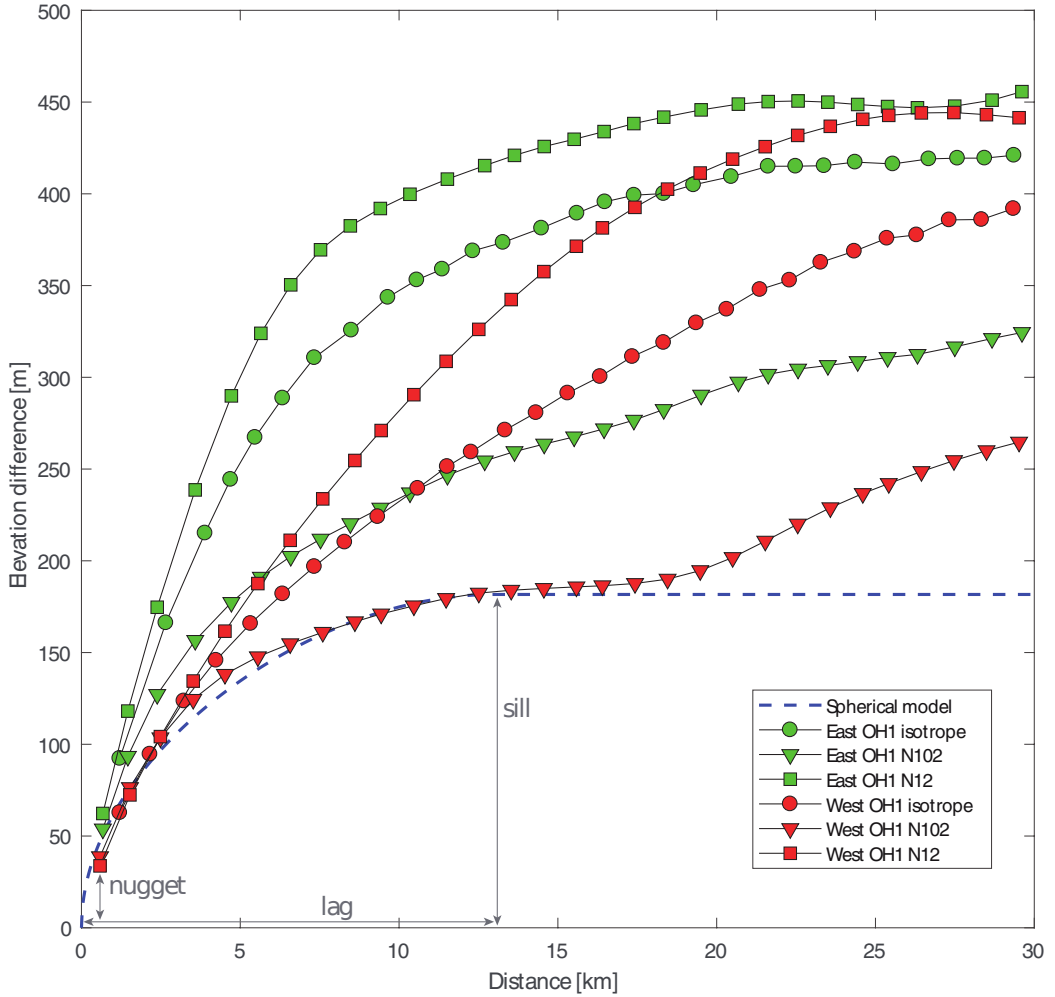


Figure 8: Variograms of bathymetry in the study area. Variograms are calculated in different ways in order to outline the variation of relief with directions, on both flanks of the ridge: two directions are used (N102 and N12 along and perpendicular to the direction of accretion) as well as non directional (isotropic) variogram. An example of a theoretical fit by a spherical variogram is shown for the case West OH1 N102: only the first part of the experimental variogram is used to determine the nugget effect, sill and lag values.

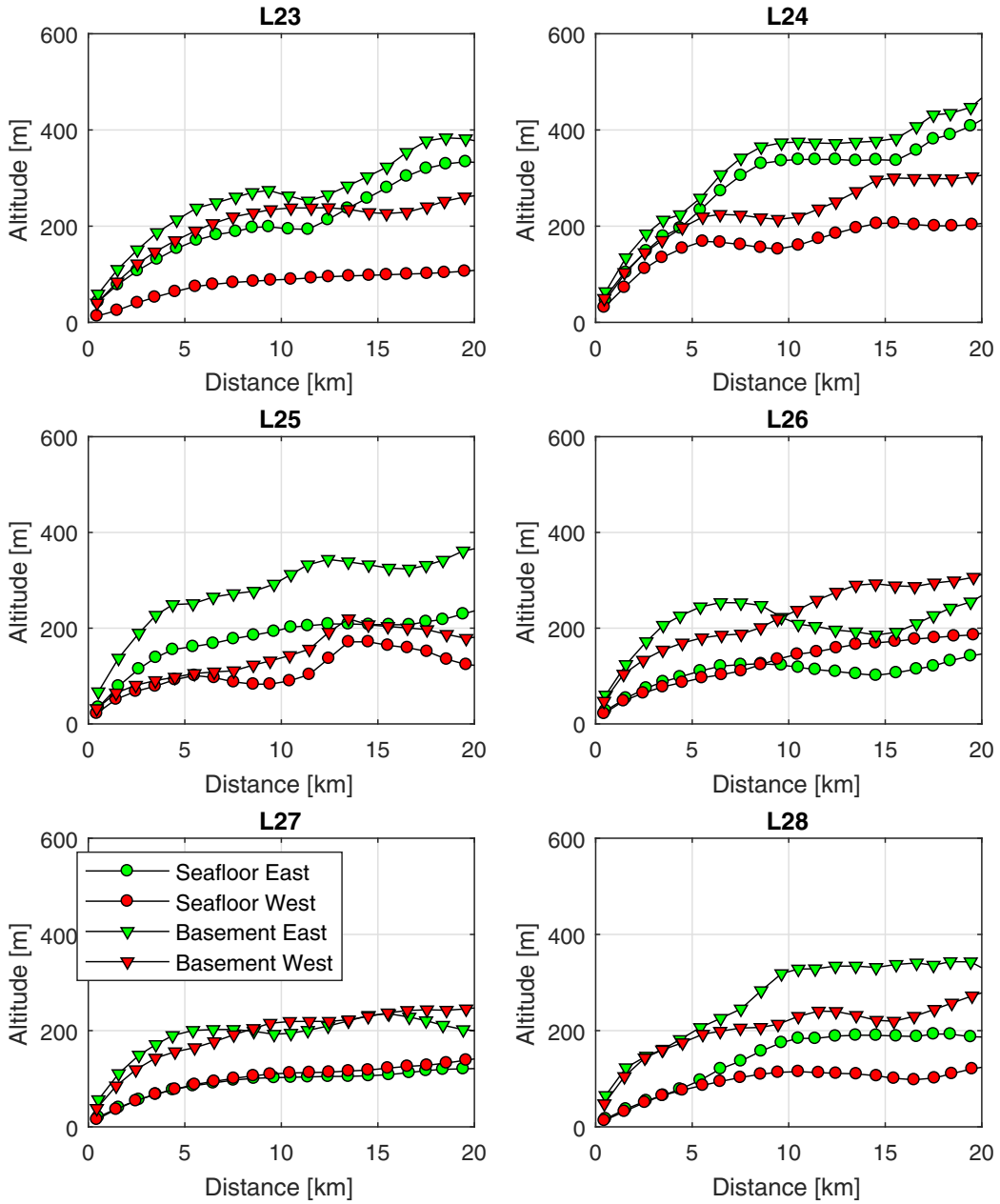


Figure 9: Variograms of seafloor and basement topography along seismic profiles where heat flow was measured. Spatial resolution is 500 m.

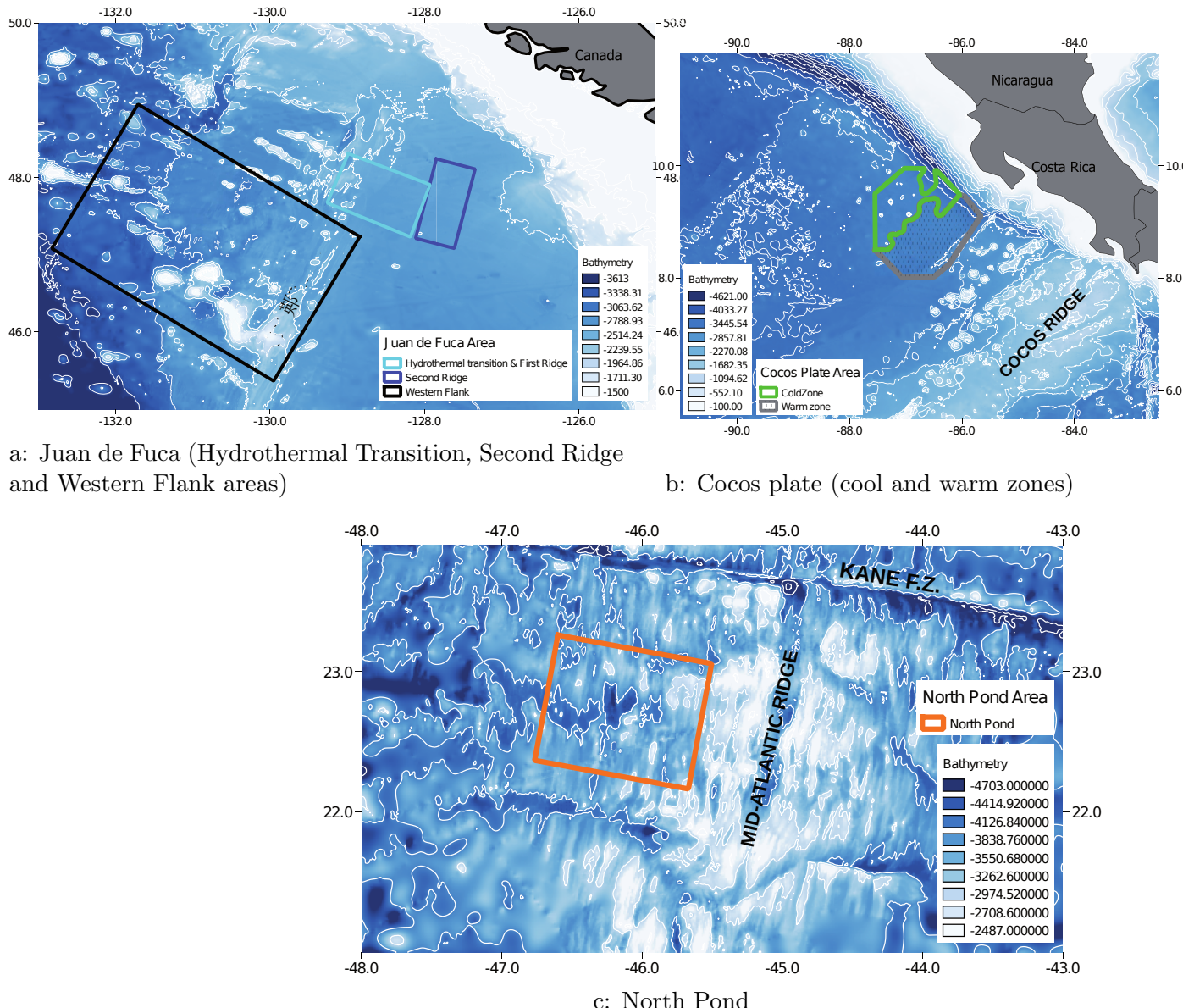


Figure 10: Location of regional studies.

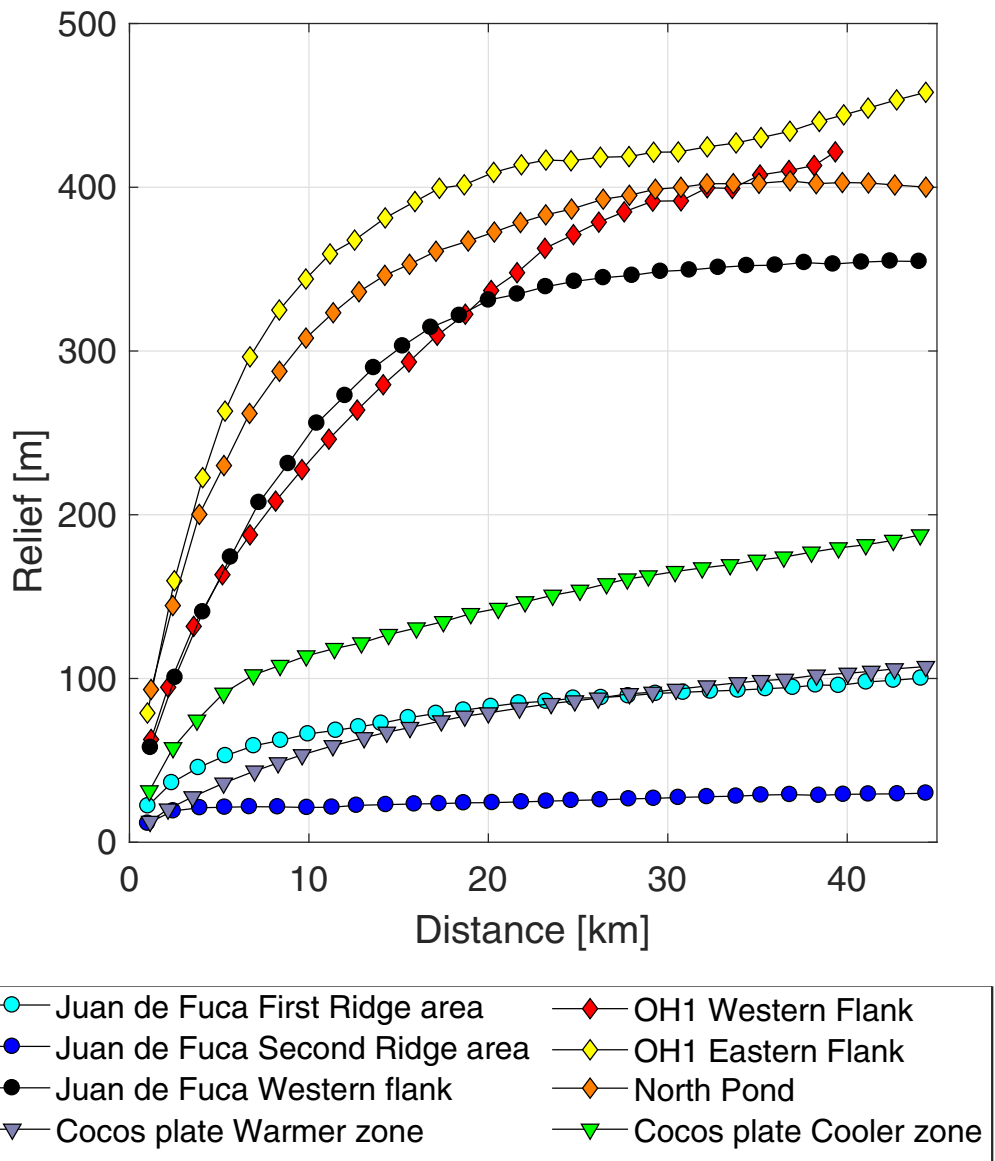


Figure 11: Comparison of variograms for several areas where hydrothermal effects on surface heat flow was studied.

## References

- Bullard, E. C.: The flow of heat through the floor of the Atlantic Ocean, Proceeding of the Royal Society London Serie A, 222, 408–429, doi: 10.1098/rspa.1954.0085, 1954.
- Cannat, M. et al.: Campagne SudAçores, N.O. L'Atalante, rapport de mission, Tech. rep., CNRS / Université Paris 6, 1999.
- Davis, E., Chapman, D., Villinger, H., Robinson, S., Grigel, J., Rosenberger, A., and Pribnow, D.: Seafloor heat flow on the eastern flank of the Juan de Fuca ridge: data from “FLANK-FLUX” studies through 1995, in: Proceedings of the Ocean Drilling Program, Initial Reports, vol. 168, pp. 23–33, URL [http://www-odp.tamu.edu/publications/168\\_IR/TABLES/CHAP\\_02/02\\_01.TXT](http://www-odp.tamu.edu/publications/168_IR/TABLES/CHAP_02/02_01.TXT), 1997.
- Davis, E. E., Chapman, N. R., Mottl, M. J., Bentkowski, W. J., Dadey, K., Forster, C. B., Harris, R. N., Nagihara, S., Rohr, K., Wheat, C. G., and Whiticar, M.: Flankflux: an experiment to study the nature of hydrothermal circulation in young oceanic crust, Canadian Journal of Earth Sciences, 29, 925–952, doi:10.1139/e92-078, 1992.
- Davis, E. E., Wang, K. L., Becker, K., Thomson, R. E., and Yashayaev, I.: Deep-ocean temperature variations and implications for errors in seafloor heat flow determinations, Journal of Geophysical Research, 108, 2034–10, doi:10.1029/2001JB00169, 2003.
- Escartìn, J., Cannat, M., Pouliquen, G., Rabain, A., and Lin, J.: Crustal thickness of V-shaped ridges south of the Azores: Interaction of the Mid-

Atlantic Ridge (36°–39°N) and the Azores hot spot, *Journal of Geophysical Research*, 106, 21–719, doi:10.1029/2001JB000224, 2001.

Fisher, A. T. and Wheat, C. G.: Seamounts as Conduits for Massive Fluid, Heat, and Solute Fluxes on Ridge Flanks, *Oceanography*, 23, doi: 10.5670/oceanog.2010.63, URL <http://dx.doi.org/>, 2010.

Fisher, A. T., Davis, E. E., Hutnak, M., Spiess, F. N., Zuhlsdorff, L., Cherkaoui, A., Christiansen, L. B., Edwards, K., Macdonald, R., Villinger, H., Mottl, M. J., Wheat, C. G., and Becker, K.: Hydrothermal recharge and discharge across 50 km guided by seamounts on a young ridge flank, *Nature*, 421, 618–621, doi:10.1038/nature01352, 2003.

Harris, R. N., Von Herzen, R. P., McNutt, M. K., and Jordahl, K.: Submarine hydrogeology of the Hawaiian Archipelagic apron, Part 1, Heat flow patterns north of Oahu and Maro reef, *Journal of Geophysical Research*, 105, 21 353–21 369, doi:10.1029/2000JB900165, 2000.

Hartmann, A. and Villinger, H.: Inversion of marine heat flow measurements by expansion of the temperature decay function, *Geophysical Journal International*, 148, 628–636, doi:10.1046/j.1365-246X.2002.01600.x, 2002.

Hutchison, I.: The effects of sedimentation and compaction on oceanic heat flow, *Geophysical Journal of the Royal Astronomy Society*, 82, 439–459, doi:10.1111/j.1365-246X.1985.tb05145.x, 1985.

Hutnak, M., Fisher, A. T., Zühlsdorff, L., Spiess, V., Stauffer, P. H., and Gable, C. W.: Hydrothermal recharge and discharge guided by basement outcrops on 0.7–3.6 Ma seafloor east of the Juan de Fuca Ridge: Observations and numerical models, *Geochemistry Geophysics Geosystems*, 7, Q07O02, doi:10.1029/2006GC001242, 2006.

Lee, T. c. and Von Herzen, R. P.: In-Situ Determination of Thermal-Properties of Sediments Using a Friction-Heated Probe Source, *Journal of Geophysical Research-Solid Earth*, 99, 12 121–12 132, doi: 10.1029/94JB00235, 1994.

Lister, C. R. B.: Heat Flow West of the Juan de Fuca Ridge, *Journal of Geophysical Research*, 75, 2648–2654, doi:10.1029/JB075i014p02648, 1970.

Lister, C. R. B.: On the thermal balance of a mid-ocean ridge, *Geophysical Journal of the Royal Astronomy Society*, 26, 515–535, doi:10.1111/j.1365-246X.1972.tb05766.x, 1972.

Lucaleau, F. and Le Douaran, S.: The blanketing effect of sediments in basins formed by extension : a numerical model. Application to the gulf of Lion and the Viking graben, *Earth and Planetary Science Letters*, 74, 92–102, doi:10.1016/0012-821X(85)90169-4, 1985.

Rabain, A., Cannat, M., Escartìn, J., Pouliquen, G., Deplus, C., and Rommevaux-Jestin, C.: Focused volcanism and growth of a slow spreading segment (Mid-Atlantic Ridge, 35°N), *Earth and Planetary Science Letters*, 185, 211–224, doi:10.1016/S0012-821X(00)00371-X, 2001.

Roko, R., Daemen, J., and Myers, D.: Variogram characterization of joint surface morphology and asperity deformation during shearing, *International Journal of Rock Mechanics and Mining Sciences*, 34, 71–84, doi: 10.1016/s1365-1609(97)80034-2, 1997.

Seeberg-Elverfeldt, J., Schlüter, M., Feseker, T., and Kölling, M.: Rhizone sampling of porewaters near the sediment-water interface of aquatic systems, *Limnology and Oceanography: Methods*, 3, 361–371, doi: 10.4319/lom.2005.3.361, 2005.

Stein, C. S. and Stein, S.: A model for the global variation in oceanic depth and heat flow with lithospheric age, *Nature*, 359, 123–129, doi: 10.1038/359123a0, 1992.

Von Herzen, R. P. and Maxwell, A. E.: The Measurement of Thermal Conductivity of Deep-Sea Sediments by a Needle-Probe Method, *Journal of Geophysical Research*, 64, 1551–1563, doi:10.1029/JZ064i010p01557, 1959.

Von Herzen, R. P. and Uyeda, S.: Heat flow through the eastern Pacific ocean floor, *Journal of Geophysical Research*, 68, 4219–4250, doi: 10.1029/JZ068i014p04219, 1963.

Von Herzen, R. P., Finckh, P., and Hsu, K. J.: Heat Flow Measurements In Swiss Lakes, *J. Geophys.*, 40, 141–172, 1974.

Von Herzen, R. P., Cordery, M. J., Detrick, R. S., and Fang, C.: Heat flow and the thermal origin of hotspot swells: the Hawaiian swell revisited, *Journal of Geophysical Research*, 94, 13–783, doi:10.1029/JB094iB10p13783, 1989.

Wheat, C. G. and Fisher, A. T.: Massive, low-temperature hydrothermal flow from a basaltic outcrop on 23 Ma seafloor of the Cocos Plate: Chemical constraints and implications, *Geochemistry, Geophysics, Geosystems*, 9, doi:10.1029/2008GC002136, q12O14, 2008.

## Additionnal figures

Figure 12: Heat flow and seismic profiles. Upper panel shows heat flow (dots, black line) and tilt (grey line). Black line represents raw heat flow values, while dots represent heat flow corrected for sedimentation, topography and heat refraction, with the associated error ( $3\sigma$  or 99.7% confidence interval). Red line represents the conductive heat flow based on Stein and Stein (1992) model. Top of the panel shows isochrons locations. Bottom of the panel is the distance to the ridge axis. Middle panel represents temperature versus depth profiles with arbitrary temperature scale. Surface temperature is indicated at the top of each profile. Dotted lines represent extrapolations. Bottom panel represents the seismic profile at the same horizontal scale and position of each site (multi penetration or core) above. The vertical scale is Two Way Travel time (s).

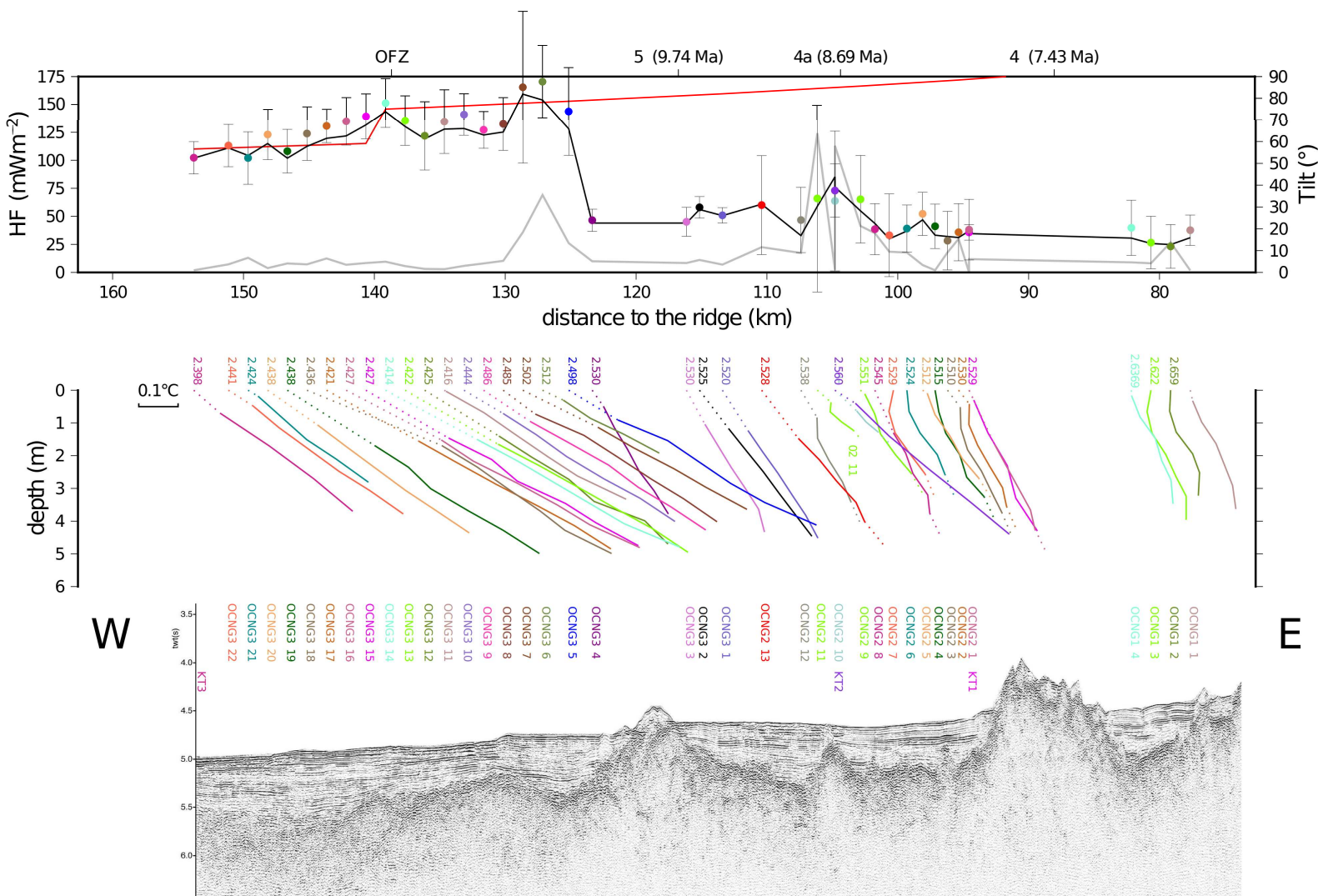


Figure 12a: Heat flow measurements along seismic profile 23W.

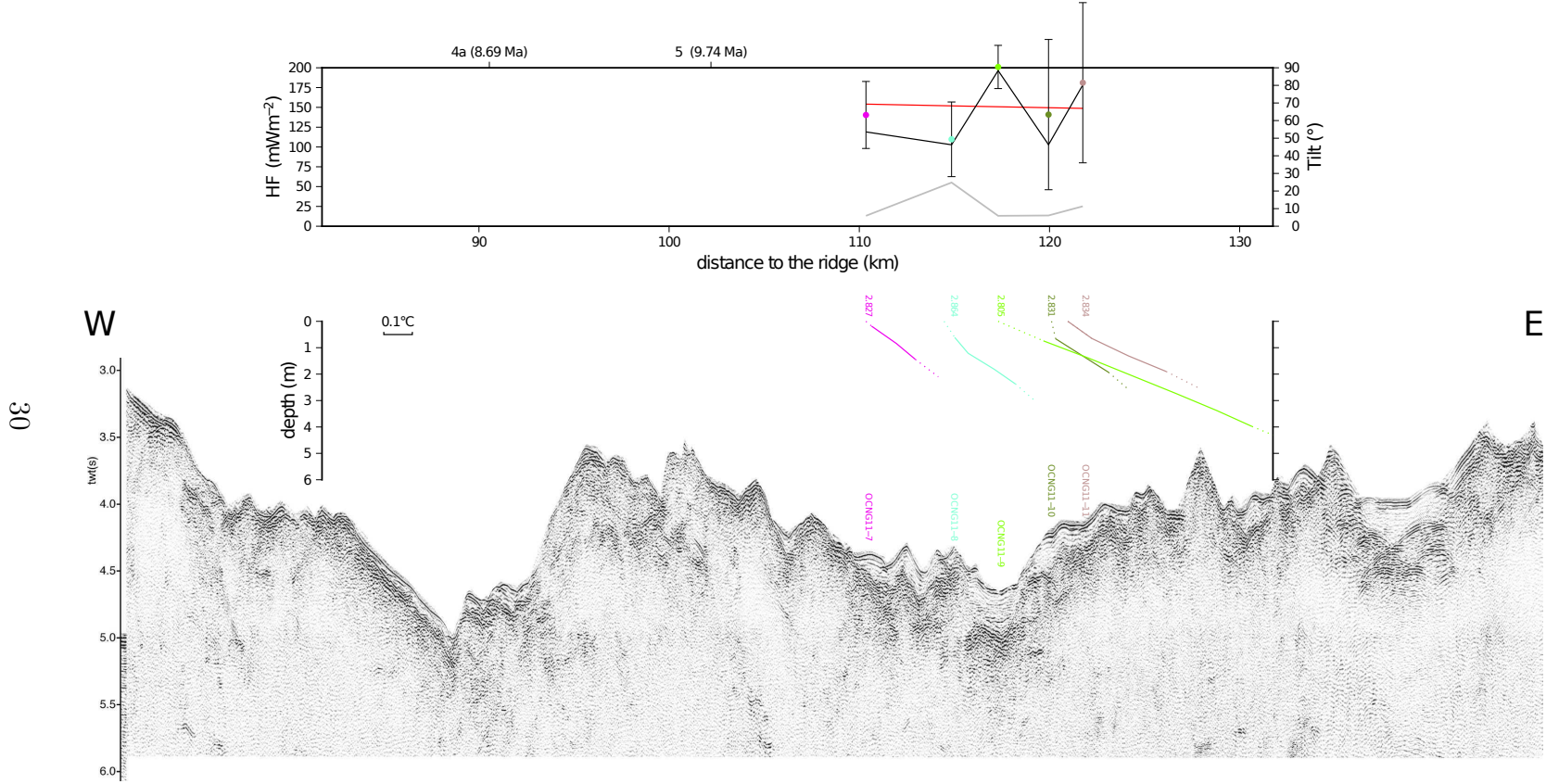
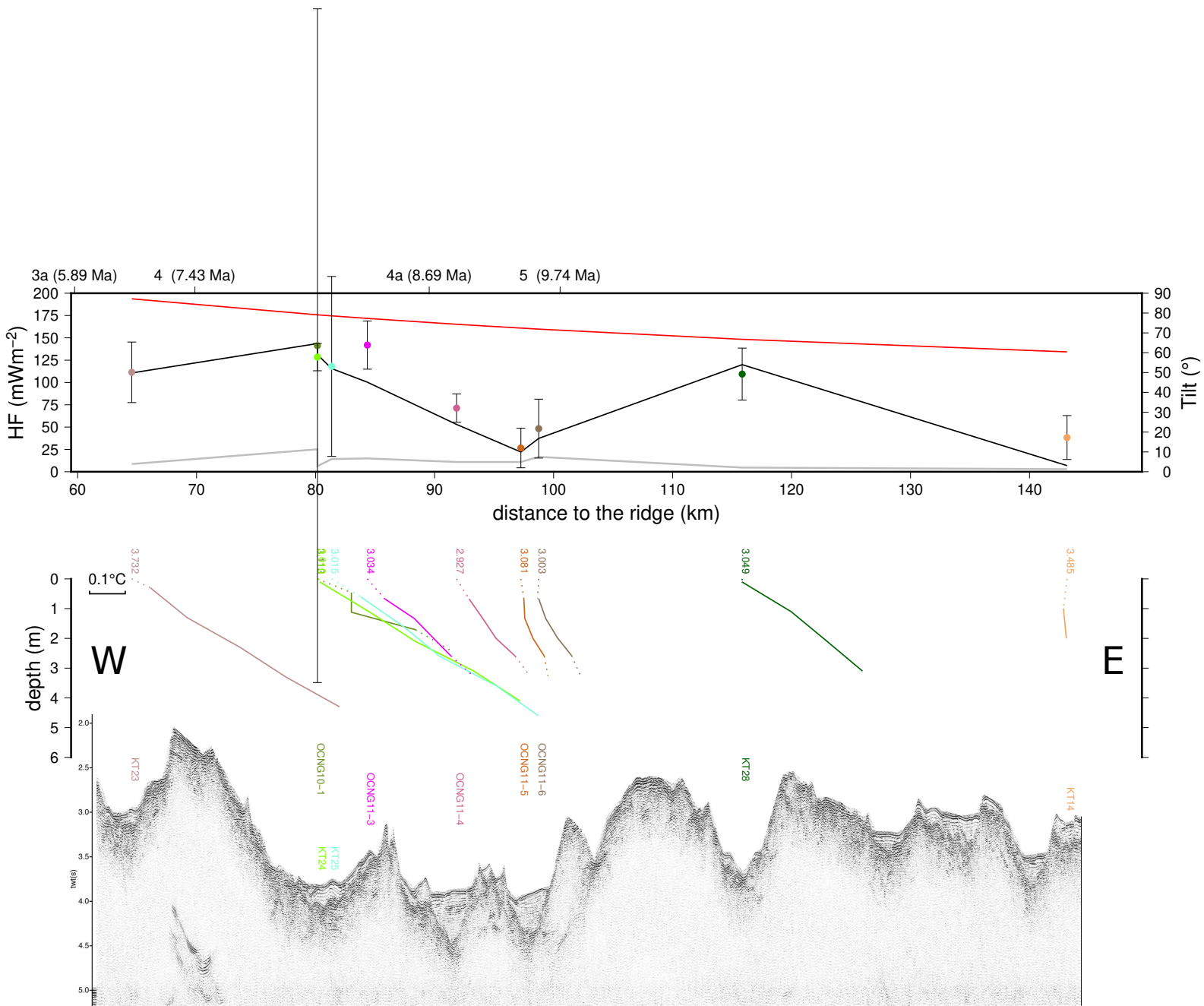


Figure 12b: Heat flow measurements along seismic profile 23E.



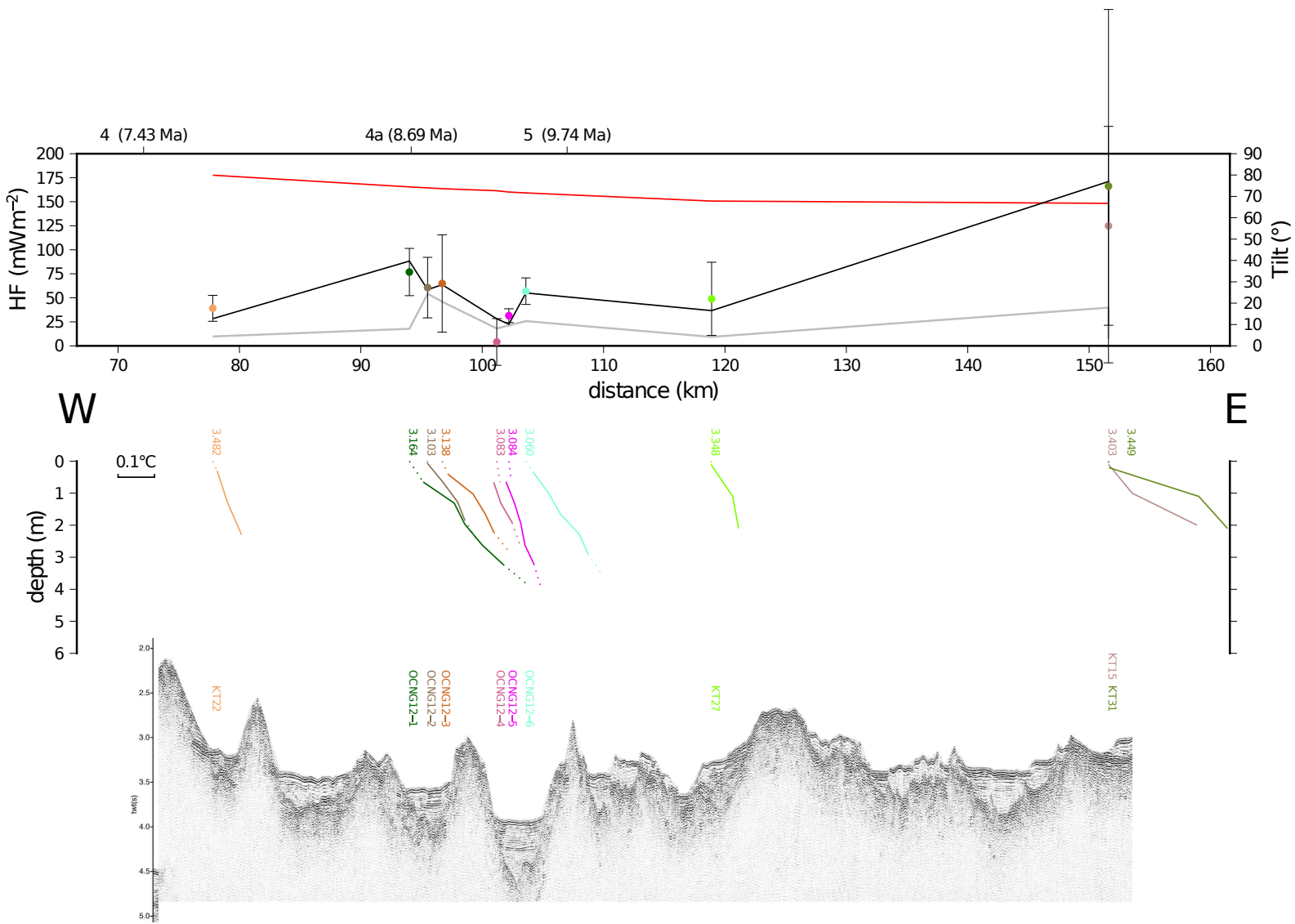


Figure 12d: Heat flow measurements along seismic profile 25E.

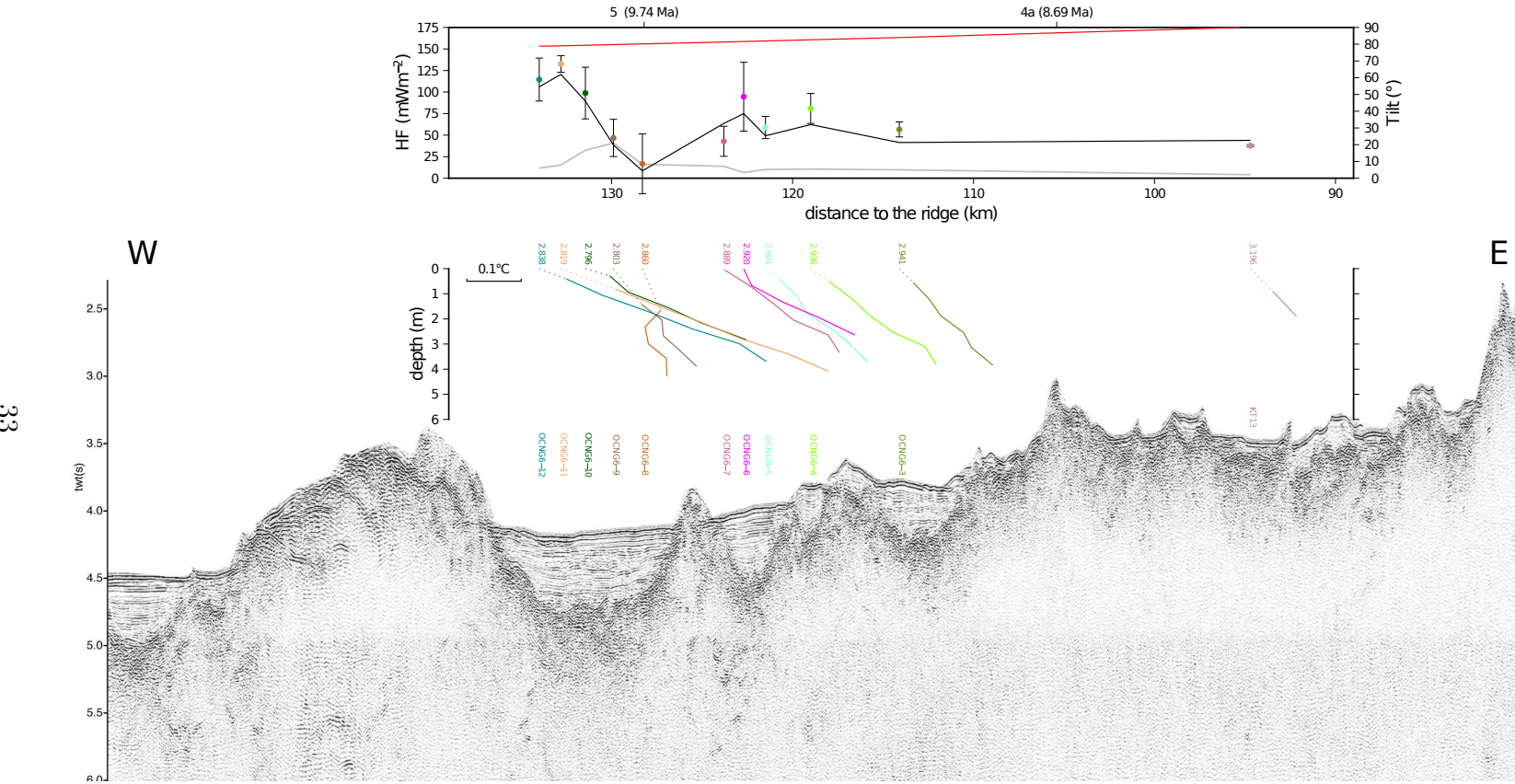


Figure 12e: Heat flow measurements along seismic profile 26W.

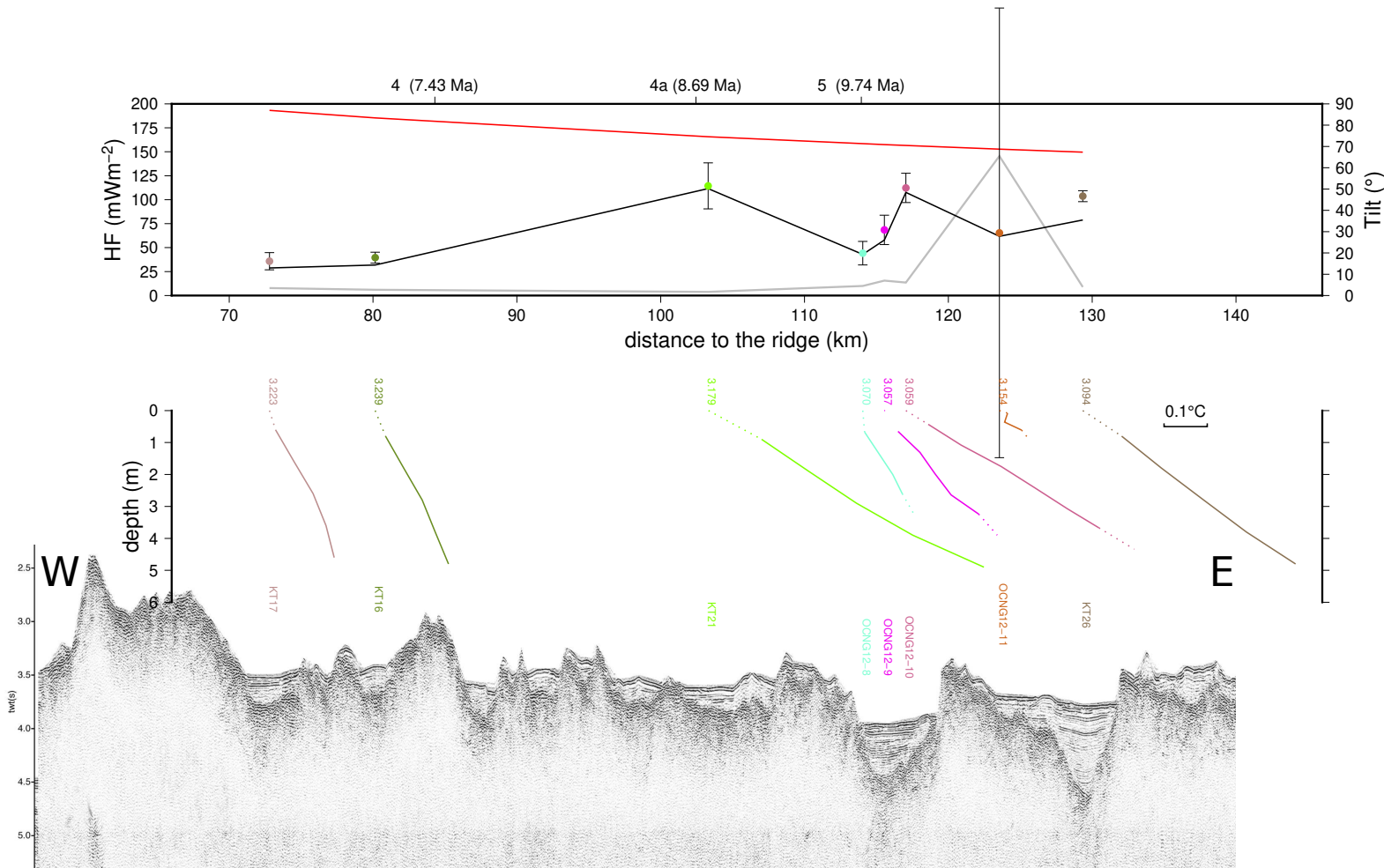


Figure 12f: Heat flow measurements along seismic profile 26E.

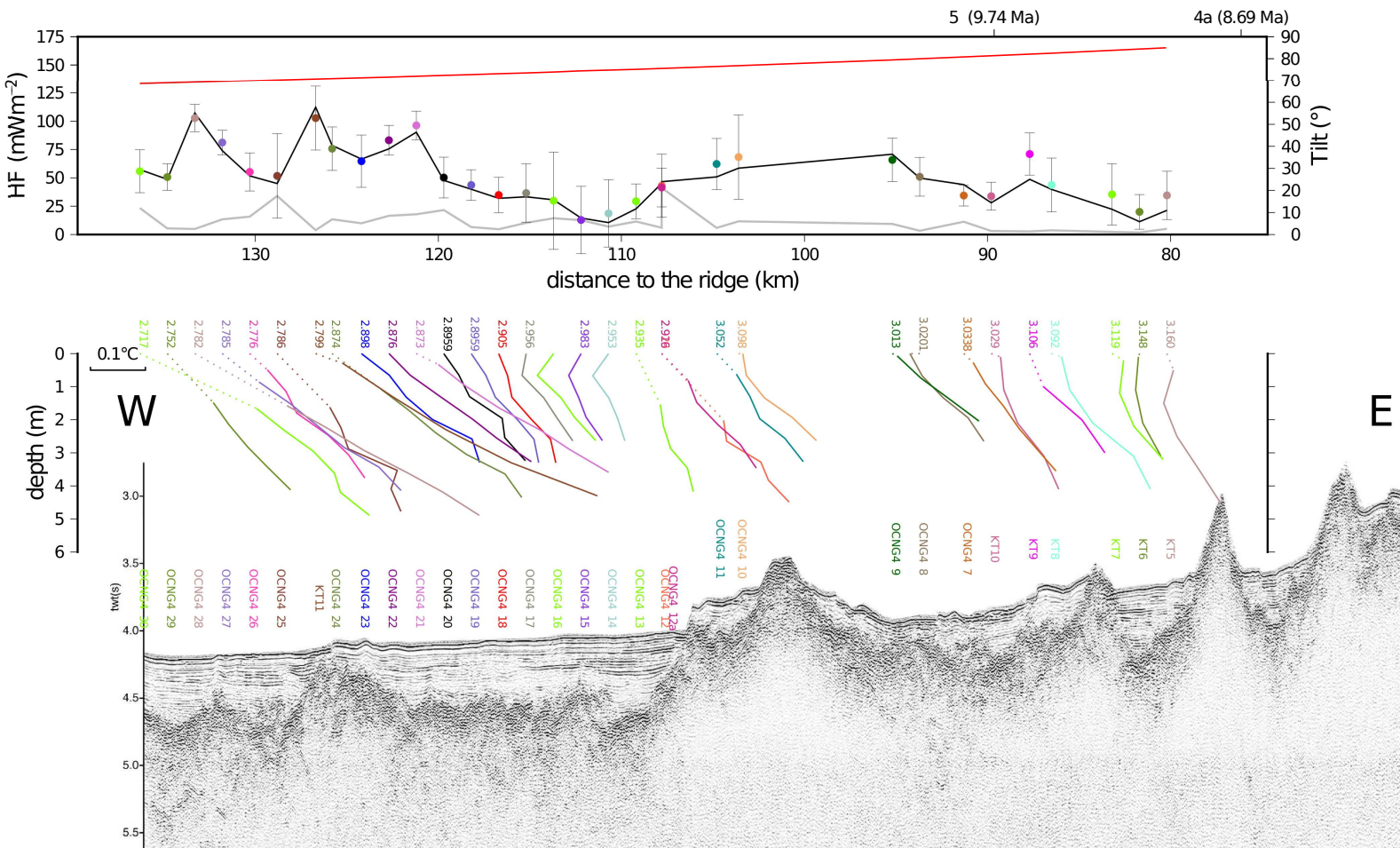


Figure 12g: Heat flow measurements along seismic profile 27W.

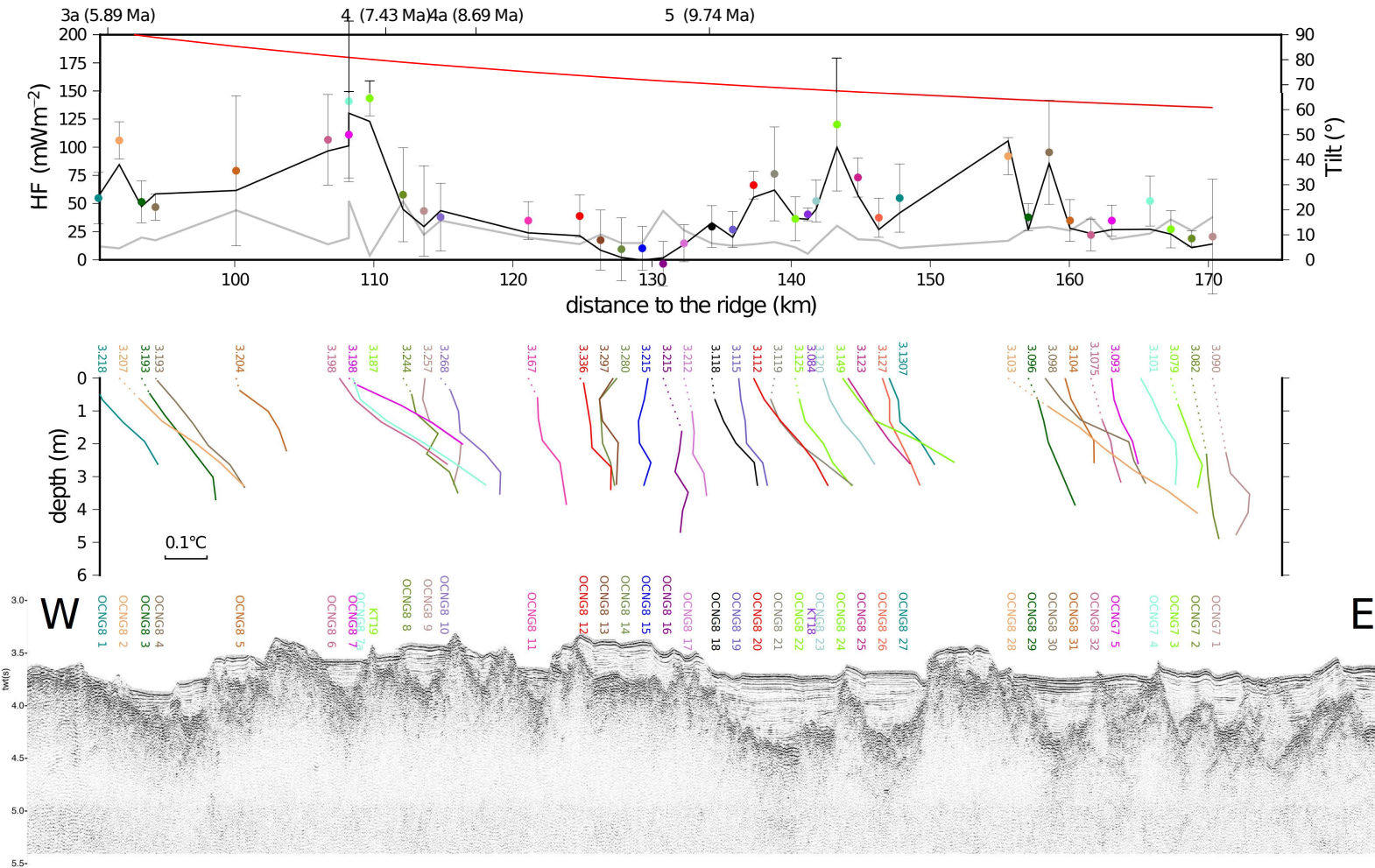


Figure 12h: Heat flow measurements along seismic profile 27E.

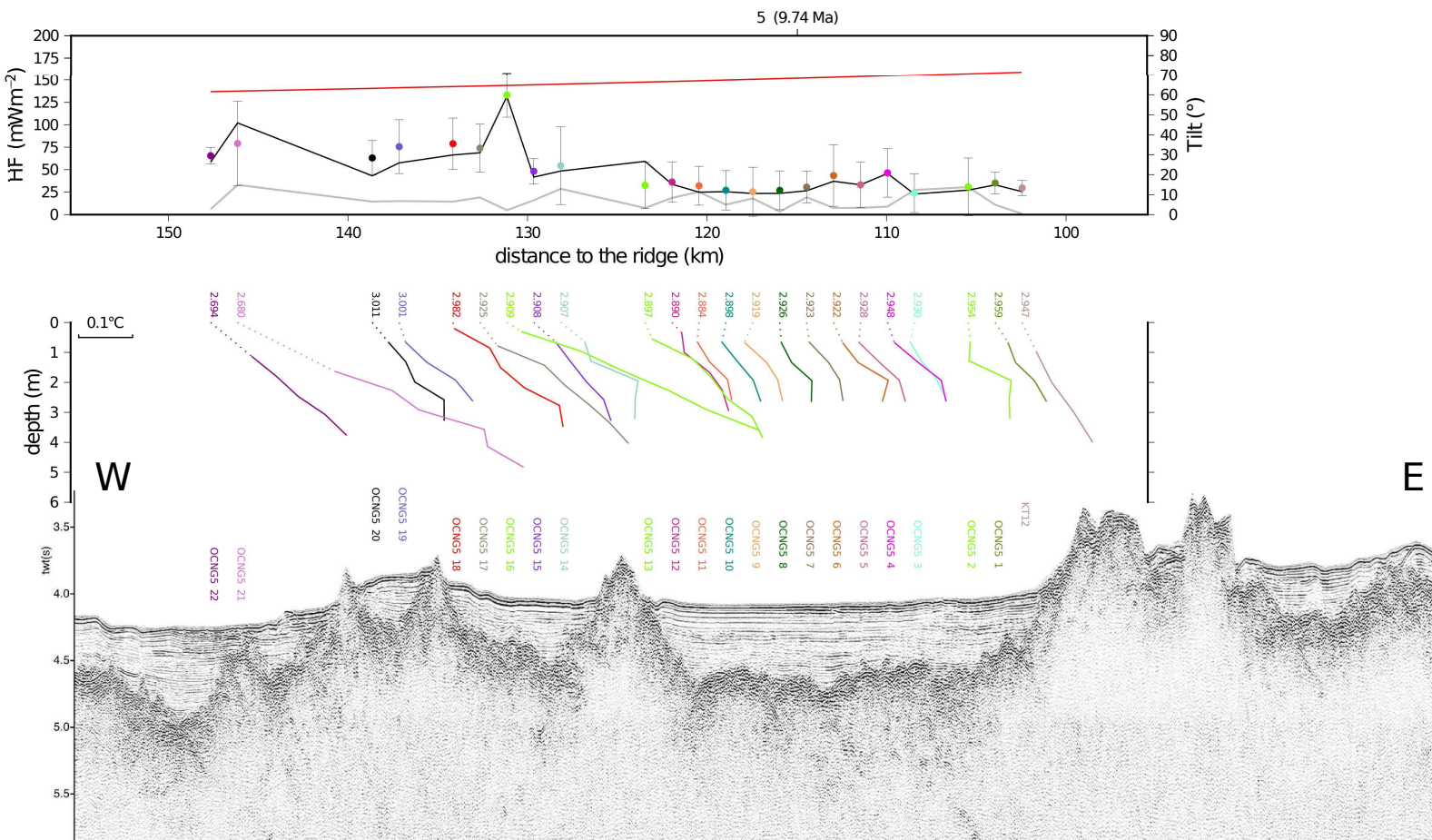


Figure 12i: Heat flow measurements along seismic profile 28W.

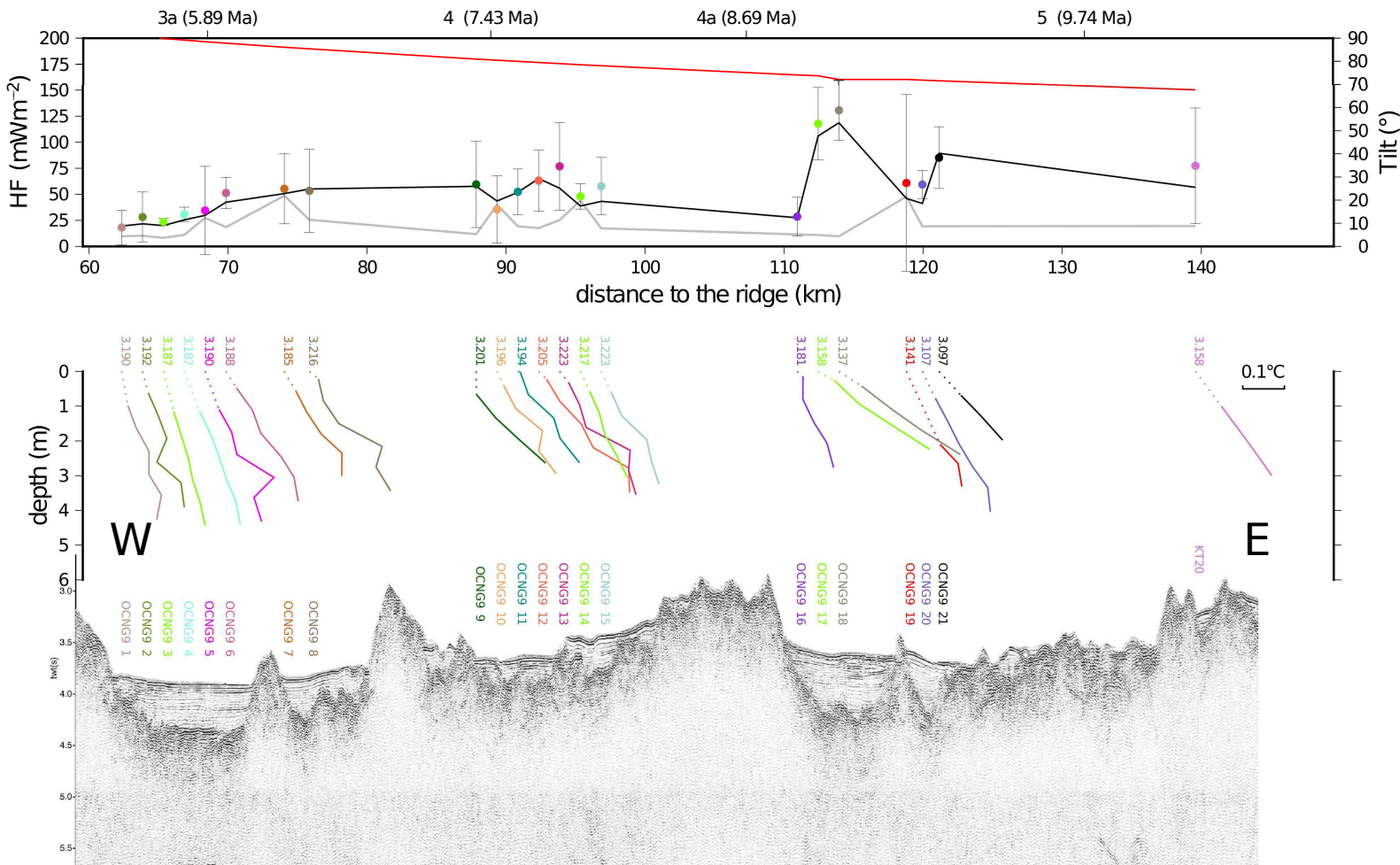


Figure 12j: Heat flow measurements along seismic profile 28E.

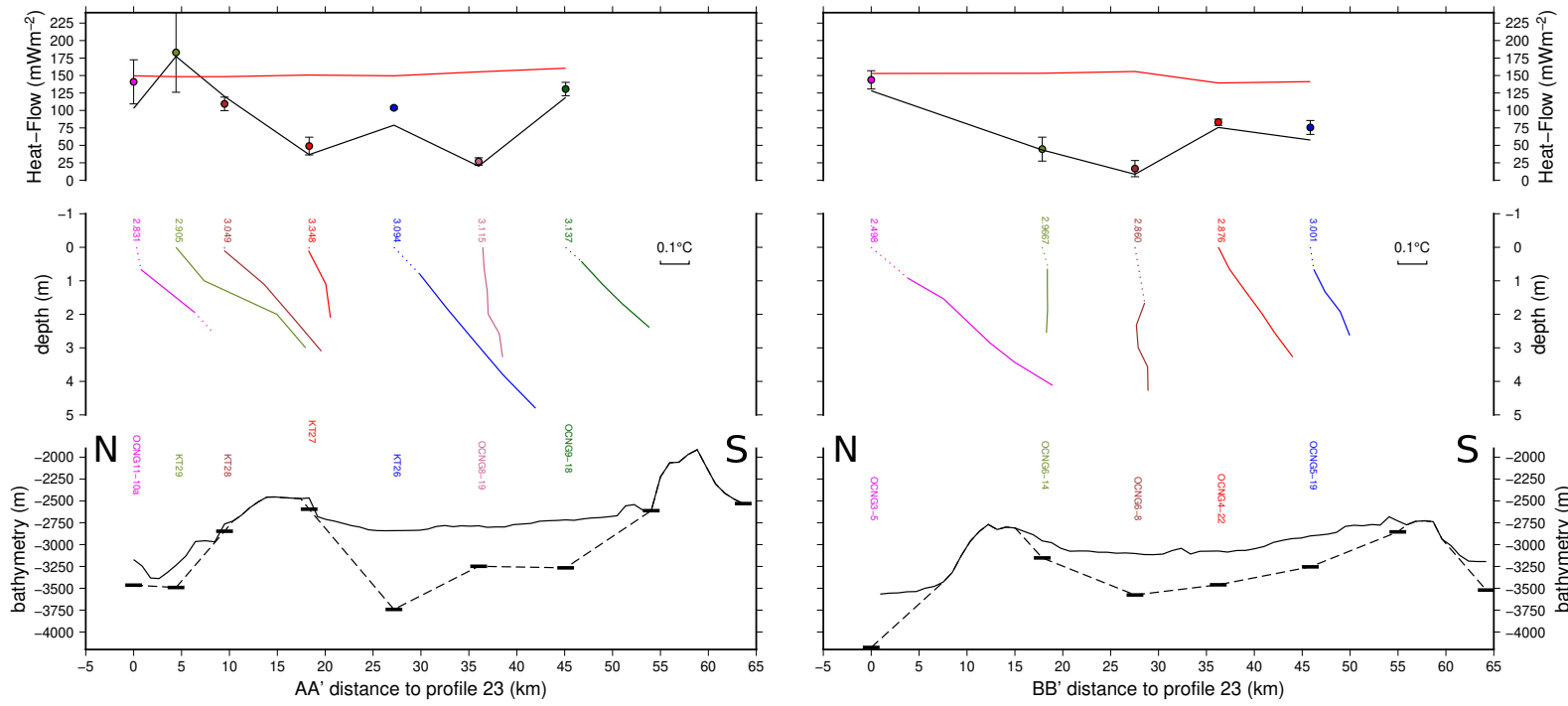


Figure 12k: Heat flow measurements along profiles AA' and BB' (locations in Figure 1). Bottom panel represents the topographic section (line), top of basement (line segment) and position of each site (multi penetration or core) above.

Figure 13: Heat flow and conductivity profiles at each measurement site

Figure 13a: Plot of OCEANOGRAPHY conductivity and temperature profiles

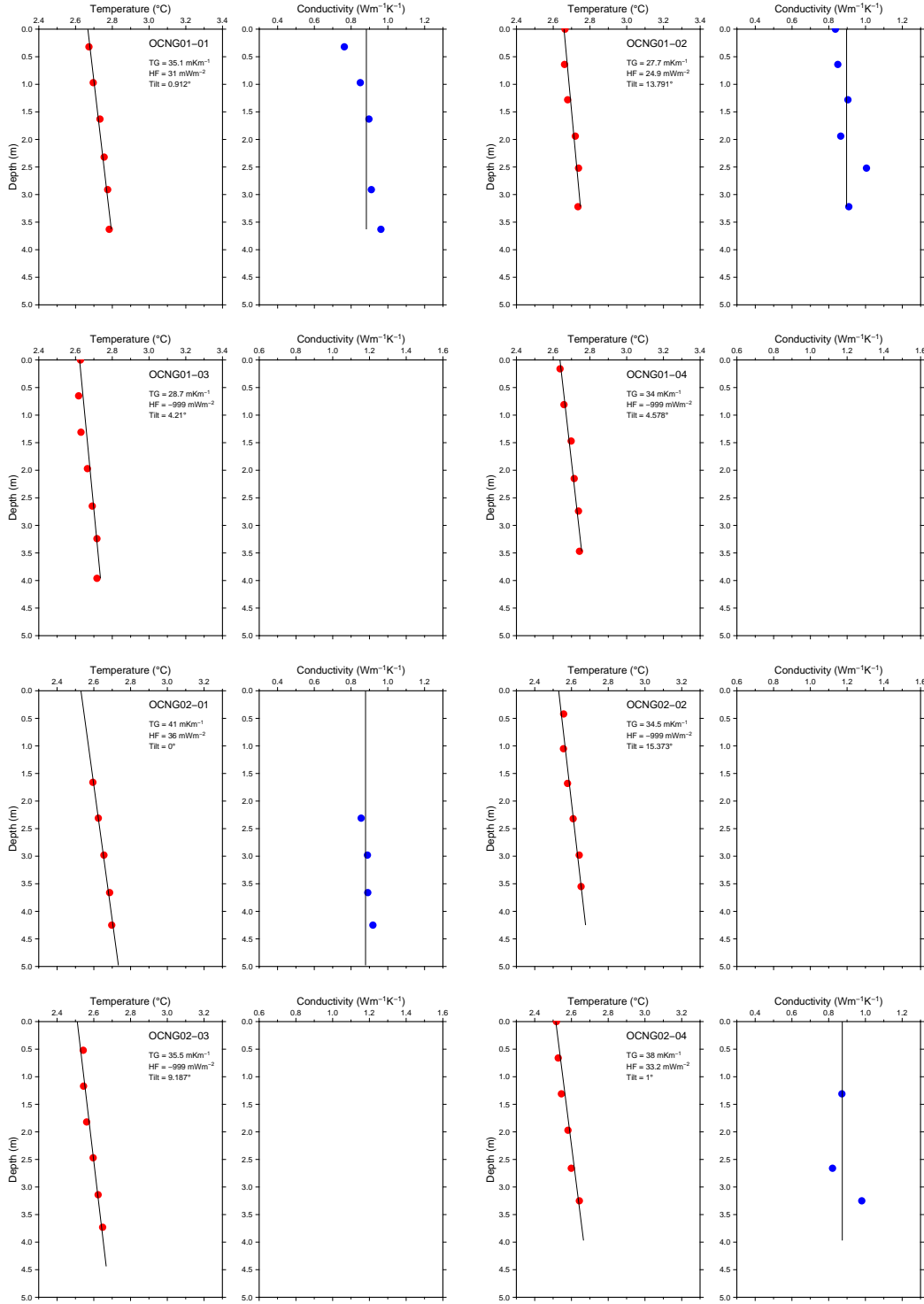


Figure 13b: Plot of OCEANOGRAPHY conductivity and temperature profiles

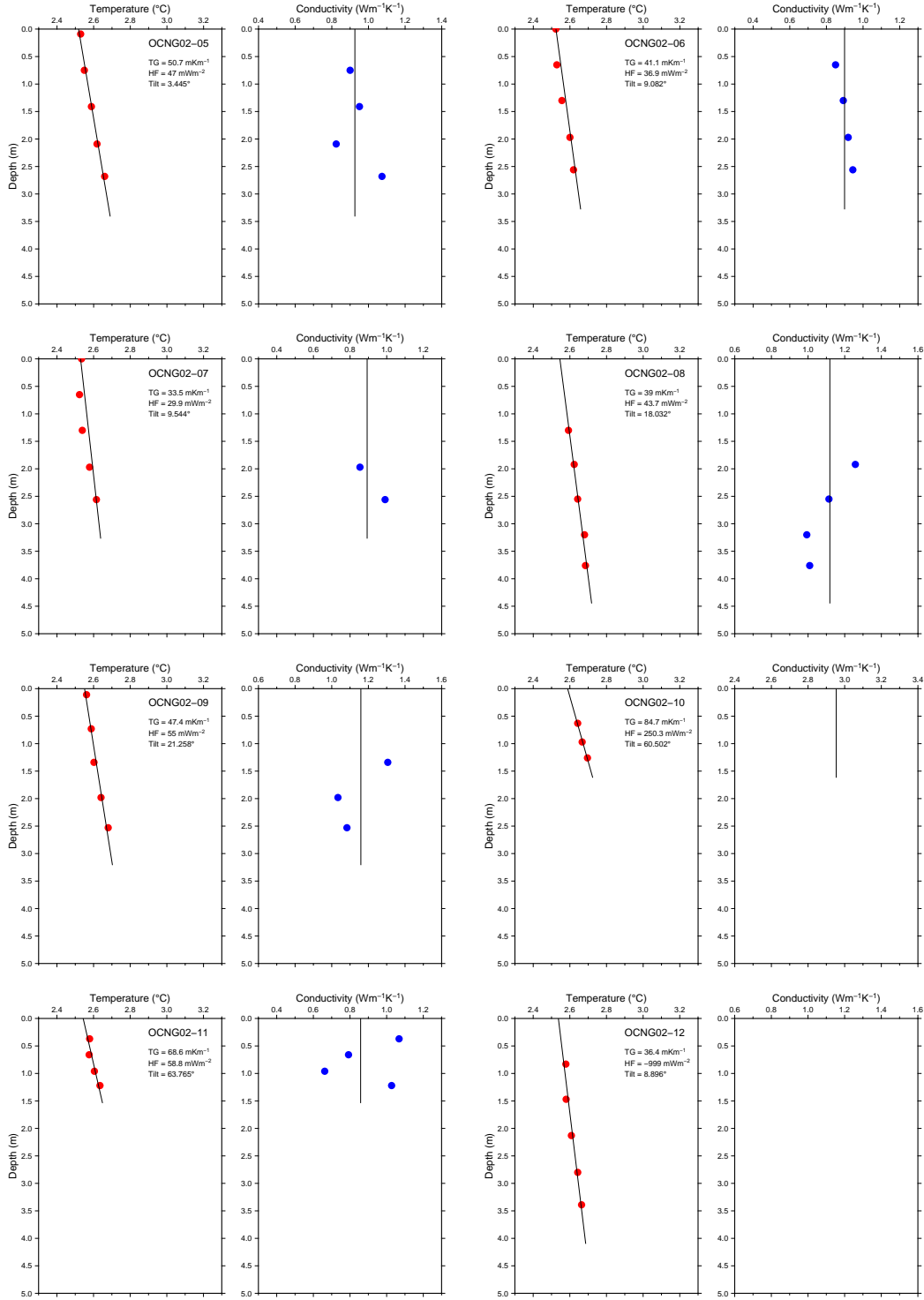


Figure 13c: Plot of OCEANOGRAPHY conductivity and temperature profiles

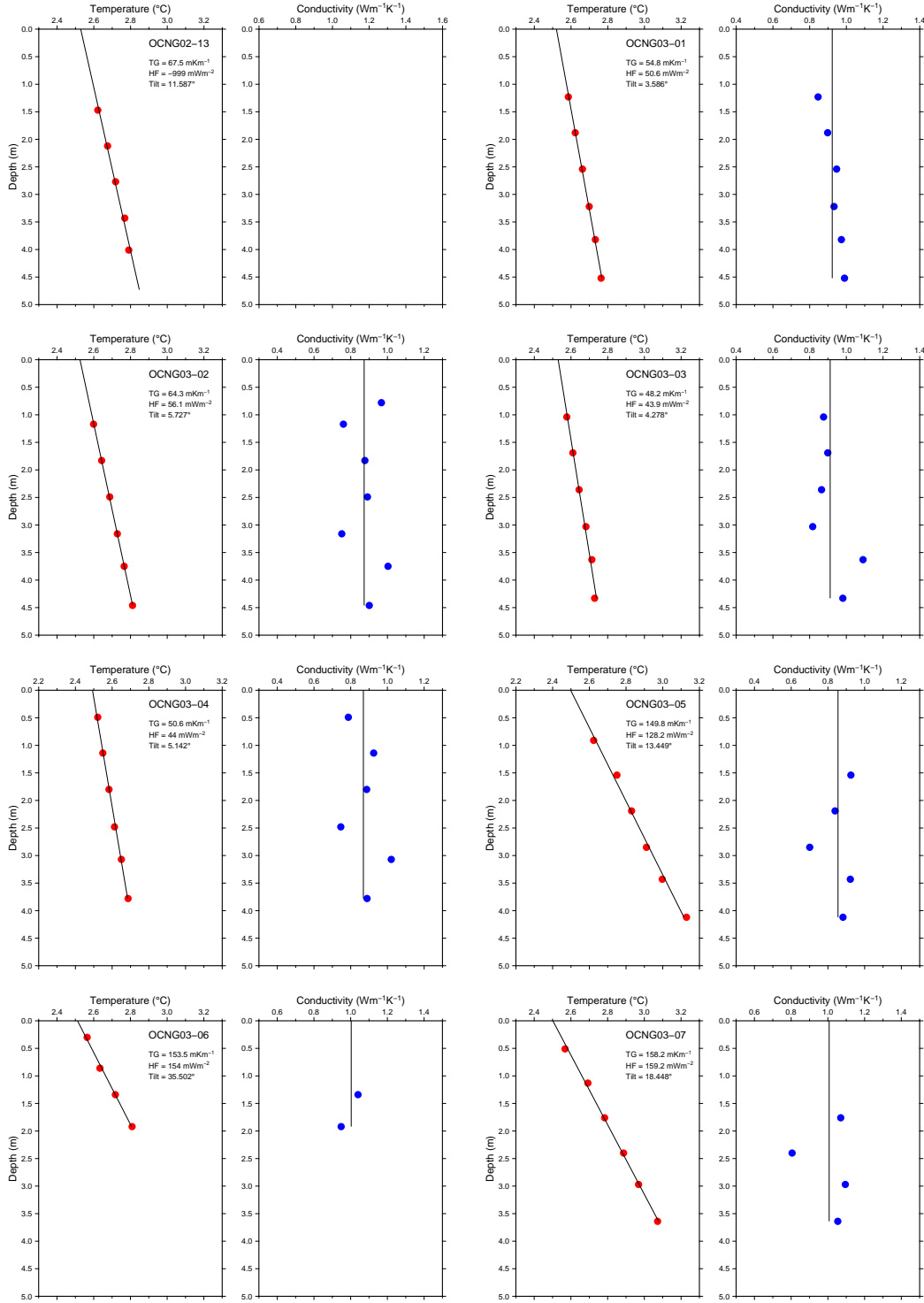


Figure 13d: Plot of OCEANOGRAPHY conductivity and temperature profiles

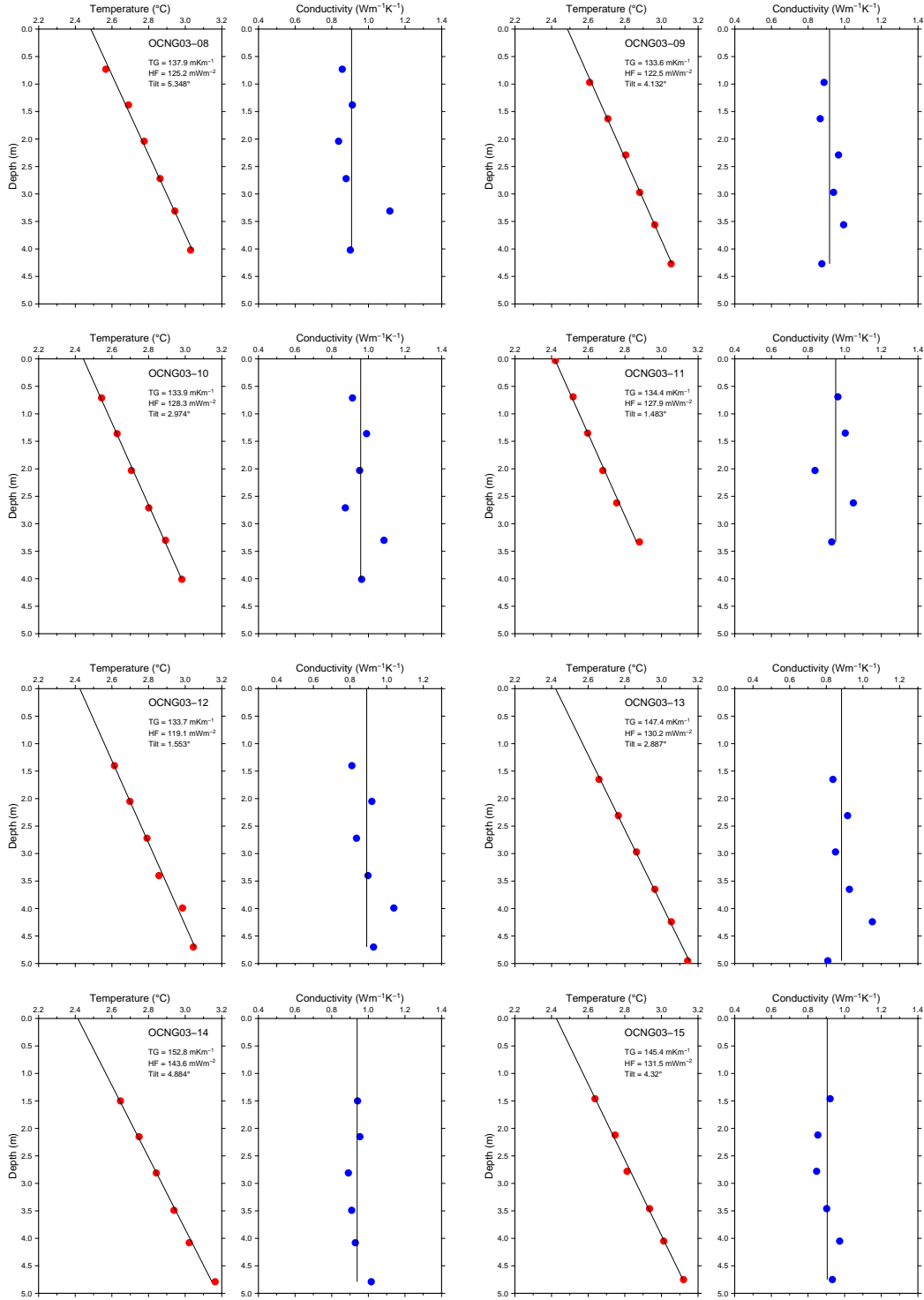


Figure 13e: Plot of OCEANOGRAFLU conductivity and temperature profiles

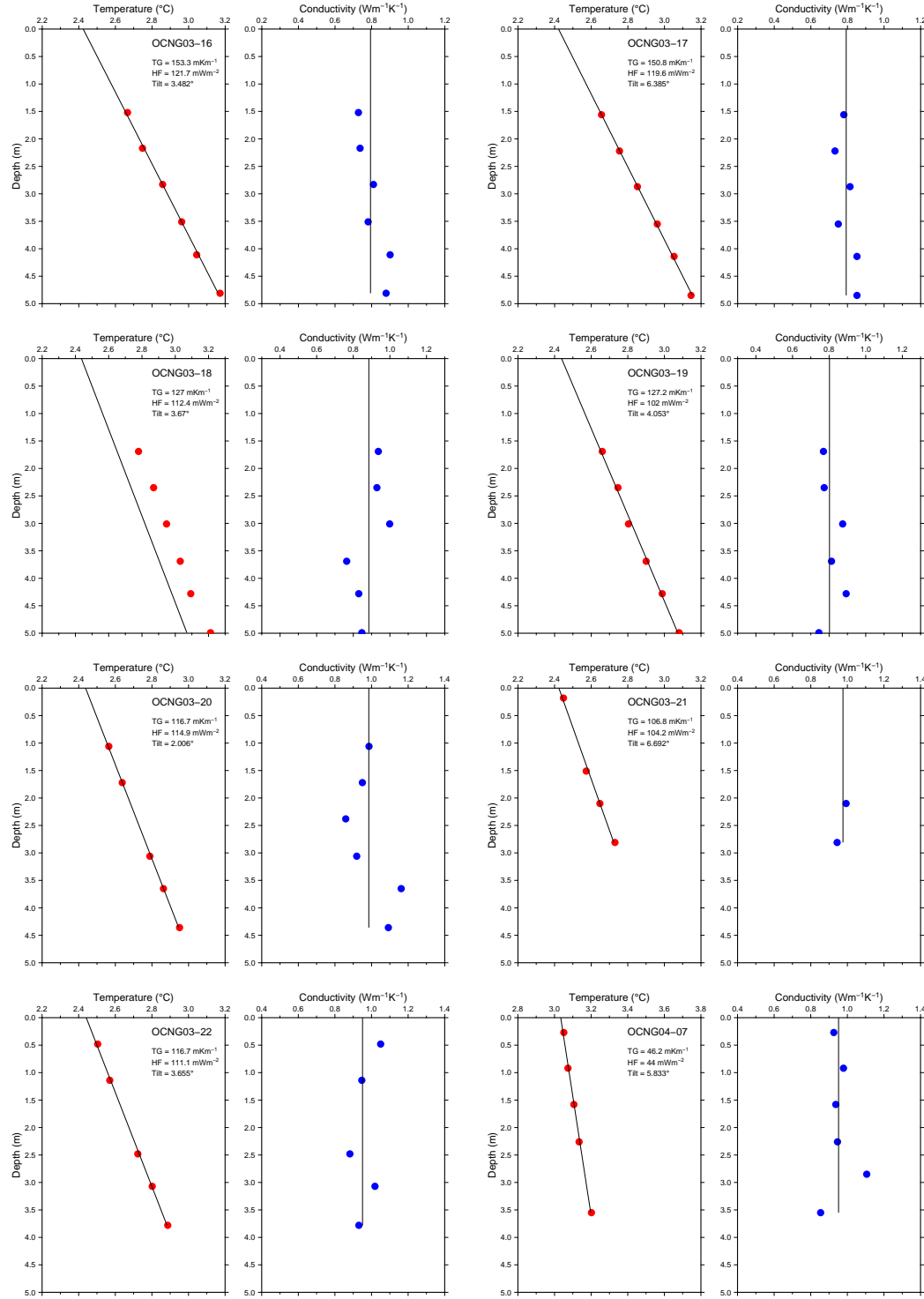


Figure 13f: Plot of OCEANOGRAPHY conductivity and temperature profiles

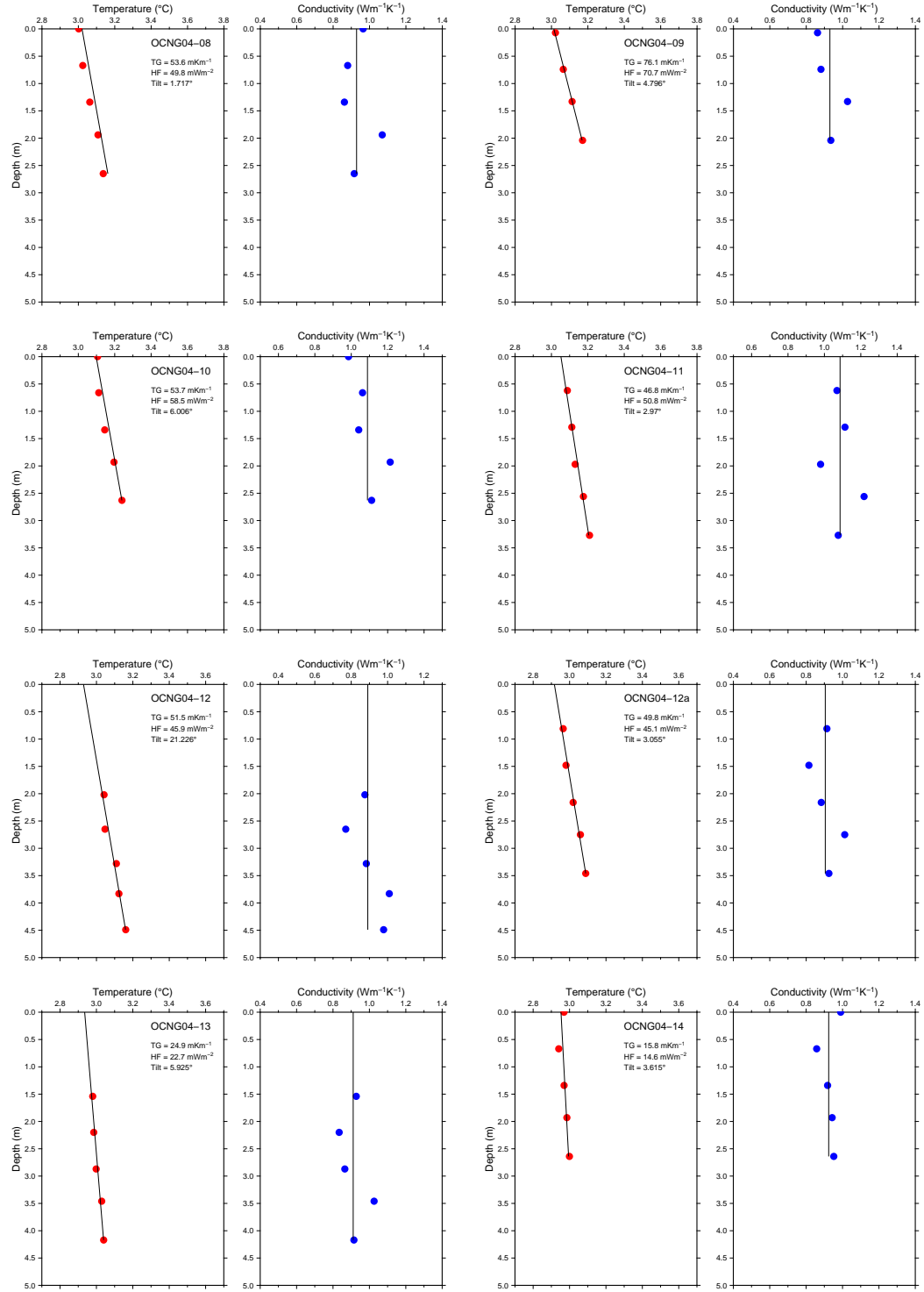


Figure 13g: Plot of OCEANOGRAPHY conductivity and temperature profiles

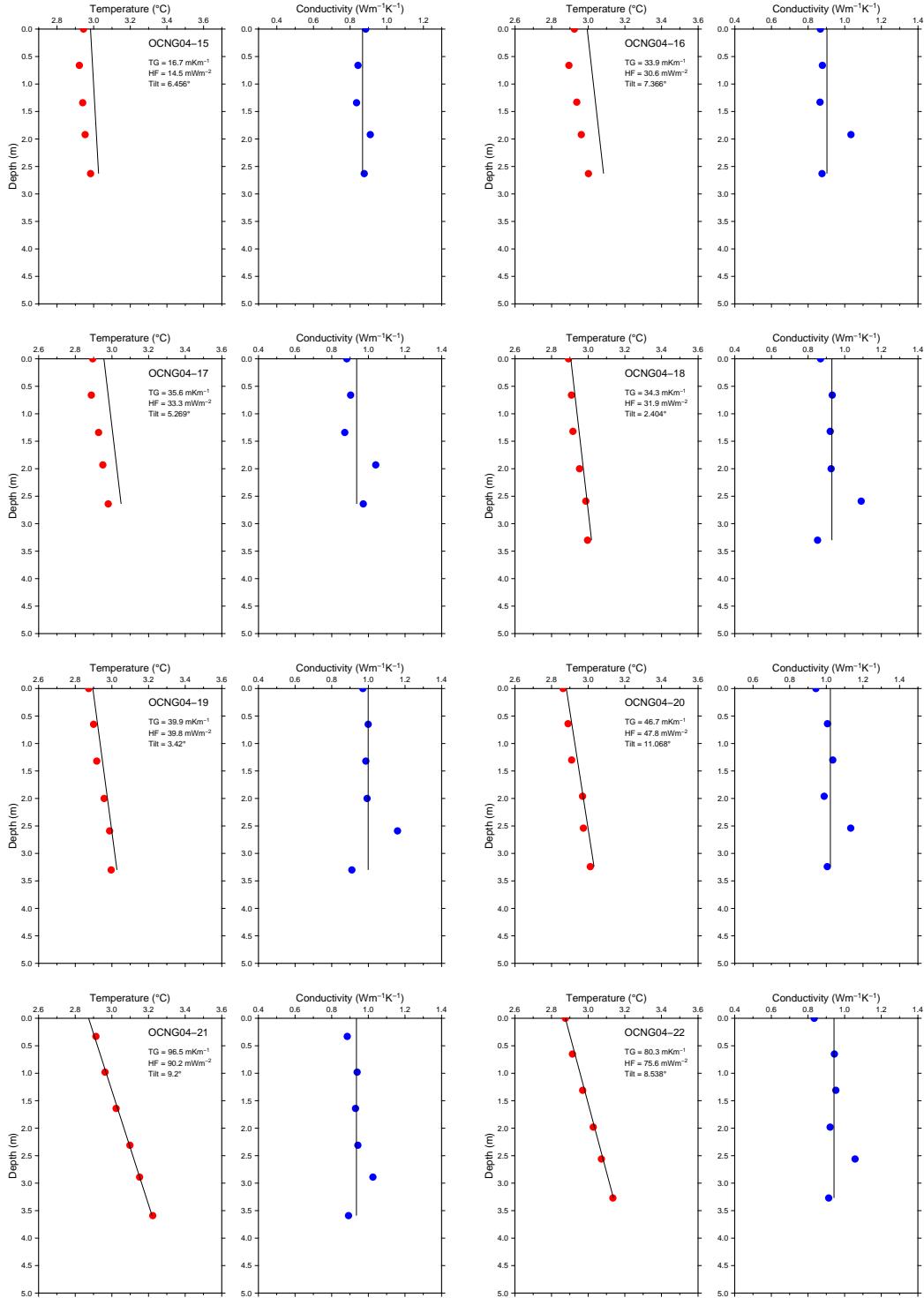


Figure 13h: Plot of OCEANOGRAPHY conductivity and temperature profiles

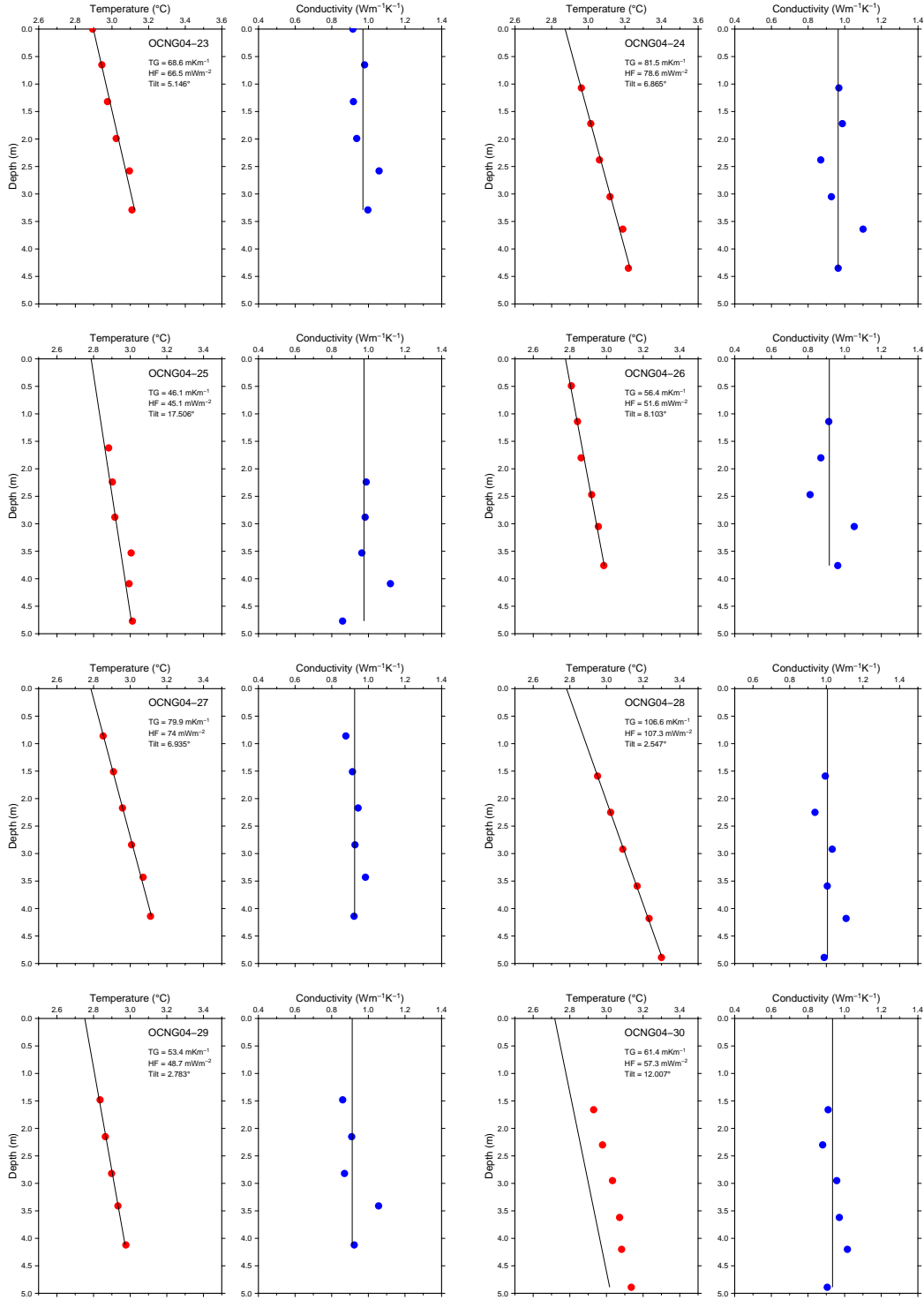


Figure 13i: Plot of OCEANOGRAPHY conductivity and temperature profiles

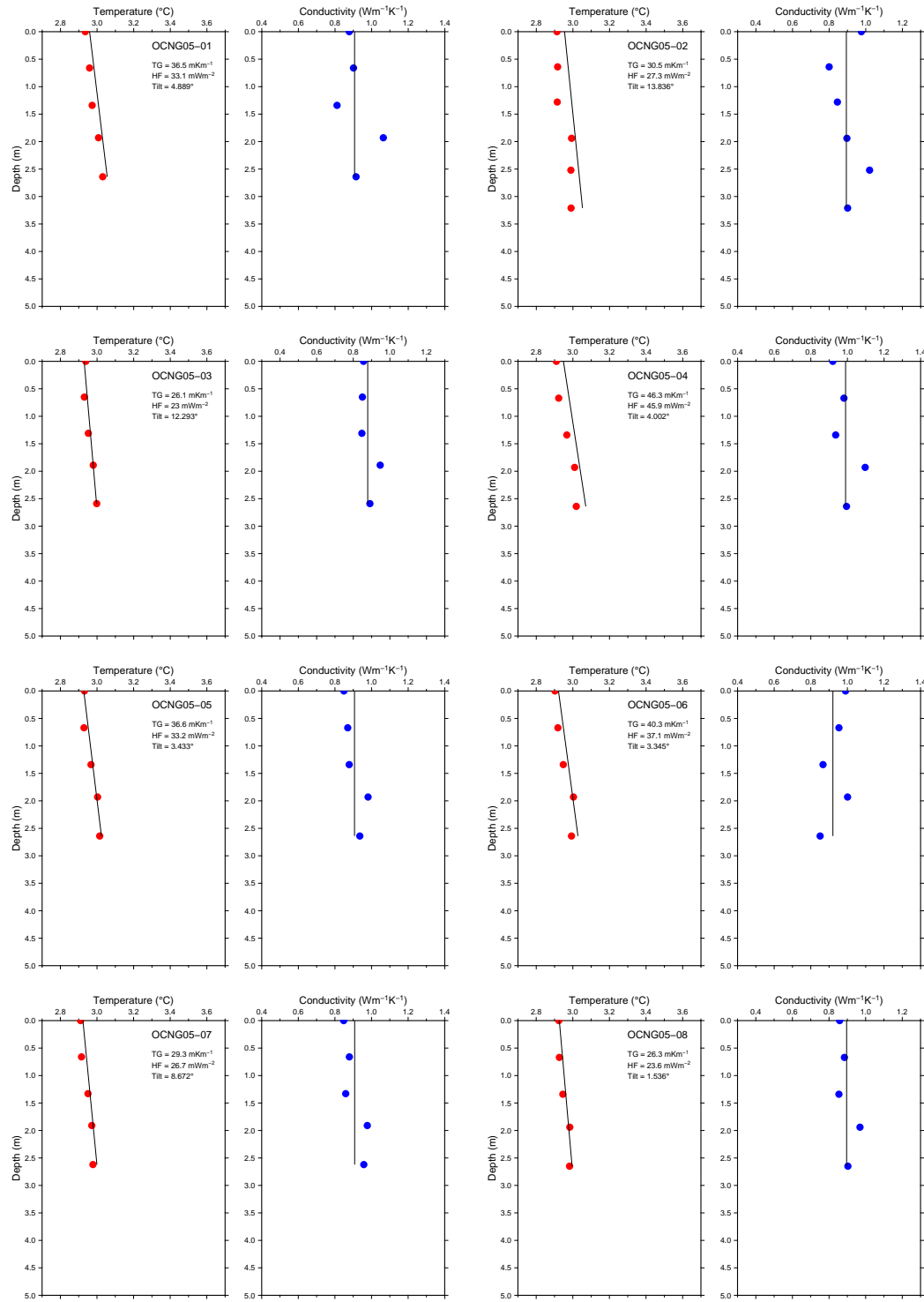


Figure 13j: Plot of OCEANOGRAFLU conductivity and temperature profiles

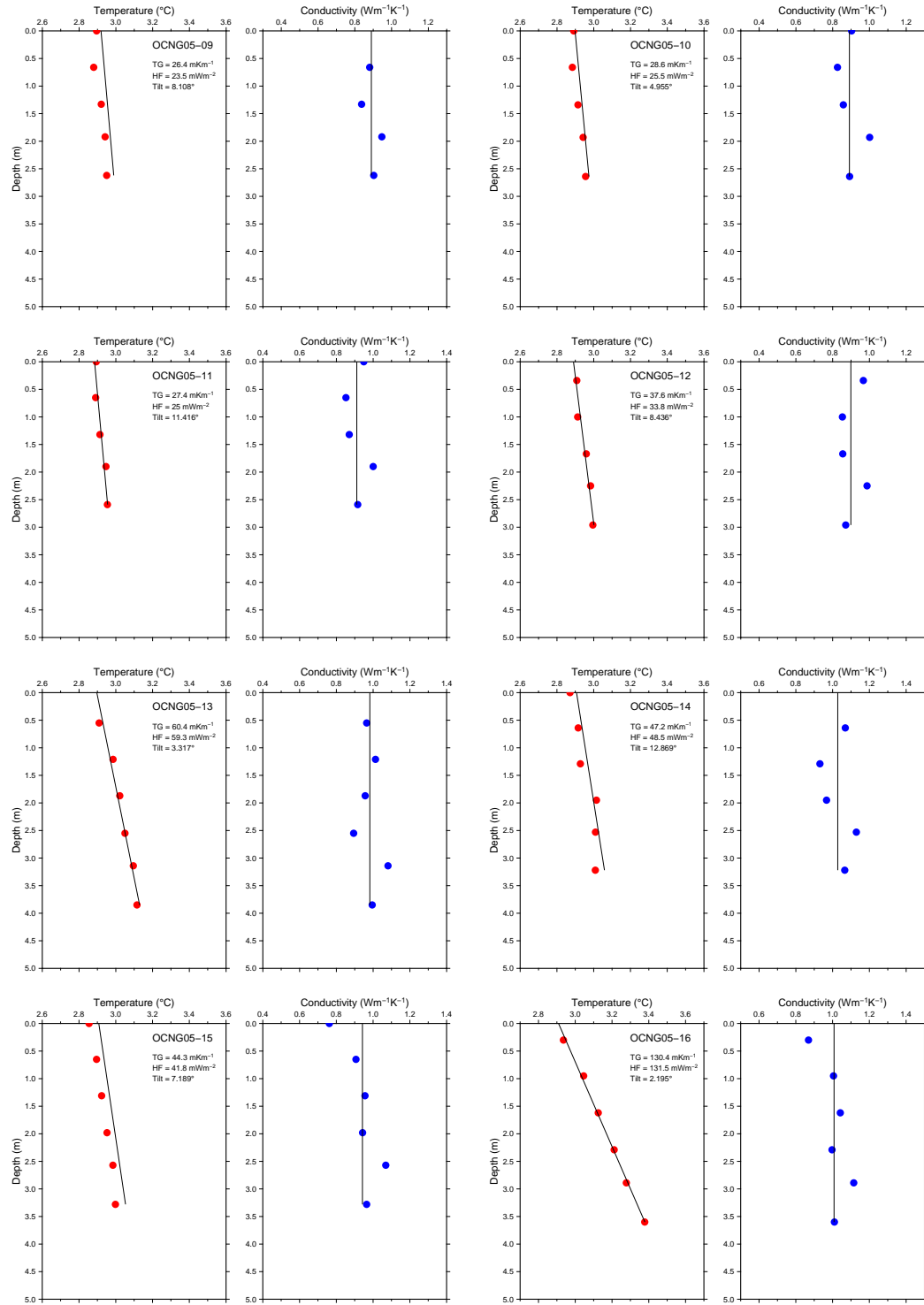


Figure 13k: Plot of OCEANOGRAPHY conductivity and temperature profiles

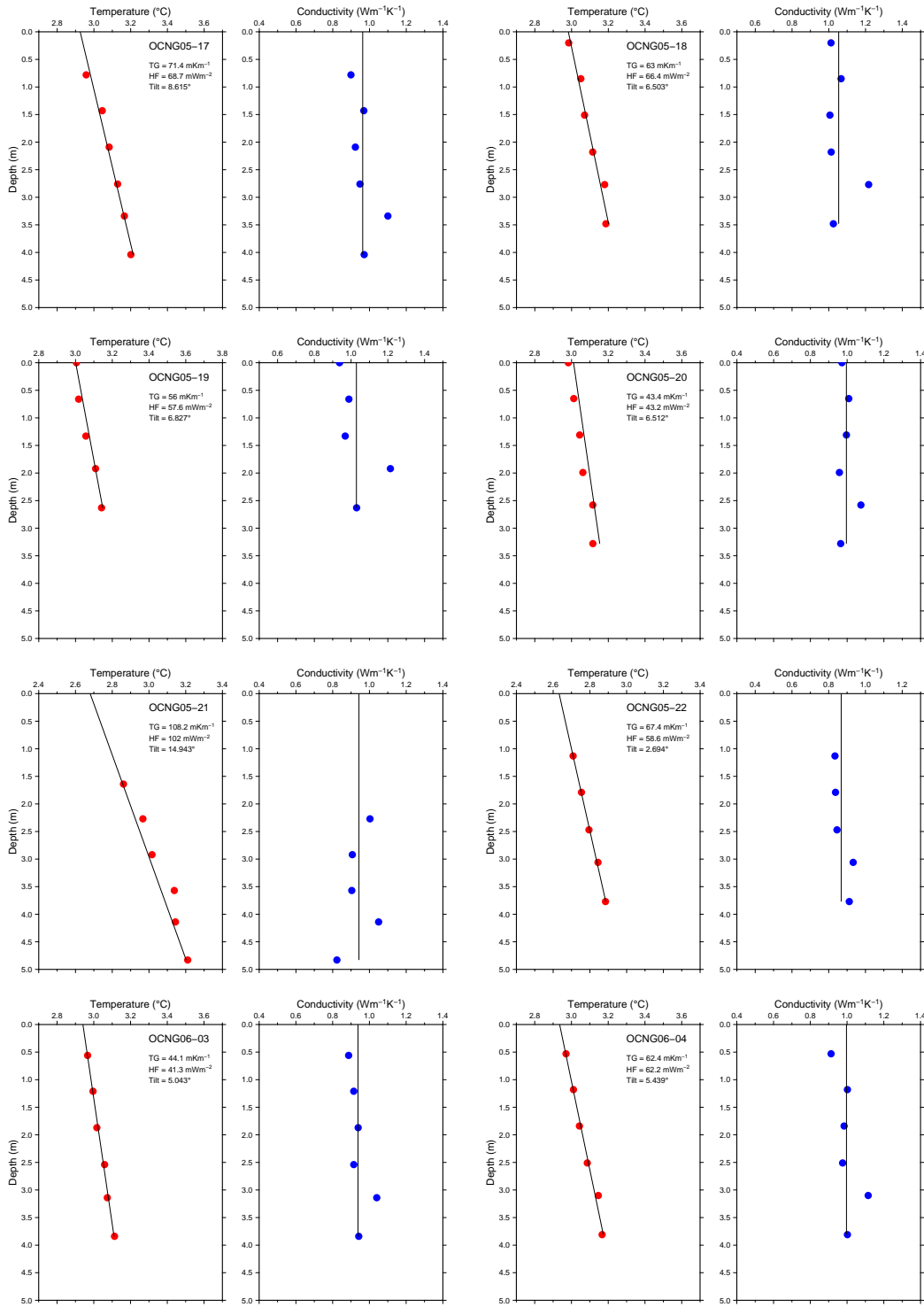


Figure 13l: Plot of OCEANOGRAPHY conductivity and temperature profiles

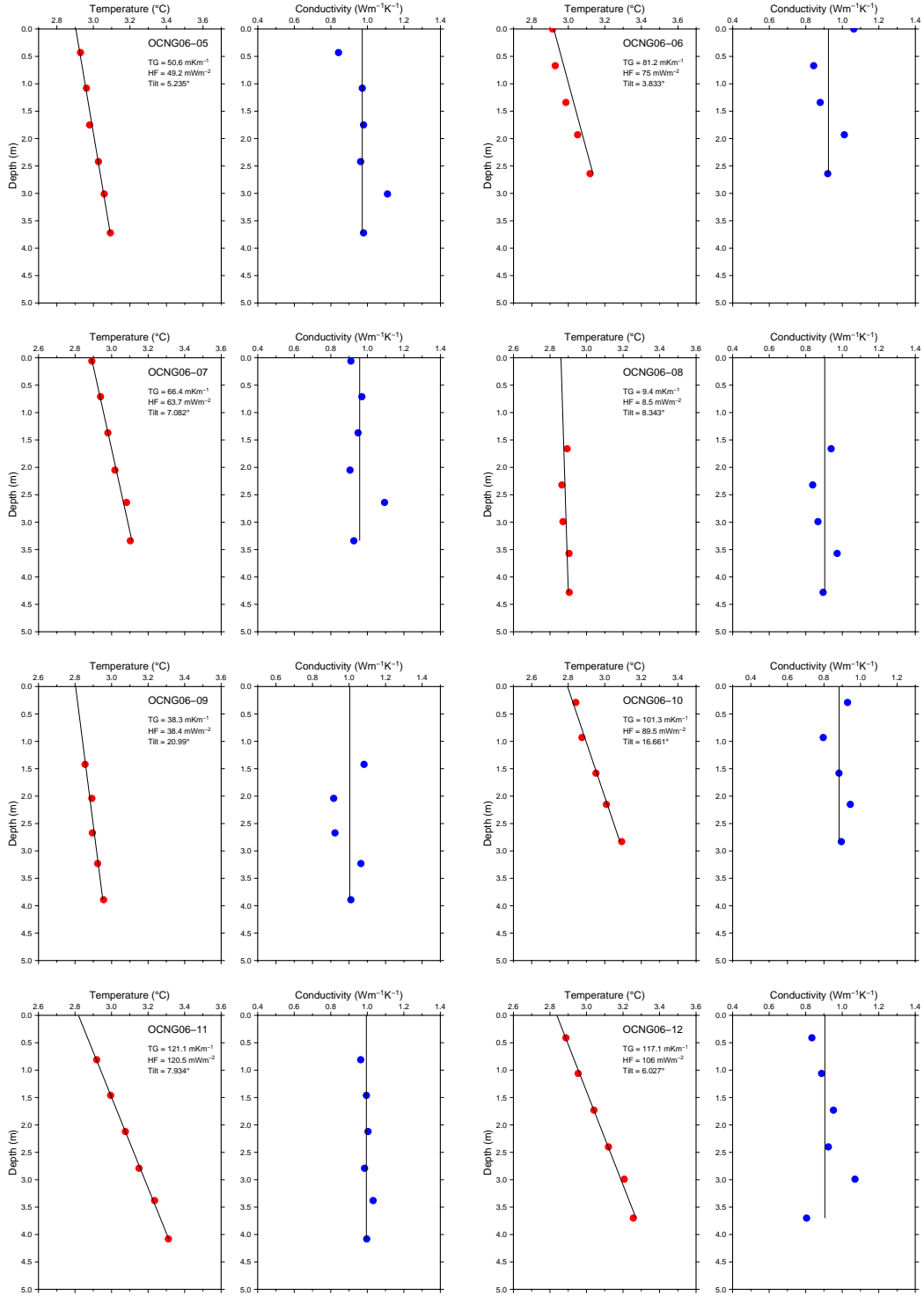


Figure 13m: Plot of OCEANOGRAPHY conductivity and temperature profiles

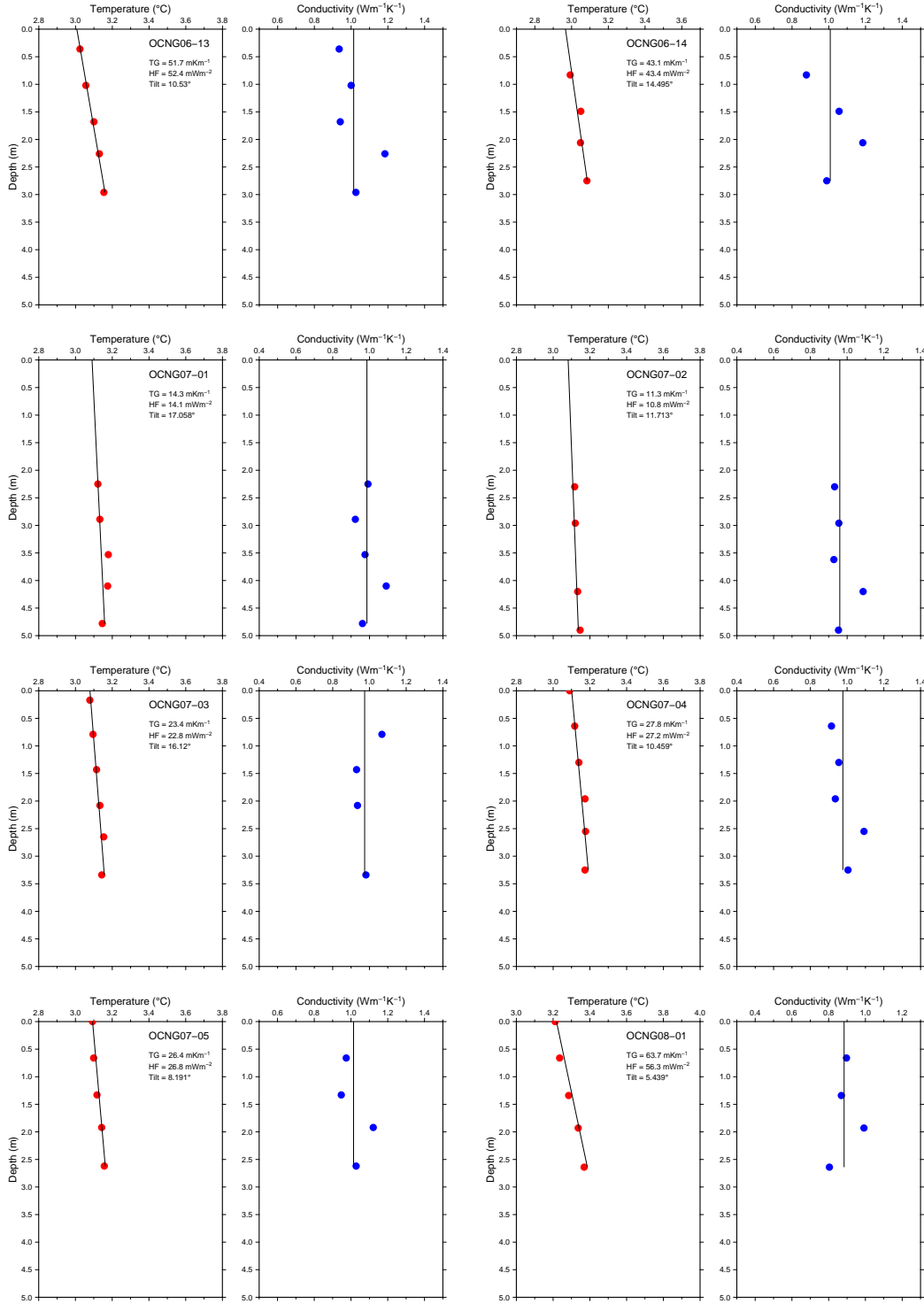


Figure 13n: Plot of OCEANOGRAPHY conductivity and temperature profiles

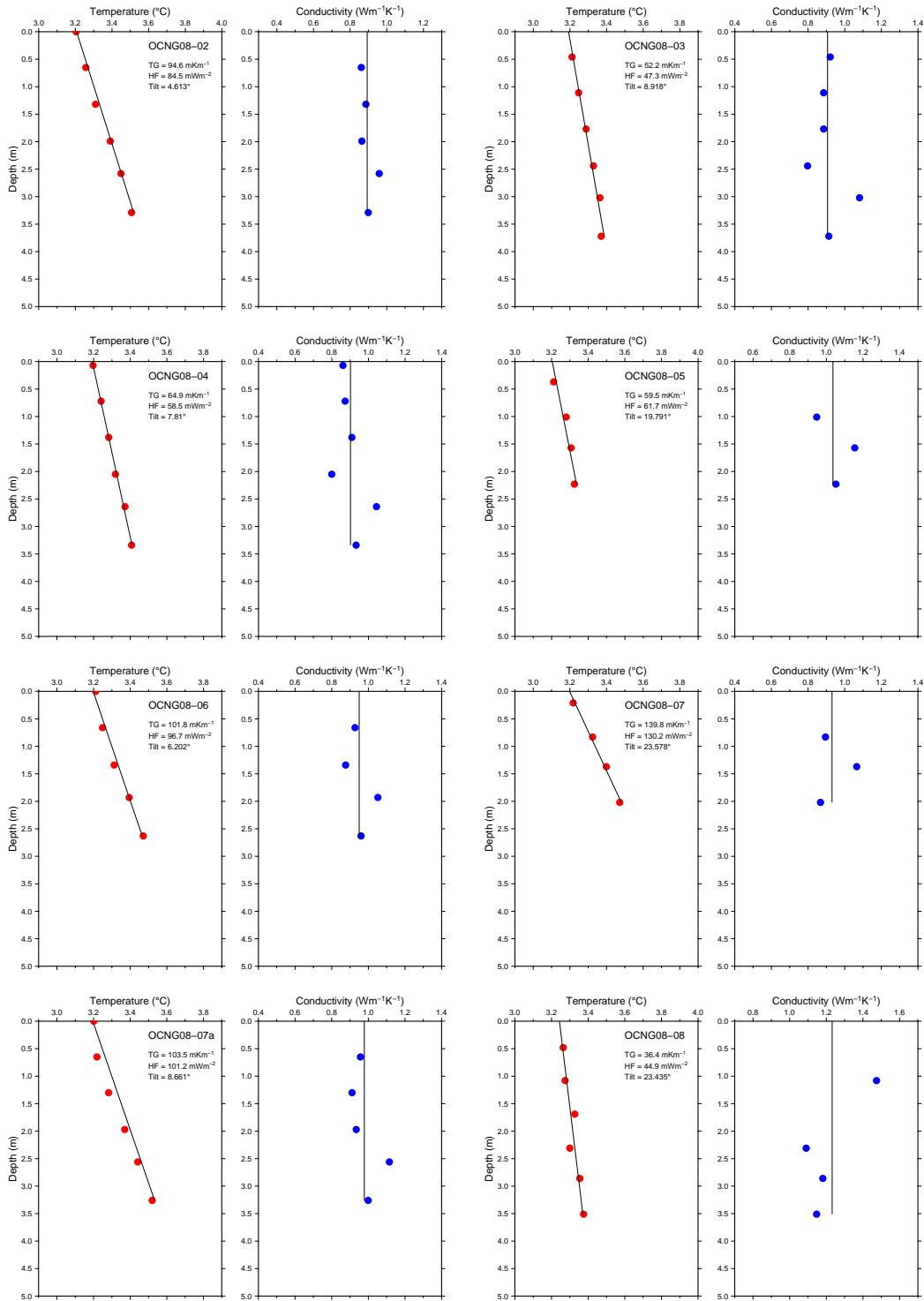


Figure 13o: Plot of OCEANOGRAPHY conductivity and temperature profiles

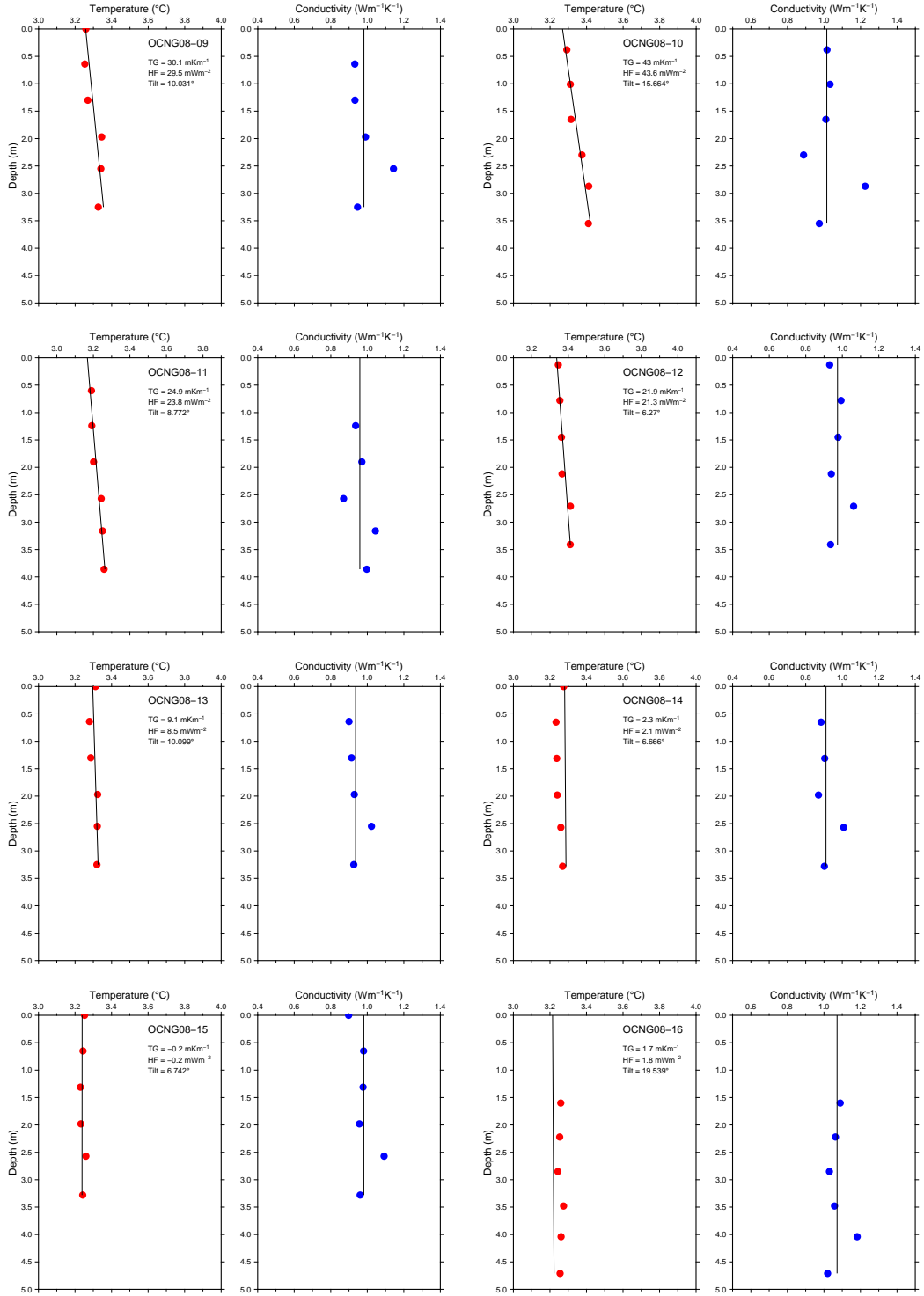


Figure 13p: Plot of OCEANOGRAPHY conductivity and temperature profiles

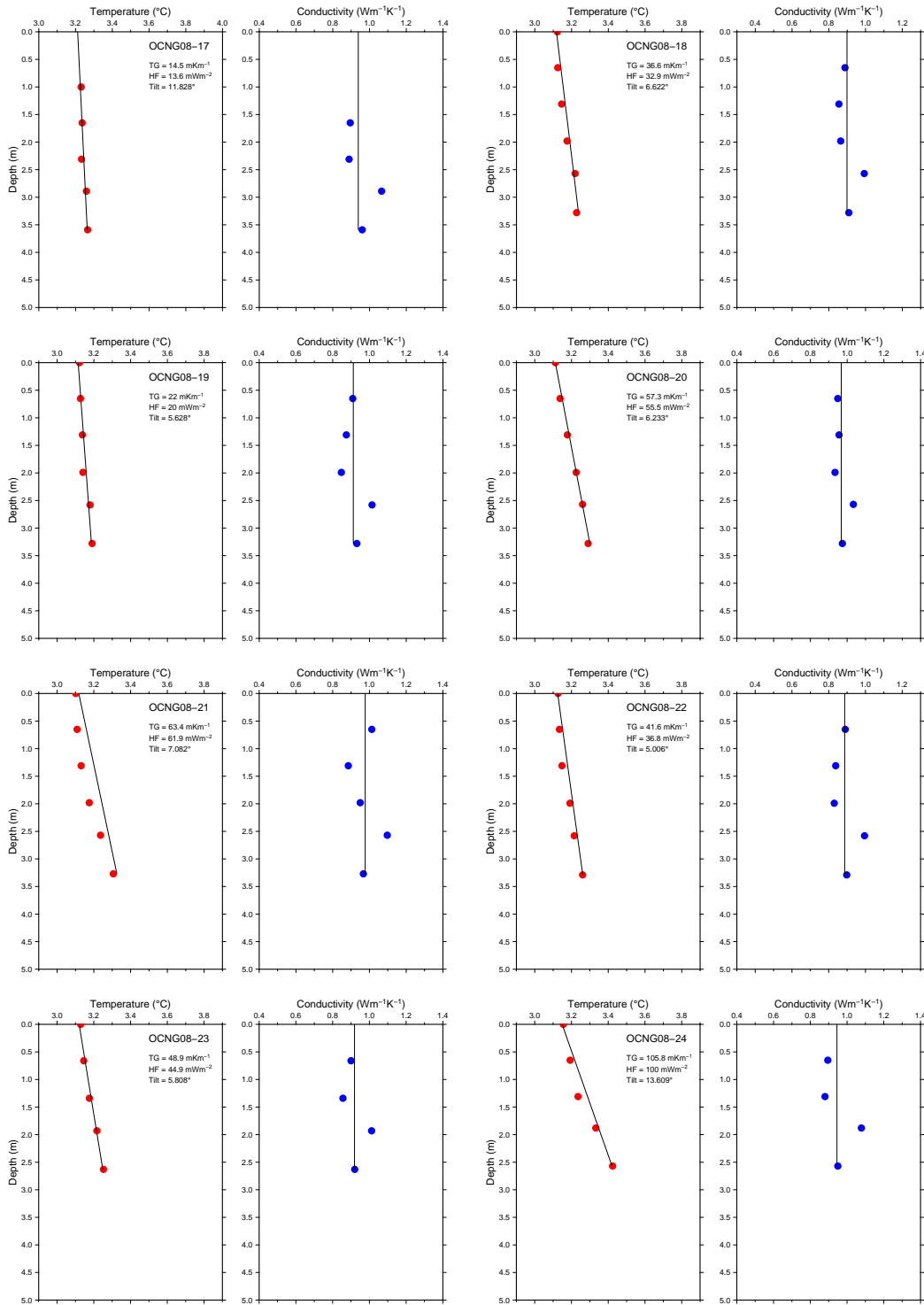


Figure 13q: Plot of OCEANOGRAPHY conductivity and temperature profiles

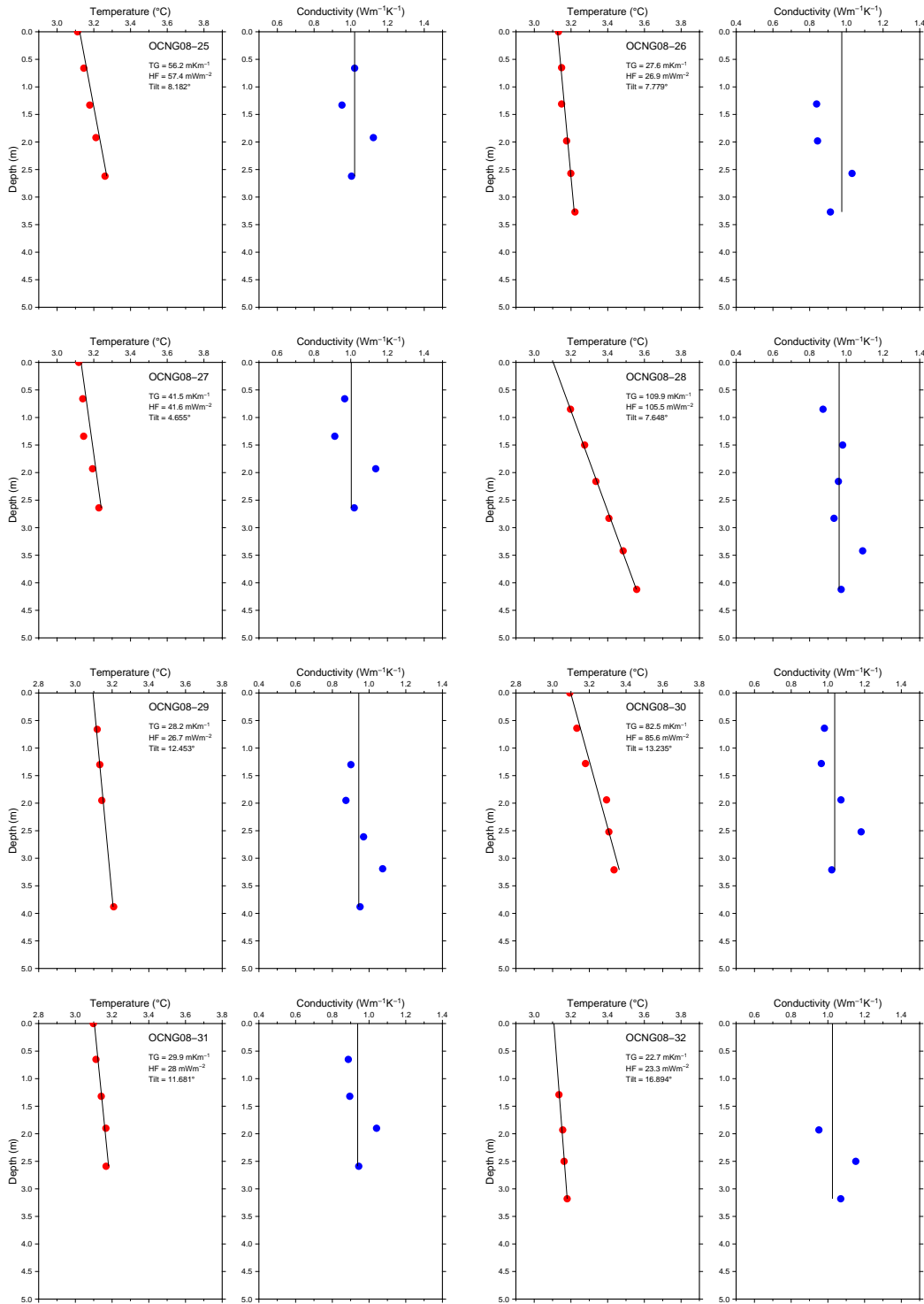


Figure 13r: Plot of OCEANOGRAPHY conductivity and temperature profiles

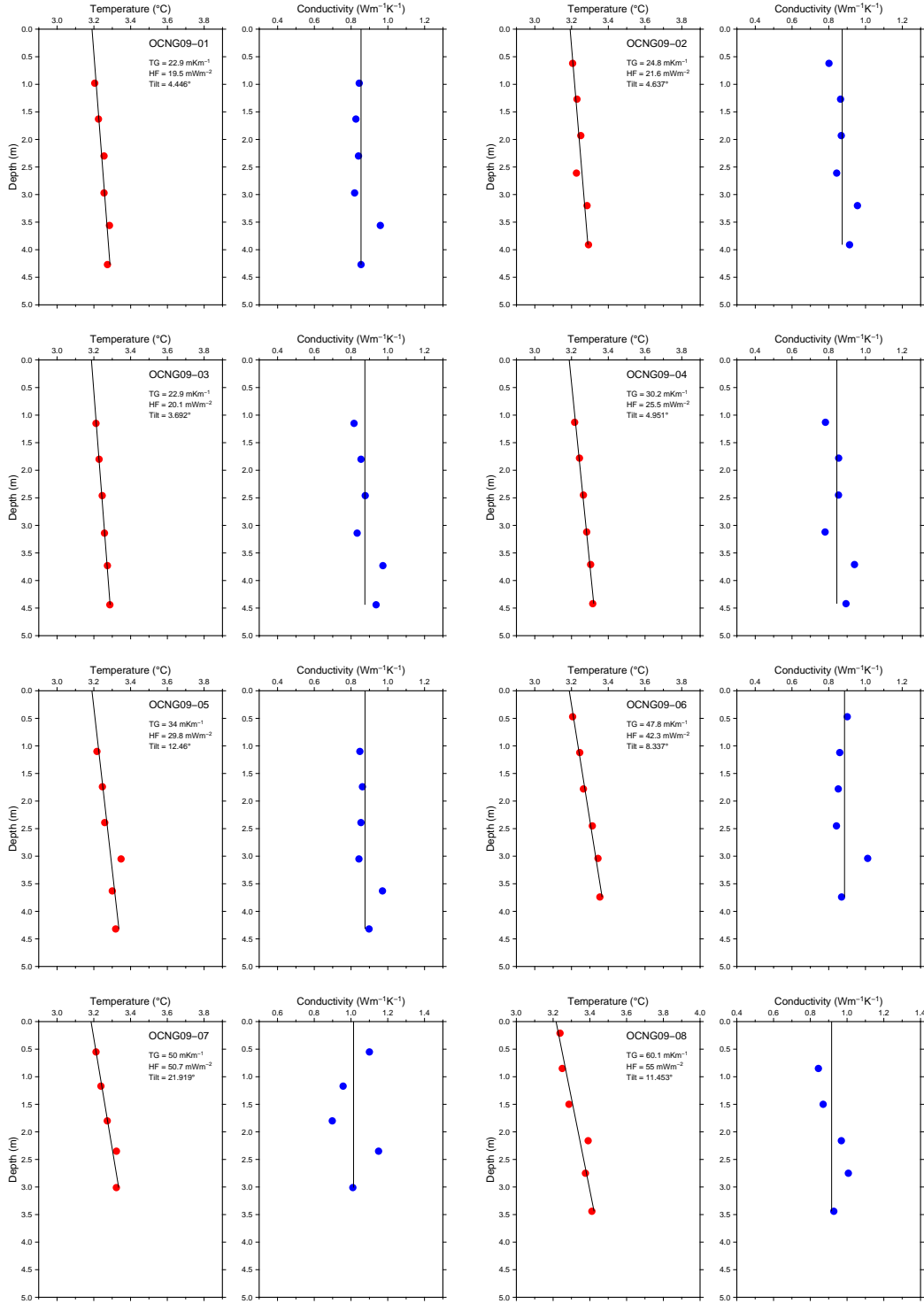


Figure 13s: Plot of OCEANOGRAFLU conductivity and temperature profiles

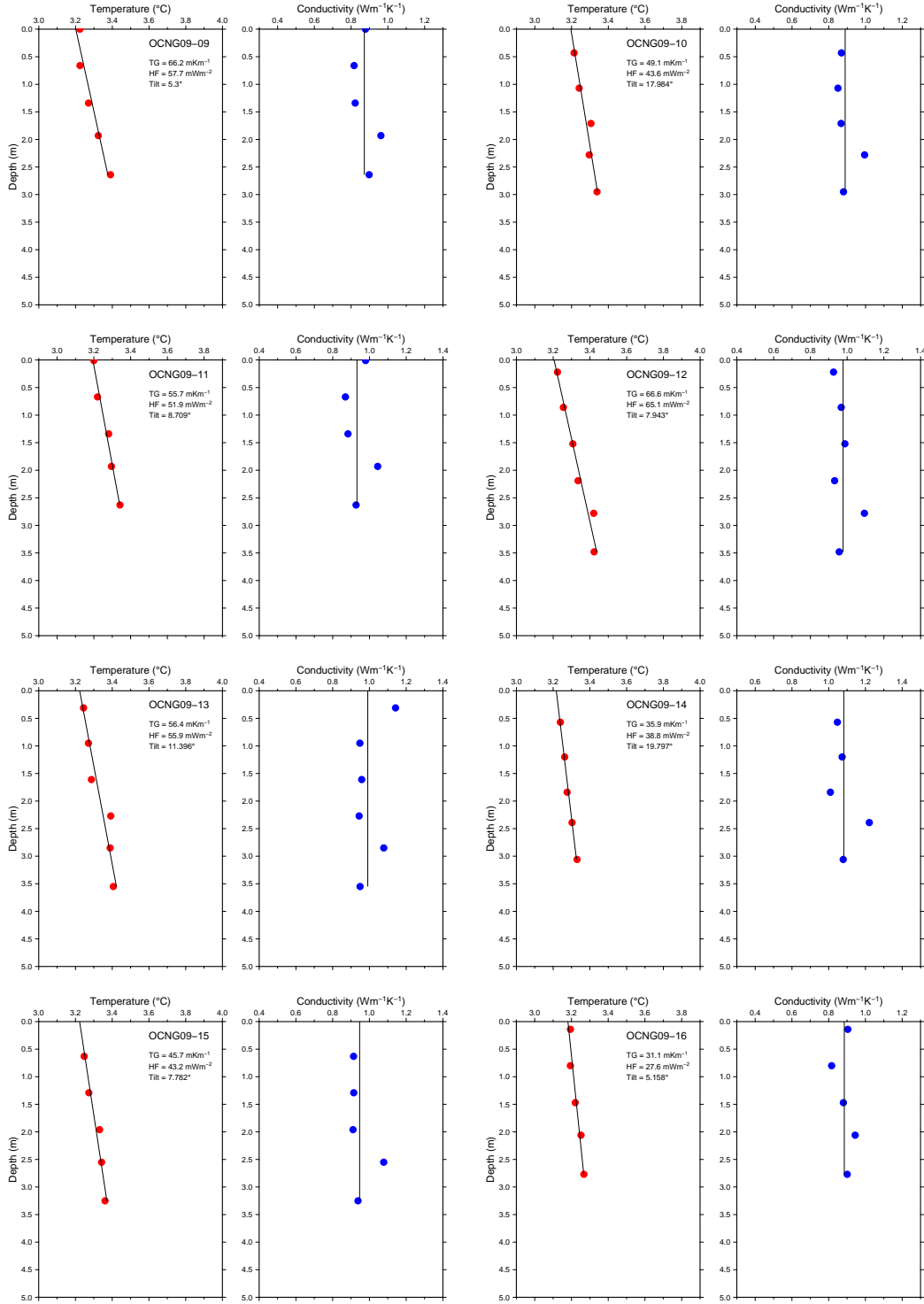


Figure 13t: Plot of OCEANOGRAPHY conductivity and temperature profiles

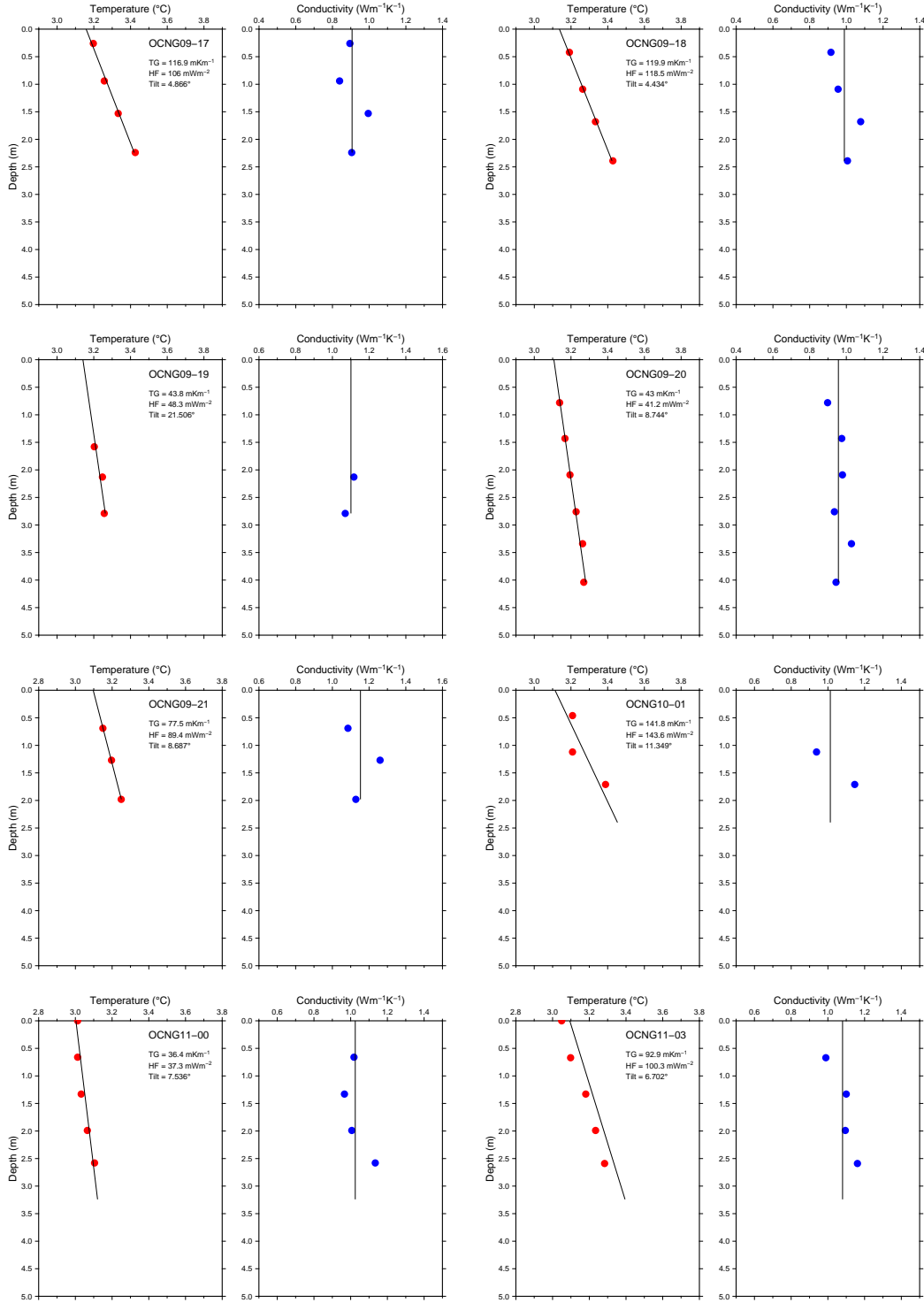


Figure 13u: Plot of OCEANOGRAPHY conductivity and temperature profiles

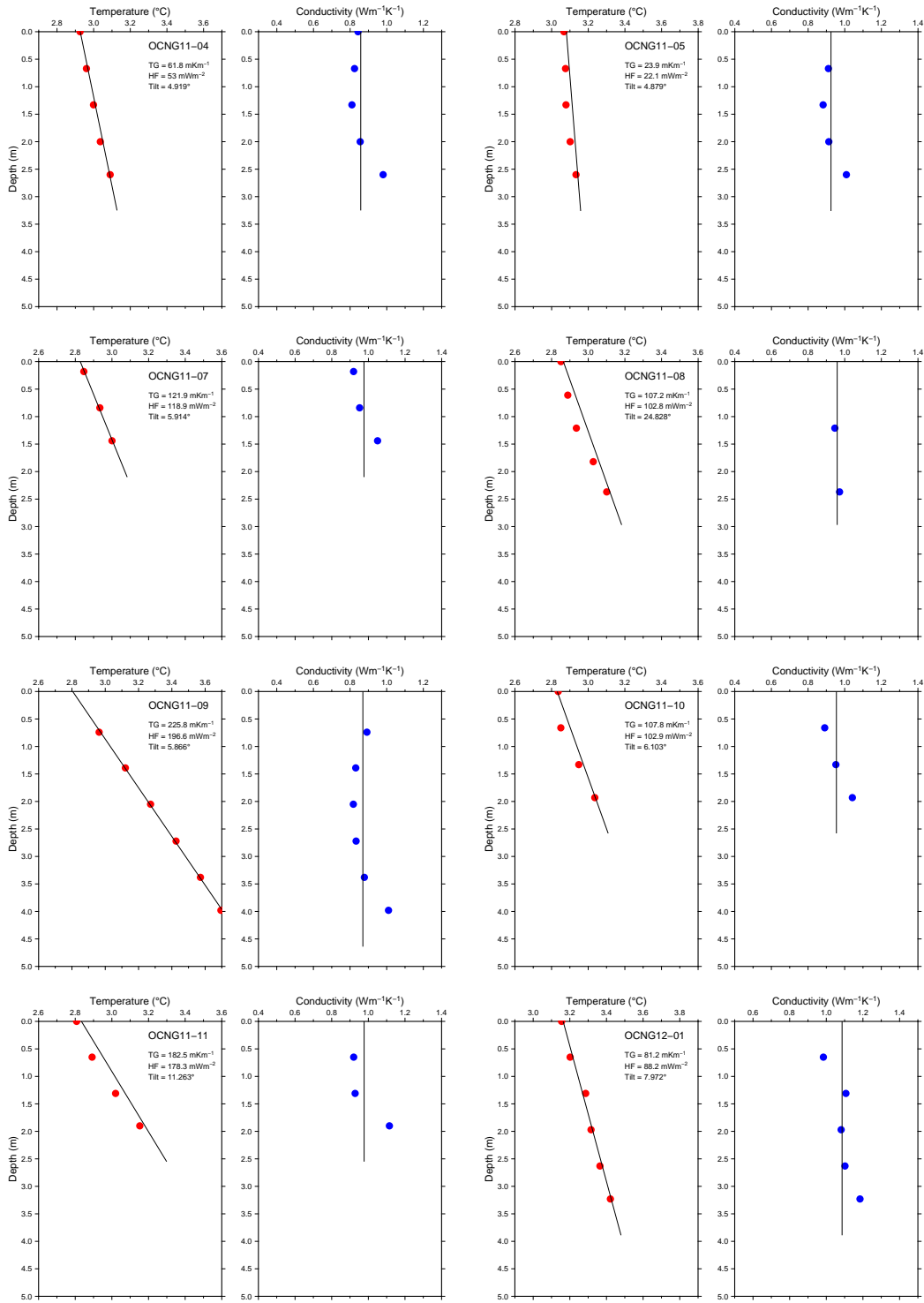


Figure 13v: Plot of OCEANOGRAPHY conductivity and temperature profiles

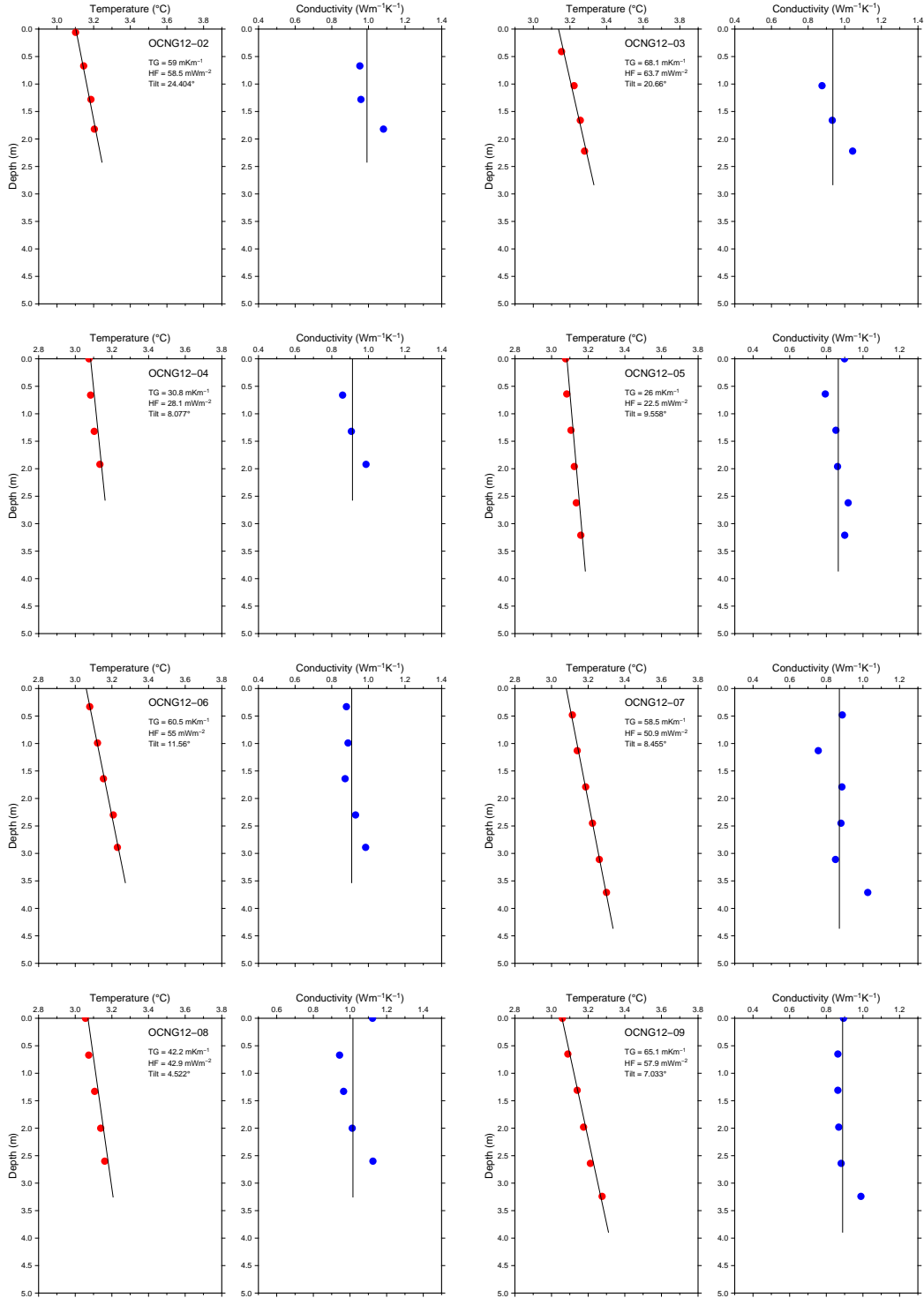


Figure 14: Plot of OCEANOGRAFLU conductivity and temperature profiles (coring)

Figure 14a: Plot of OCEANOGRAPHY conductivity and temperature profiles (coring)

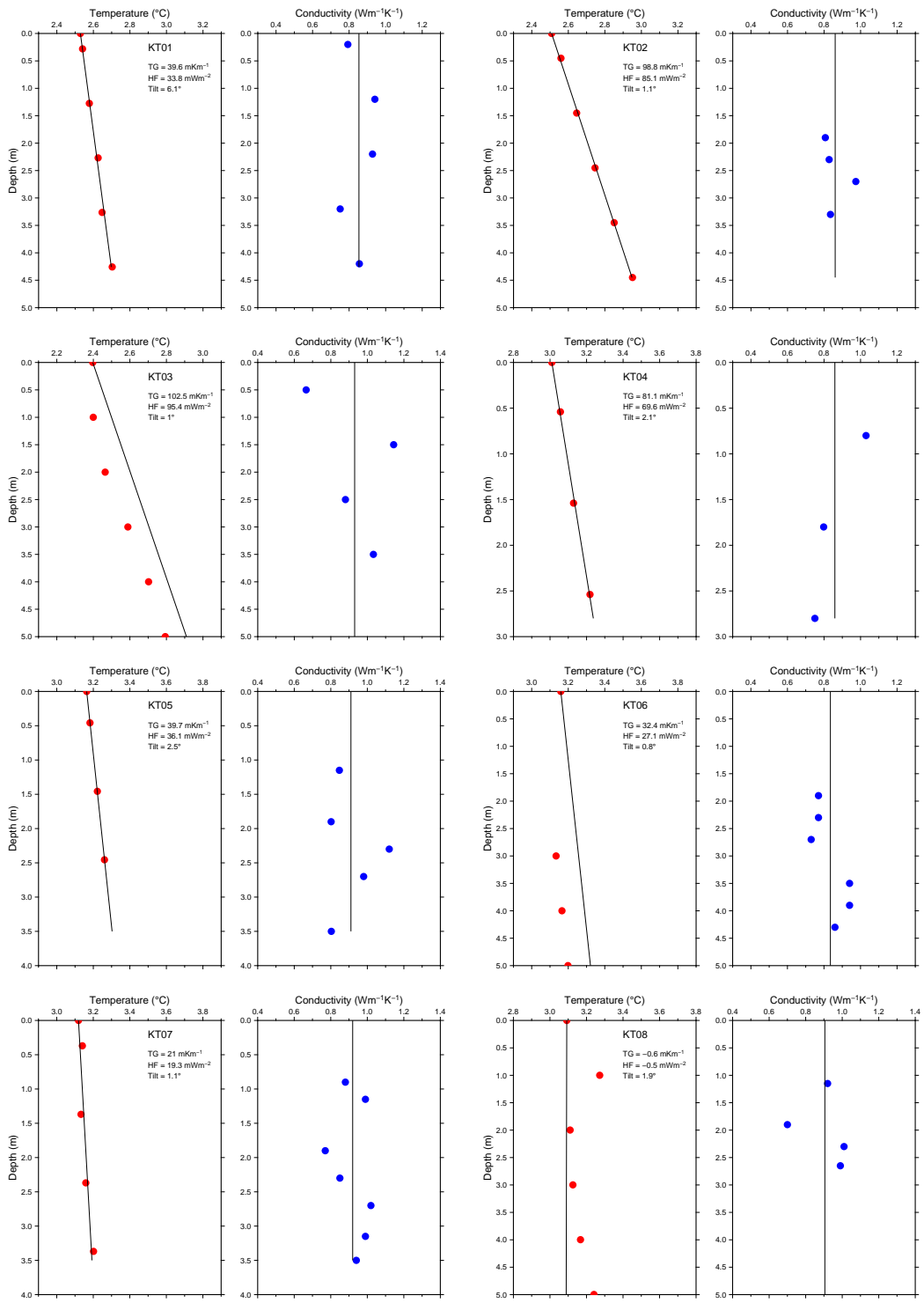


Figure 14b: Plot of OCEANOGRAPHY conductivity and temperature profiles (coring)

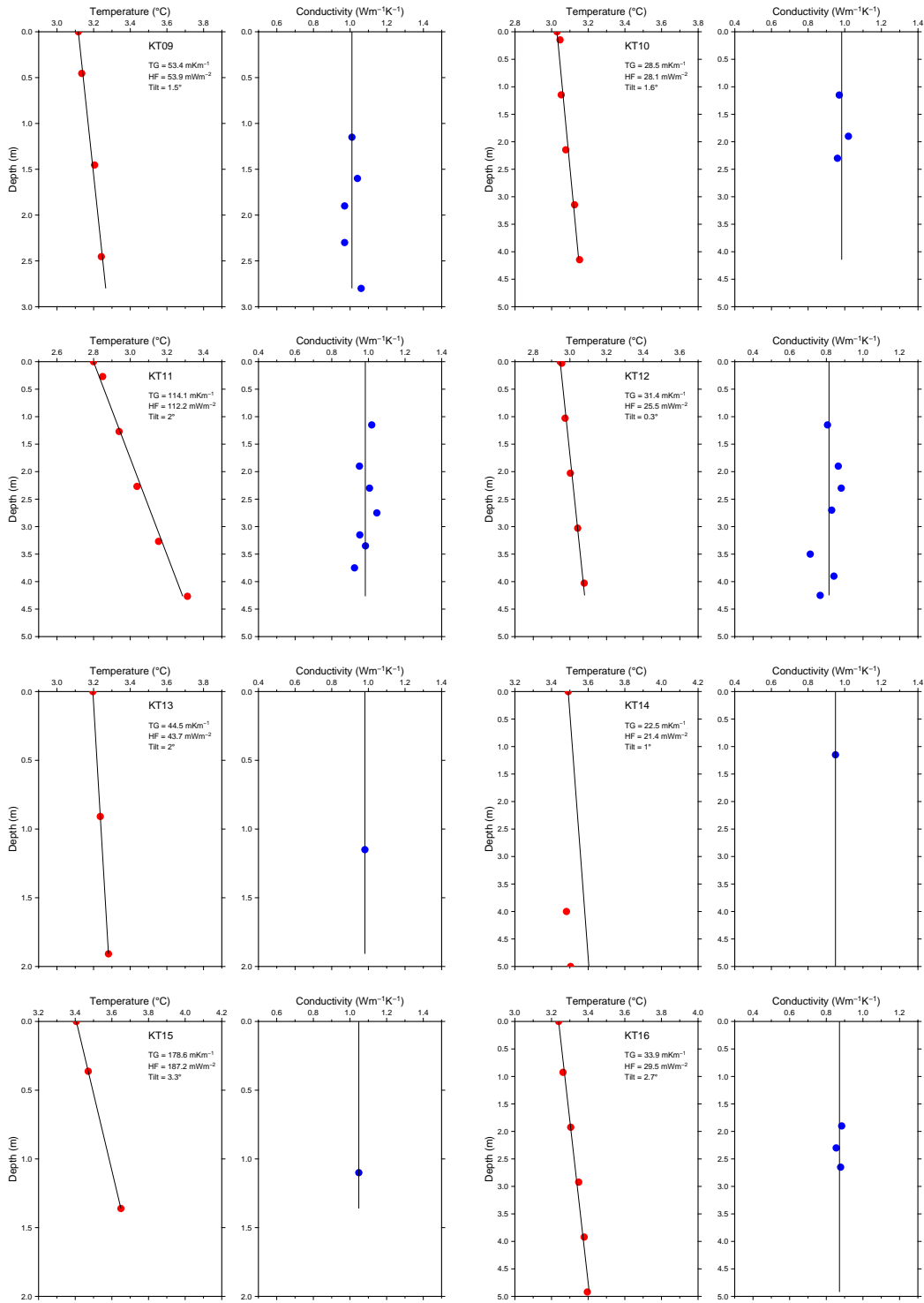


Figure 14c: Plot of OCEANOGRAPHY conductivity and temperature profiles (coring)

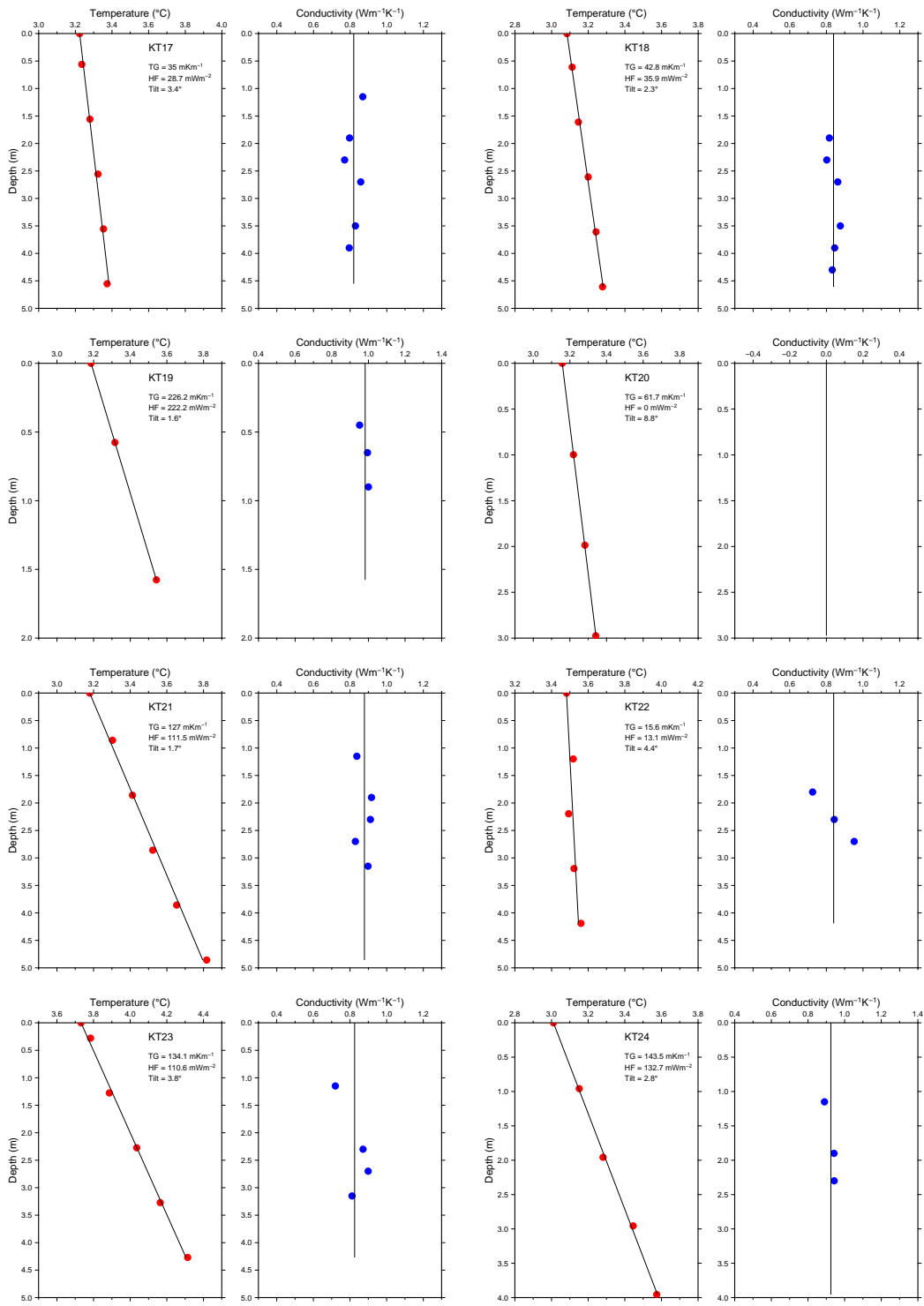
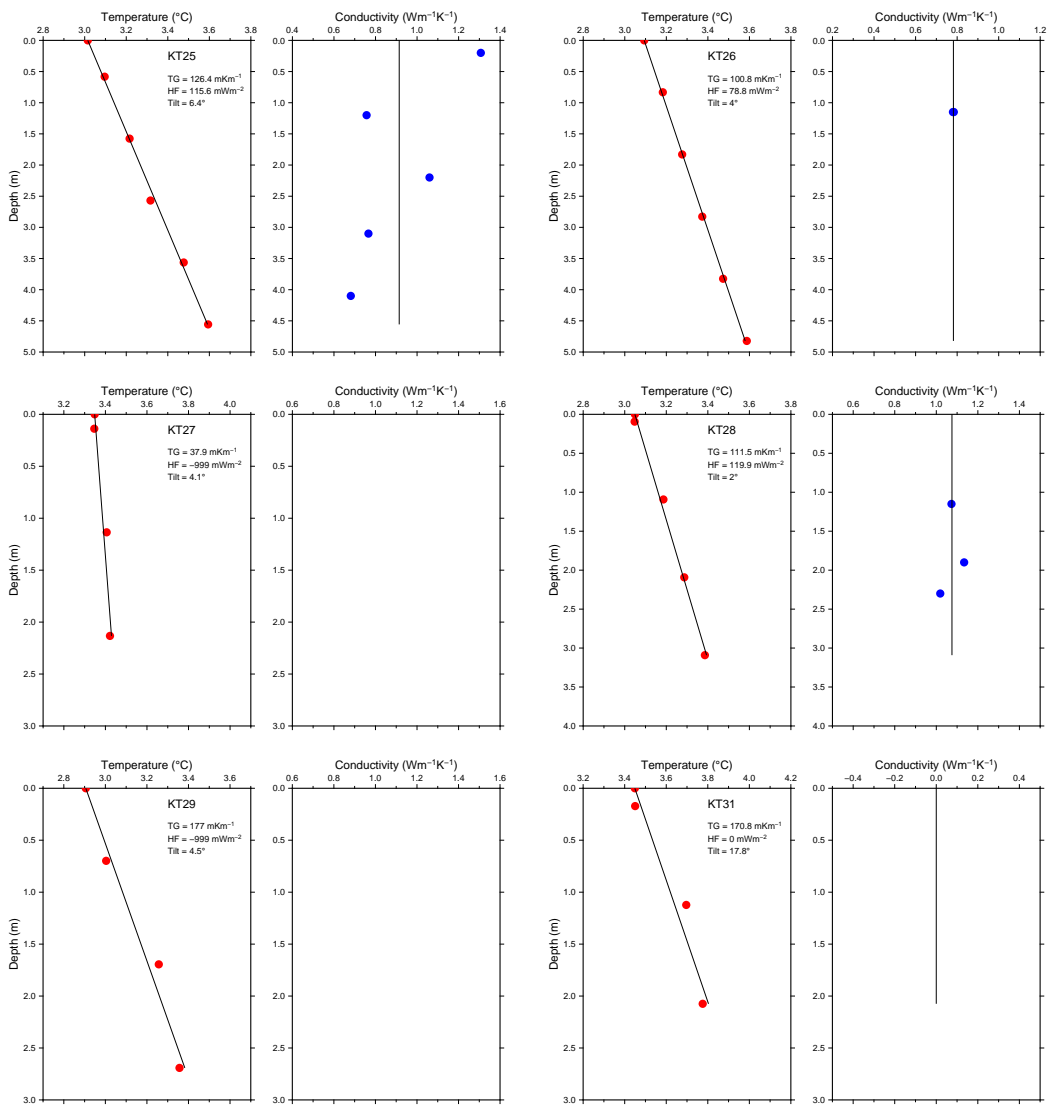


Figure 14d: Plot of OCEANOGRAPHY conductivity and temperature profiles (coring)



## Tables

Table 1: Table of sedimentation corrections assuming two different sediment velocities (1850 and 2050 m/s) and three models cor1 (Von Herzen et al., 1974), cor2 (Hutchison, 1985) and cor3 (Lucazeau and Le Douaran, 1985). All corrections are percentage of surface heat flow. ec and ed are respectively compacted and decomapacted thicknesses.

id	t(Ma)	ec(m)	ed(m)	cor1	cor2	cor3	ec(m)	ed(m)	cor1	cor2	cor3
OCNG1-1	6.8	239.1	262.6	3.5	3.9	3.9	264.5	293	3.8	4.2	4.2
OCNG1-2	7	230.4	252.2	3.3	3.7	3.7	255.2	281.8	3.6	4	4
OCNG1-3	7.1	329.5	373.2	4.6	5	5	364.9	418.2	5	5.4	5.4
OCNG1-4	7.2	344.7	392.4	4.7	5.1	5.1	381.3	439.3	5.2	5.5	5.5
KT1	8.1	277.8	309.2	3.7	4	4	307.5	345.8	4	4.4	4.4
OCNG2-1	8.1	277.8	309.2	3.7	4	4	307.5	345.8	4	4.4	4.4
OCNG2-2	8.1	371.5	426.7	4.8	5.1	5.1	411	478.1	5.3	5.6	5.6
OCNG2-3	8.2	322.1	363.9	4.2	4.5	4.5	356.7	407.7	4.6	4.9	4.9
OCNG2-4	8.3	466.8	552.4	5.9	6.1	6.1	516.6	620.5	6.4	6.6	6.6
OCNG2-5	8.3	409.6	476.2	5.2	5.5	5.5	454.1	535.3	5.7	6	5.9
OCNG2-6	8.4	394.3	456.1	5	5.3	5.3	436.6	512	5.5	5.8	5.7
OCNG2-7	8.5	411.1	478.2	5.2	5.4	5.4	455.1	536.6	5.7	5.9	5.9
OCNG2-8	8.6	289.5	323.5	3.7	4.1	4.1	320.8	362.4	4.1	4.4	4.4
OCNG2-9	8.7	425.9	497.7	5.3	5.5	5.5	471.5	558.8	5.8	6	6
OCNG2-10	8.8	170.1	182.1	2.2	2.5	2.5	188.6	203.3	2.4	2.8	2.8
KT2	8.8	367.8	421.9	4.6	4.9	4.9	188.6	203.3	2.4	2.8	2.8
OCNG2-11	8.9	585.1	716.7	6.9	7	7	406.9	472.7	5	5.3	5.3
OCNG2-12	9	329.7	373.4	4.1	4.4	4.4	647.8	807.4	7.5	7.6	7.5
OCNG2-13	9.2	170.1	182.1	2.2	2.5	2.5	364.9	418.2	4.4	4.8	4.7
OCNG3-1	9.4	265.2	293.9	3.3	3.6	3.6	294.2	329.3	3.6	3.9	3.9
OCNG3-2	9.5	209.7	227.8	2.6	2.9	2.9	232.7	254.9	2.9	3.2	3.2
OCNG3-3	9.6	193.4	208.9	2.4	2.7	2.7	214.2	233.1	2.6	3	3
OCNG3-4	10.1	375.2	431.4	4.4	4.7	4.6	415.1	483.5	4.8	5.1	5
OCNG3-5	10.3	536.2	647.8	6	6.1	6.1	593.5	728.7	6.5	6.6	6.6

---

... continuing next page...

... table 1 continuing...

id	t(Ma)	ec(m)	ed(m)	cor1	cor2	cor3	ec(m)	ed(m)	cor1	cor2	cor3
OCNG3-6	10.4	540.1	653.2	6	6.1	6.1	598.6	736.1	6.6	6.7	6.6
OCNG3-7	10.5	415	483.3	4.7	5	4.9	459.2	542.2	5.1	5.4	5.3
OCNG3-8	10.6	390.9	451.8	4.4	4.7	4.7	432.5	506.5	4.8	5.1	5.1
OCNG3-9	10.7	346.3	394.5	3.9	4.3	4.2	383.4	442	4.3	4.6	4.6
OCNG3-10	10.8	378.3	435.5	4.2	4.6	4.5	419.2	488.9	4.7	4.9	4.9
OCNG3-11	11	403	467.5	4.5	4.7	4.7	445.9	524.3	4.9	5.1	5.1
OCNG3-12	11.1	429.8	502.9	4.7	5	4.9	475.6	564.3	5.2	5.4	5.3
OCNG3-13	11.2	439.8	516.2	4.8	5	5	486.9	579.7	5.3	5.5	5.4
OCNG3-14	11.3	494	589.4	5.3	5.5	5.5	547.3	663.3	5.8	6	5.9
OCNG3-15	11.4	537	648.8	5.7	5.9	5.8	594.5	730.2	6.2	6.3	6.3
OCNG3-16	11.5	649.3	809.6	6.7	6.7	6.6	719.5	913.9	7.3	7.3	7.2
OCNG3-17	11.6	612.7	756.3	6.3	6.4	6.3	678.5	852.7	6.9	6.9	6.8
OCNG3-18	11.7	604.4	744.3	6.2	6.3	6.3	669.3	839	6.8	6.8	6.7
OCNG3-19	11.8	579	708	6	6.1	6	641.7	798.4	6.6	6.6	6.5
OCNG3-20	11.9	523.5	630	5.4	5.6	5.6	580.2	709.7	6	6.1	6
OCNG3-21	12	472.2	559.7	4.9	5.2	5.1	522.8	629	5.4	5.6	5.5
OCNG3-22	12.1	436.5	511.7	4.6	4.8	4.8	483.8	575.5	5	5.2	5.2
KT3	12.3	414.4	482.6	4.3	4.6	4.6	459.2	542.2	4.8	5	5
KT4	10	278.5	310	3.3	3.7	3.6	308.5	347	3.6	4	4
KT5	8.8	203.8	220.9	2.6	3	3	225.5	246.4	2.9	3.2	3.2
KT6	8.9	319.3	360.5	4	4.3	4.3	353.6	403.8	4.4	4.7	4.7
KT7	9.1	246.9	271.9	3.1	3.5	3.4	273.7	304.2	3.4	3.8	3.8
KT8	9.3	191.4	206.5	2.4	2.7	2.7	212.2	230.7	2.6	3	3
KT9	9.4	240.3	263.9	3	3.3	3.3	266.5	295.5	3.3	3.6	3.6
KT10	9.6	288.6	322.4	3.5	3.8	3.8	319.8	361.1	3.8	4.2	4.2

... continuing next page...

... table 1 continuing...

---

id	t(Ma)	ec(m)	ed(m)	cor1	cor2	cor3	ec(m)	ed(m)	cor1	cor2	cor3
OCNG4-7	9.7	160.9	171.6	2	2.3	2.3	178.4	191.5	2.2	2.5	2.5
OCNG4-8	9.9	153.6	163.5	1.9	2.1	2.2	170.1	182.2	2.1	2.4	2.4
OCNG4-9	10.1	149.6	158.9	1.8	2.1	2.1	166.1	177.5	2	2.3	2.3
OCNG4-10	10.8	143.3	151.8	1.7	1.9	1.9	158.9	169.4	1.9	2.1	2.1
OCNG4-11	10.9	230.4	252.2	2.6	3	3	255.2	281.8	2.9	3.2	3.2
OCNG4-12	11.1	168.1	179.8	1.9	2.2	2.2	186.6	200.9	2.1	2.4	2.4
OCNG4-12a	11.1	168.1	179.8	1.9	2.2	2.2	186.6	200.9	2.1	2.4	2.4
OCNG4-13	11.2	435	509.8	4.7	5	5	481.8	572.7	5.2	5.4	5.4
OCNG4-14	11.4	500.5	598.3	5.3	5.5	5.5	554.5	673.4	5.9	6	5.9
OCNG4-15	11.4	334.3	379.3	3.7	4	4	370	424.8	4	4.3	4.3
OCNG4-16	11.6	317.8	358.6	3.5	3.8	3.8	351.6	401.2	3.8	4.1	4.1
OCNG4-17	11.7	396.3	458.8	4.3	4.5	4.5	438.7	514.7	4.7	4.9	4.9
OCNG4-18	11.9	399.1	462.4	4.3	4.5	4.5	441.8	518.8	4.7	4.9	4.9
OCNG4-19	12	374.3	430.2	4	4.3	4.3	414.1	482.1	4.4	4.7	4.6
OCNG4-20	12.1	387.4	447.2	4.1	4.4	4.4	429.5	502.4	4.5	4.8	4.7
OCNG4-21	12.2	368.5	422.9	3.9	4.2	4.2	408	474	4.3	4.6	4.5
OCNG4-22	12.4	365	418.3	3.8	4.1	4.1	403.9	468.7	4.2	4.5	4.5
OCNG4-23	12.5	216	235.2	2.3	2.6	2.6	238.8	262.2	2.6	2.9	2.9
OCNG4-24	12.6	141.6	150	1.5	1.8	1.8	156.8	167.1	1.7	2	2
KT11	12.7	333.7	378.6	3.5	3.8	3.8	180.4	193.9	1.9	2.2	2.2
OCNG4-25	12.9	347.2	395.7	3.6	3.9	3.9	370	424.8	3.8	4.1	4.1
OCNG4-26	13	369.1	423.6	3.8	4.1	4	384.4	443.3	3.9	4.2	4.2
OCNG4-27	13.1	282.1	314.4	2.9	3.2	3.2	409	475.4	4.1	4.4	4.4
OCNG4-28	13.3	379.6	437.2	3.8	4.1	4.1	312.6	352.1	3.2	3.5	3.5
OCNG4-29	13.4	333.9	378.8	3.4	3.7	3.7	420.3	490.2	4.2	4.5	4.4

---

... continuing next page...

... table 1 continuing...

---

id	t(Ma)	ec(m)	ed(m)	cor1	cor2	cor3	ec(m)	ed(m)	cor1	cor2	cor3
OCNG4-30	13.5	162.7	173.7	1.7	2	2	370	424.8	3.7	4	4
KT12	9.5	298.4	334.5	3.6	4	4	330	373.9	4	4.3	4.3
OCNG5-1	9.6	367.4	421.4	4.4	4.7	4.7	406.9	472.7	4.8	5.1	5.1
OCNG5-2	9.7	484.6	576.6	5.6	5.8	5.8	537.1	649	6.2	6.3	6.3
OCNG5-3	9.9	440.4	516.9	5.1	5.4	5.3	487.9	581.1	5.6	5.8	5.8
OCNG5-4	10	451.3	531.5	5.2	5.4	5.4	500.2	597.9	5.7	5.9	5.8
OCNG5-5a	10.1	429.4	502.4	4.9	5.2	5.2	475.6	564.3	5.4	5.6	5.6
OCNG5-6	10.3	490.5	584.6	5.5	5.7	5.7	543.3	657.6	6	6.2	6.1
OCNG5-7	10.4	510.1	611.6	5.7	5.9	5.8	564.8	687.9	6.2	6.4	6.3
OCNG5-8	10.5	500.1	597.8	5.6	5.8	5.7	553.5	672	6.1	6.2	6.2
OCNG5-9	10.6	465	549.9	5.2	5.4	5.4	514.5	617.7	5.7	5.9	5.8
OCNG5-10	10.7	445	523.1	4.9	5.2	5.2	493	588.1	5.4	5.7	5.6
OCNG5-11	10.8	489.2	582.9	5.4	5.6	5.5	542.2	656.2	5.9	6.1	6
OCNG5-12	10.9	340.6	387.2	3.8	4.1	4.1	377.2	434	4.2	4.5	4.5
OCNG5-13	11	70.9	73	0.8	1	1	78.9	81.6	0.9	1.1	1.1
OCNG5-14	11.4	310.4	349.4	3.4	3.7	3.7	343.4	390.8	3.8	4.1	4.1
OCNG5-15	11.5	365.6	419.1	4	4.3	4.3	404.9	470	4.4	4.7	4.6
OCNG5-16	11.6	269.9	299.5	3	3.3	3.3	299.3	335.6	3.3	3.6	3.6
OCNG5-17	11.7	245.4	270.1	2.7	3	3	271.6	301.7	3	3.3	3.3
OCNG5-18	11.8	223.2	243.7	2.5	2.8	2.8	247	272	2.7	3	3
OCNG5-19	12	314.7	354.7	3.4	3.7	3.7	348.5	397.3	3.7	4	4
OCNG5-20	12.2	273.2	303.6	2.9	3.3	3.2	302.4	339.4	3.2	3.6	3.5
OCNG5-21	12.7	92.4	96	1	1.2	1.2	102.5	106.9	1.1	1.3	1.3
OCNG5-22	12.8	403	467.5	4.1	4.4	4.4	445.9	524.3	4.5	4.8	4.7
KT13	7.8	29.6	30	0.4	0.5	0.5	32.8	33.3	0.5	0.6	0.6

---

... continuing next page...

... table 1 continuing...

---

id	t(Ma)	ec(m)	ed(m)	cor1	cor2	cor3	ec(m)	ed(m)	cor1	cor2	cor3
OCNG6-3	9	333	377.6	4.1	4.5	4.5	369	423.5	4.5	4.9	4.8
OCNG6-4	9.3	320.2	361.6	3.9	4.3	4.2	354.6	405.1	4.3	4.6	4.6
OCNG6-5	9.5	342.6	389.8	4.1	4.5	4.4	379.3	436.7	4.5	4.8	4.8
OCNG6-6	9.5	469.8	556.4	5.5	5.8	5.7	520.7	626.2	6.1	6.2	6.2
OCNG6-7	9.6	83.3	86.2	1.1	1.2	1.2	92.3	95.8	1.2	1.4	1.4
OCNG6-8	9.9	435.2	510	5	5.3	5.3	481.8	572.7	5.5	5.8	5.7
OCNG6-9	10	508.7	609.5	5.8	6	5.9	563.8	686.4	6.3	6.5	6.4
OCNG6-10	10.1	478.3	568	5.4	5.7	5.6	529.9	639	6	6.1	6.1
OCNG6-11	10.2	511.8	613.9	5.8	5.9	5.9	566.8	690.8	6.3	6.4	6.4
OCNG6-12	10.2	425.2	496.7	4.9	5.1	5.1	470.5	557.4	5.3	5.6	5.5
OCNG6-13	10.1	309.7	348.5	3.6	4	4	343.4	390.8	4	4.3	4.3
OCNG6-14	10.2	178.3	191.5	2.1	2.5	2.4	197.8	214	2.4	2.7	2.7
KT14	13.3	162.7	173.7	1.7	2	2	180.4	193.9	1.9	2.2	2.2
KT15	12.9	165	176.3	1.8	2	2	182.4	196.2	1.9	2.2	2.2
OCNG7-1	13.1	386.4	445.9	3.9	4.2	4.2	428.5	501.1	4.3	4.6	4.5
OCNG7-2	13	255.8	282.5	2.7	3	3	282.9	315.4	2.9	3.3	3.2
OCNG7-3	12.9	319.7	360.9	3.3	3.6	3.6	353.6	403.8	3.7	4	3.9
OCNG7-4	12.7	380.2	437.9	3.9	4.2	4.2	421.3	491.6	4.3	4.6	4.6
OCNG7-5	12.5	170.6	182.6	1.9	2.1	2.1	188.6	203.3	2	2.3	2.3
OCNG8-32	12.3	255.4	282.1	2.8	3.1	3.1	92.3	95.8	1	1.2	1.2
OCNG8-31	12.2	248	273.2	2.7	3	3	204	221.1	2.2	2.5	2.5
OCNG8-30	12.1	68.2	70.2	0.8	0.9	0.9	419.2	488.9	4.4	4.7	4.6
OCNG8-29	11.9	144.3	153	1.6	1.9	1.9	447.9	527	4.7	5	4.9
OCNG8-28	11.8	191.9	207.2	2.1	2.4	2.4	114.8	120.3	1.3	1.5	1.5
OCNG8-27	11.1	125.2	131.8	1.5	1.7	1.7	307.5	345.8	3.4	3.8	3.8

---

... continuing next page...

... table 1 continuing...

---

id	t(Ma)	ec(m)	ed(m)	cor1	cor2	cor3	ec(m)	ed(m)	cor1	cor2	cor3
OCNG8-26	10.9	205.7	223.2	2.4	2.7	2.7	505.3	604.9	5.5	5.7	5.7
OCNG8-25	10.8	183.7	197.7	2.1	2.4	2.4	556.6	676.3	6	6.2	6.1
OCNG8-24	10.7	165.8	177.2	1.9	2.2	2.2	271.6	301.7	3.1	3.5	3.4
OCNG8-23	10.5	165.8	177.2	2	2.3	2.3	384.4	443.3	4.4	4.7	4.6
KT18	10.5	252.4	278.4	2.9	3.3	3.3	428.5	501.1	4.8	5.1	5.1
OCNG8-22	10.4	280.1	312.1	3.3	3.6	3.6	423.3	494.3	4.8	5.1	5
OCNG8-21	10.2	192.7	208	2.3	2.6	2.6	671.4	842	7.3	7.3	7.2
OCNG8-20	10.1	249.1	274.4	3	3.3	3.3	635.5	789.4	7	7	7
OCNG8-19	10	254.5	281	3	3.4	3.4	473.5	561.5	5.4	5.7	5.6
OCNG8-18	9.8	300.1	336.6	3.6	3.9	3.9	288	321.7	3.4	3.8	3.8
OCNG8-17	9.6	323.6	365.9	3.9	4.2	4.2	194.8	210.4	2.4	2.7	2.7
OCNG8-16	9.5	242.3	266.3	3	3.3	3.3	157.9	168.2	2	2.3	2.3
OCNG8-15	9.4	142.6	151.1	1.8	2.1	2.1	268.5	297.9	3.3	3.6	3.6
OCNG8-14	9.2	175.9	188.8	2.2	2.5	2.5	358.8	410.3	4.4	4.7	4.7
OCNG8-13	9.1	260.3	287.9	3.3	3.6	3.6	332.1	376.5	4.1	4.4	4.4
OCNG8-12	9	427.5	499.8	5.2	5.5	5.4	281.9	314.2	3.5	3.9	3.9
OCNG8-11	8.6	573.3	700	6.9	7	7	275.7	306.7	3.5	3.9	3.9
OCNG8-10	8	606.1	746.8	7.5	7.6	7.5	213.2	231.9	2.9	3.2	3.2
OCNG8-9	7.9	382.2	440.5	5	5.3	5.3	310.6	349.6	4.1	4.5	4.5
OCNG8-8	7.8	346.7	395	4.6	5	4.9	279.8	311.7	3.8	4.1	4.1
KT19	7.6	245.5	270.2	3.4	3.7	3.7	105.6	110.3	1.5	1.7	1.8
OCNG8-7	7.4	502.1	600.5	6.6	6.8	6.8	183.5	197.4	2.6	2.9	2.9
OCNG8-7a	7.4	455.8	537.6	6.1	6.3	6.3	183.5	197.4	2.6	2.9	2.9
OCNG8-6	7.3	277.6	309	3.9	4.2	4.2	204	221.1	2.9	3.3	3.3
OCNG8-5	6.7	103.6	108.1	1.6	1.8	1.8	227.6	248.8	3.3	3.7	3.7

---

... continuing next page...

... table 1 continuing...

---

id	t(Ma)	ec(m)	ed(m)	cor1	cor2	cor3	ec(m)	ed(m)	cor1	cor2	cor3
OCNG8-4	6.1	404.4	469.3	6	6.3	6.3	138.4	146.4	2.2	2.5	2.5
OCNG8-3	6.1	378.9	436.2	5.6	6	6	212.2	230.7	3.3	3.7	3.7
OCNG8-2	5.9	184.5	198.6	2.9	3.3	3.3	159.9	170.5	2.5	2.9	2.9
OCNG8-1	5.8	83.1	86	1.3	1.6	1.6	75.8	78.3	1.2	1.5	1.5
KT17	6.4	386.7	446.3	5.6	5.9	5.9	274.7	305.4	4.1	4.5	4.5
KT16	7	95	98.8	1.4	1.6	1.7	282.9	315.4	4	4.4	4.4
OCNG9-1	5.8	152.9	162.6	2.4	2.8	2.8	169.1	181	2.7	3.1	3.1
OCNG9-2a	5.9	347.4	395.9	5.3	5.6	5.7	384.4	443.3	5.8	6.1	6.1
OCNG9-3	6	377.3	434.2	5.6	6	6	418.2	487.5	6.2	6.5	6.5
OCNG9-4	6.1	407.8	473.8	6	6.3	6.3	452	532.5	6.6	6.9	6.9
OCNG9-5	6.2	400.8	464.7	5.9	6.2	6.2	443.8	521.5	6.4	6.7	6.7
OCNG9-6	6.3	413.4	481.2	6	6.3	6.3	458.2	540.8	6.6	6.9	6.8
OCNG9-7	6.6	211.1	229.5	3.1	3.5	3.5	233.7	256.1	3.4	3.8	3.8
OCNG9-8	6.7	181	194.6	2.7	3	3.1	200.9	217.6	3	3.3	3.3
OCNG9-9	7.4	68.9	70.9	1	1.2	1.2	75.8	78.3	1.1	1.3	1.3
OCNG9-10	7.5	89.1	92.5	1.3	1.5	1.5	98.4	102.5	1.4	1.6	1.7
OCNG9-11	7.6	64	65.8	0.9	1.1	1.1	70.7	72.8	1	1.2	1.2
OCNG9-12	7.7	134.2	141.7	1.9	2.2	2.2	148.6	157.8	2.1	2.4	2.4
OCNG9-13	7.8	63.5	65.2	0.9	1.1	1.1	70.7	72.8	1	1.2	1.2
OCNG9-14	7.9	320.1	361.5	4.2	4.6	4.6	354.6	405.1	4.7	5	5
OCNG9-15	8	312.3	351.7	4.1	4.5	4.5	345.4	393.4	4.5	4.9	4.9
OCNG9-16	8.9	257.9	285.1	3.3	3.6	3.6	286	319.2	3.6	3.9	3.9
OCNG9-17	8.9	487.3	580.2	5.9	6.1	6.1	540.2	653.3	6.5	6.6	6.6
OCNG9-18	9	443.4	521	5.4	5.6	5.6	491	585.3	5.9	6.1	6.1
OCNG9-19	9.3	228.1	249.5	2.8	3.2	3.2	253.2	279.4	3.1	3.5	3.5

---

... continuing next page...

... table 1 continuing...

---

id	t(Ma)	ec(m)	ed(m)	cor1	cor2	cor3	ec(m)	ed(m)	cor1	cor2	cor3
OCNG9-20	9.4	457.2	539.5	5.4	5.7	5.6	506.4	606.4	5.9	6.1	6.1
OCNG9-21	9.5	86	89.1	1.1	1.3	1.3	95.3	99.1	1.2	1.4	1.4
KT20	10.6	143.3	151.8	1.7	2	2	158.9	169.4	1.9	2.2	2.2
KT21	8.7	187	201.4	2.4	2.8	2.8	207.1	224.7	2.7	3	3
KT22	7.6	328.4	371.8	4.4	4.8	4.8	363.9	416.9	4.9	5.2	5.2
KT23	6.4	96.3	100.2	1.5	1.7	1.8	106.6	111.4	1.6	1.9	1.9
OCNG10-1	7.8	175.5	188.2	2.4	2.8	2.8	194.8	210.4	2.7	3	3
KT24	7.8	175.5	188.2	2.4	2.8	2.8	194.8	210.4	2.7	3	3
KT25	7.9	177.5	190.6	2.4	2.8	2.8	196.8	212.8	2.7	3	3
OCNG11-3	8.1	132.8	140.2	1.8	2.1	2.1	147.6	156.7	2	2.3	2.3
OCNG11-4	8.8	493.6	588.8	6	6.2	6.2	546.3	661.9	6.6	6.7	6.6
OCNG11-5	9.3	294	329.1	3.6	4	4	326	368.8	4	4.3	4.3
OCNG11-6a	9.4	316	356.3	3.8	4.2	4.2	349.5	398.6	4.2	4.5	4.5
OCNG11-7	10.1	163.9	175.1	2	2.3	2.3	181.4	195.1	2.2	2.5	2.5
OCNG11-9	10.6	360.2	412.2	4.1	4.4	4.4	398.7	462	4.5	4.8	4.8
OCNG11-10a	10.7	195	210.7	2.3	2.6	2.6	216.3	235.5	2.5	2.8	2.8
OCNG11-11	10.8	101	105.3	1.2	1.4	1.4	111.7	117	1.3	1.5	1.5
OCNG12-1	8.8	140.6	148.8	1.8	2.1	2.1	155.8	165.9	2	2.3	2.3
OCNG12-2	8.9	335	380.2	4.2	4.5	4.5	371	426.1	4.6	4.9	4.9
OCNG12-3	9	219.7	239.6	2.8	3.1	3.1	242.9	267.1	3.1	3.4	3.4
OCNG12-4	9.2	405.6	470.9	4.9	5.2	5.2	449	528.4	5.4	5.6	5.6
OCNG12-5	9.4	591.4	725.7	6.8	6.9	6.8	655	817.9	7.5	7.5	7.4
OCNG12-6	9.5	496.7	593.1	5.8	6	6	550.4	667.7	6.4	6.5	6.4
OCNG12-7	9.5	328.6	372.1	4	4.3	4.3	363.9	416.9	4.4	4.7	4.7
OCNG12-8	9.6	160.5	171.2	2	2.3	2.3	177.3	190.4	2.2	2.5	2.5

---

... continuing next page...

... table 1 continuing...

---

id	t(Ma)	ec(m)	ed(m)	cor1	cor2	cor3	ec(m)	ed(m)	cor1	cor2	cor3
OCNG12-9	9.7	455.4	537.1	5.3	5.6	5.5	504.3	603.5	5.8	6	6
OCNG12-10	9.8	344.5	392.1	4.1	4.4	4.4	381.3	439.3	4.5	4.8	4.8
OCNG12-11	10.3	151.2	160.8	1.8	2.1	2.1	167.1	178.7	2	2.3	2.3
KT26	10.7	832.4	1087.4	8.6	8.4	8.2	921.5	1229.1	9.4	9	8.8
KT27	10.6	110.6	115.7	1.3	1.5	1.6	133.3	140.7	1.6	1.8	1.8
KT28	10.9	236	258.8	2.7	3	3	123	129.3	1.4	1.7	1.7
KT29	10.9	162.7	173.7	1.9	2.2	2.2	261.4	289.2	3	3.3	3.3

---

Table 2: Table of heat flow measurements. First column is the site name (OCNG\*-\* for POGO measurements and KT\* for Kullenberg cores equipped with thermistors). Second and third columns are longitude and latitude (decimal degrees). z is bathymetry from echosounding (meters). Tw is sea-bottom temperature (in °C). tilt is the angle of the instrument in the sediment (°). nT is the number of available thermistors (maximum 7). G is the uncorrected temperature gradient ( $\text{mKm}^{-1}$ ). nλ is the number of thermal conductivity measurements. λ is the thermal conductivity ( $\text{Wm}^{-1}\text{K}^{-1}$ ). UHF is the uncorrected heat flow ( $\text{mWm}^{-2}$ ). UHF is the heat flow corrected for topographic, refraction and sedimentation effects ( $\text{mWm}^{-2}$ ). σHF is the standard error on corrected heat flow values ( $\text{mWm}^{-2}$ ).

---

Site	long	lat	z	Tw	tilt	nT	G	nλ	λ	UHF	CTHF	σHF
profile 23W												
OCNG1-1	-37.0717	35.3807	3321	2.67	0.9	6	35.1	6	0.88	31.0	37.6	4.5
OCNG1-2	-37.0889	35.3829	3330	2.66	13.8	6	27.7	6	0.90	24.8	23.2	6.5
OCNG1-3	-37.1057	35.3870	3355	2.62	4.2	6	28.7	0	0.90	25.8	26.6	7.8
OCNG1-4	-37.1227	35.3897	3350	2.64	4.6	6	34.0	0	0.90	30.6	39.8	8.2

---

... continuing next page...

... table 2 continuing...

Site	long	lat	z	Tw	tilt	nT	G	nλ	λ	UHF	CTHF	$\sigma_{HF}$
KT1	-37.2625	35.4159	3430	2.53	6.1	5	39.7	1	0.87	34.6	35.7	2.3
OCNG2-1	-37.2621	35.4158	3429	2.53	0.0	5	41.0	4	0.90	36.9	38.1	9.0
OCNG2-2	-37.2707	35.4252	3469	2.53	15.4	6	34.5	0	0.90	31.1	35.8	8.5
OCNG2-3	-37.2809	35.4193	3466	2.51	9.2	6	35.5	0	0.90	32.0	28.3	8.7
OCNG2-4	-37.2909	35.4207	3473	2.51	1.0	6	38.0	3	0.87	33.2	41.1	6.6
OCNG2-5	-37.3015	35.4234	3475	2.52	3.4	5	50.7	4	0.93	46.9	52.2	6.4
OCNG2-6	-37.3147	35.4265	3491	2.52	9.1	5	41.1	4	0.90	36.9	39.1	7.0
OCNG2-7	-37.3298	35.4283	3503	2.53	9.5	5	33.5	2	0.89	29.9	33.1	12.3
OCNG2-8	-37.3421	35.4308	3504	2.55	18.0	5	39.0	4	1.12	43.6	38.5	7.6
OCNG2-9	-37.3537	35.4336	3504	2.55	21.3	5	47.4	3	1.16	54.9	65.2	13.0
OCNG2-10	-37.3755	35.4374	3473	2.59	58.1	3	84.7	0	0.90	76.2	63.7	20.8
KT2	-37.3758	35.4371	3469	2.51	1.1	5	99.0	4	0.86	85.2	73.0	7.9
OCNG2-11	-37.3902	35.4403	3482	2.54	63.8	4	68.6	2	0.86	58.9	65.9	27.8
OCNG2-12	-37.4039	35.4428	3469	2.54	8.9	6	36.4	0	0.90	32.8	46.7	9.7
OCNG2-13	-37.4378	35.4488	3468	2.53	11.6	5	67.5	0	0.90	60.8	60.0	14.7
OCNG3-1	-37.4710	35.4551	3471	2.52	3.6	6	54.8	6	0.92	50.6	50.9	2.3
OCNG3-2	-37.4923	35.4590	3463	2.52	5.7	6	64.3	7	0.87	56.1	58.0	3.2
OCNG3-3	-37.5011	35.4611	3464	2.53	4.3	6	48.2	6	0.91	44.0	45.1	4.3
OCNG3-4	-37.5811	35.4757	3576	2.49	5.1	6	50.6	6	0.87	44.0	46.5	3.3
OCNG3-5	-37.6013	35.4797	3577	2.50	13.4	6	149.8	6	0.86	128.1	143.7	13.1
OCNG3-6	-37.6231	35.4833	3580	2.51	35.5	4	153.5	2	1.00	154.0	170.4	10.8
OCNG3-7	-37.6395	35.4866	3576	2.50	18.4	6	158.2	5	1.01	159.3	165.4	22.6
OCNG3-8	-37.6556	35.4897	3577	2.48	5.3	6	137.9	6	0.91	125.2	132.5	7.9
OCNG3-9	-37.6718	35.4930	3618	2.49	4.1	6	133.6	6	0.92	122.5	127.2	5.5
OCNG3-10	-37.6880	35.4952	3645	2.44	3.0	6	133.9	6	0.96	128.3	141.0	6.2

... continuing next page...

... table 2 continuing...

---

Site	long	lat	z	Tw	tilt	nT	G	nλ	λ	UHF	CTHF	$\sigma_{HF}$
OCNG3-11	-37.7040	35.4988	3658	2.42	1.5	6	134.4	5	0.95	127.8	134.6	9.5
OCNG3-12	-37.7201	35.5016	3663	2.42	1.6	6	133.7	6	0.89	119.1	121.9	10.2
OCNG3-13	-37.7361	35.5044	3657	2.42	2.9	6	147.4	6	0.88	130.2	135.5	7.4
OCNG3-14	-37.7521	35.5078	3659	2.41	4.9	6	152.8	6	0.94	143.5	151.2	7.3
OCNG3-15	-37.7686	35.5107	3664	2.43	4.3	6	145.4	6	0.91	131.6	139.3	6.7
OCNG3-16	-37.7846	35.5136	3674	2.42	3.5	6	153.3	6	0.79	121.7	134.9	7.1
OCNG3-17	-37.8014	35.5170	3693	2.42	6.4	6	150.8	6	0.79	119.6	130.7	5.0
OCNG3-18	-37.8170	35.5202	3692	2.44	3.7	6	127.0	6	0.89	112.4	123.9	8.0
OCNG3-19	-37.8335	35.5228	3691	2.44	4.1	6	127.0	6	0.80	101.9	108.1	6.5
OCNG3-20	-37.8498	35.5262	3730	2.44	2.0	5	116.7	6	0.99	114.9	123.0	7.5
OCNG3-21	-37.8658	35.5291	3737	2.42	6.7	4	106.8	2	0.98	104.2	102.0	7.8
OCNG3-22	-37.8820	35.5323	3715	2.44	3.7	5	116.7	5	0.95	111.0	113.1	6.3
KT3	-37.9108	35.5372	3753	2.40	1.0	4	112.7	1	0.90	101.9	102.2	4.8
profile 25W												
KT4	-37.6837	35.3416	2859	3.01	2.2	3	81.0	3	0.86	69.6	86.9	13.0
profile 27W												
KT5	-37.3608	35.1271	2726	3.16	2.6	5	23.4	6	0.91	21.3	34.5	7.1
KT6	-37.3783	35.1301	2769	3.15	0.9	4	13.5	6	0.84	11.3	20.0	5.1
KT7	-37.3952	35.1338	2786	3.12	1.2	4	24.1	7	0.92	22.2	35.4	9.0
KT8	-37.4320	35.1402	2766	3.09	1.9	5	44.0	4	0.91	39.8	43.7	7.9
KT9	-37.4458	35.1436	2757	3.11	1.4	4	48.2	5	1.01	48.7	71.0	6.2

---

... continuing next page...

... table 2 continuing...

Site	long	lat	z	Tw	tilt	nT	G	nλ	λ	UHF	CTHF	$\sigma_{HF}$
KT10	-37.4675	35.1475	2886	3.03	1.6	5	28.6	3	0.98	28.0	33.8	4.1
OCNG4-7	-37.4853	35.1505	2926	3.03	5.8	5	46.2	6	0.95	44.0	34.4	3.1
OCNG4-8	-37.5119	35.1555	2937	3.02	1.7	5	53.6	5	0.93	49.8	50.9	5.7
OCNG4-9	-37.5281	35.1586	2951	3.01	4.8	4	76.1	4	0.93	70.8	65.8	6.4
OCNG4-10	-37.6202	35.1762	2774	3.10	6.0	5	53.7	5	1.09	58.5	68.3	12.4
OCNG4-11	-37.6334	35.1783	2830	3.05	3.0	5	46.8	5	1.09	50.8	62.2	7.5
OCNG4-12	-37.6641	35.1848	3010	2.92	21.2	5	51.5	0	0.91	46.6	43.0	9.3
OCNG4-12a	-37.6641	35.1848	3010	2.92	3.1	5	49.8	5	0.91	45.1	41.5	5.7
OCNG4-13	-37.6793	35.1869	3023	2.94	5.9	5	24.9	5	0.91	22.7	29.3	5.1
OCNG4-14	-37.6959	35.1902	3034	2.95	3.6	5	11.4	5	0.92	10.5	18.6	9.9
OCNG4-15	-37.7127	35.1939	3037	2.98	6.5	5	16.7	5	0.87	14.5	12.8	9.9
OCNG4-16	-37.7296	35.1963	3038	2.99	7.4	5	33.9	5	0.90	30.6	29.8	14.3
OCNG4-17	-37.7461	35.1995	3067	2.96	5.3	5	35.6	5	0.94	33.3	36.6	8.6
OCNG4-18	-37.7623	35.2027	3058	2.90	2.4	6	34.3	6	0.93	31.9	34.8	5.2
OCNG4-19	-37.7777	35.2063	3057	2.90	3.4	6	39.9	6	1.00	39.9	43.6	4.5
OCNG4-20	-37.7941	35.2084	3078	2.88	11.1	6	46.7	6	1.02	47.7	50.2	6.0
OCNG4-21	-37.8097	35.2118	3081	2.87	9.2	6	96.5	6	0.94	90.2	96.2	4.2
OCNG4-22	-37.8311	35.2149	3077	2.88	8.5	6	80.3	6	0.94	75.6	83.1	4.4
OCNG4-23	-37.8428	35.2181	3077	2.90	5.1	6	68.6	6	0.97	66.5	64.7	7.7
OCNG4-24	-37.8603	35.2212	3070	2.87	6.9	6	81.5	6	0.96	78.6	75.7	6.4
KT11	-37.8703	35.2226	3099	2.80	2.0	5	114.2	7	0.98	112.3	102.7	9.4
OCNG4-25	-37.8930	35.2278	3126	2.79	17.5	6	46.1	5	0.98	45.0	51.7	12.4
OCNG4-26	-37.9094	35.2305	3134	2.78	8.1	6	56.4	5	0.92	51.7	55.2	5.6
OCNG4-27	-37.9259	35.2335	3026	2.79	6.9	6	79.9	6	0.93	73.9	81.1	3.6
OCNG4-28	-37.9420	35.2367	3158	2.78	2.5	6	106.6	6	1.01	107.2	102.7	4.0

... continuing next page...

... table 2 continuing...

---

Site	long	lat	z	Tw	tilt	nT	G	nλ	λ	UHF	CTHF	$\sigma_{HF}$
OCNG4-29	-37.9585	35.2397	3160	2.75	2.8	5	53.4	5	0.91	48.7	50.7	3.9
OCNG4-30	-37.9753	35.2431	3156	2.72	12.0	6	61.4	6	0.93	57.3	55.8	6.3
profile 28W												
KT12	-37.5348	35.0831	2997	2.95	0.4	5	31.4	7	0.81	25.6	29.6	2.8
OCNG5-1	-37.5507	35.0859	3022	2.96	4.9	5	36.5	6	0.91	33.1	35.1	4.0
OCNG5-2	-37.5662	35.0886	3045	2.95	13.8	6	30.5	6	0.89	27.3	30.9	10.7
OCNG5-3	-37.5979	35.0945	3049	2.93	12.3	5	26.1	5	0.88	22.9	23.9	7.2
OCNG5-4	-37.6136	35.0977	3066	2.95	4.0	5	46.3	5	0.99	45.8	46.5	9.0
OCNG5-5a	-37.6294	35.1008	3069	2.93	3.4	5	36.6	5	0.91	33.2	33.1	8.4
OCNG5-6	-37.6449	35.1041	3070	2.92	3.3	5	40.3	5	0.92	37.1	43.4	11.4
OCNG5-7	-37.6607	35.1064	3073	2.92	8.7	5	29.3	5	0.91	26.6	30.6	5.9
OCNG5-8	-37.6769	35.1098	3075	2.93	1.5	5	26.3	5	0.90	23.6	27.0	7.2
OCNG5-9	-37.6932	35.1128	3078	2.92	8.1	5	26.4	4	0.89	23.5	25.4	9.1
OCNG5-10	-37.7096	35.1157	3078	2.90	5.0	5	28.6	5	0.89	25.5	27.1	7.3
OCNG5-11	-37.7258	35.1173	3078	2.88	11.4	5	27.4	5	0.91	25.0	32.1	7.2
OCNG5-12	-37.7421	35.1221	3069	2.89	8.4	5	37.6	5	0.90	33.8	36.2	7.4
OCNG5-13	-37.7581	35.1252	3050	2.90	3.3	6	60.4	6	0.98	59.3	32.6	8.6
OCNG5-14	-37.8087	35.1345	3052	2.91	12.9	6	47.2	5	1.03	48.5	54.5	14.4
OCNG5-15	-37.8249	35.1376	3047	2.91	7.2	6	44.3	6	0.94	41.7	48.2	4.7
OCNG5-16	-37.8408	35.1407	2990	2.91	2.2	6	130.4	6	1.01	131.4	133.1	8.2
OCNG5-17	-37.8583	35.1439	3004	2.93	8.6	6	71.4	6	0.96	68.8	74.0	8.9
OCNG5-18	-37.8731	35.1485	2954	2.98	6.5	6	63.0	6	1.05	66.4	78.9	9.5
OCNG5-19	-37.9051	35.1531	2907	3.00	6.8	5	56.0	5	1.03	57.6	75.6	10.0

---

... continuing next page...

... table 2 continuing...

---

Site	long	lat	z	Tw	tilt	nT	G	nλ	λ	UHF	CTHF	σHF
OCNG5-20	-37.9209	35.1558	2908	3.01	6.5	6	43.4	6	1.00	43.2	63.1	6.4
OCNG5-21	-38.0044	35.1739	3191	2.68	14.9	6	108.2	5	0.94	102.0	79.2	15.7
OCNG5-22	-38.0145	35.1802	3208	2.69	2.7	5	67.4	5	0.87	58.5	65.5	3.1
profile 26W												
KT13	-37.4300	35.2167	2622	3.20	2.1	2	44.7	1	0.98	43.9	37.7	0.4
OCNG6-3	-37.6332	35.2551	2834	2.94	5.0	6	44.1	6	0.94	41.4	56.6	2.9
OCNG6-4	-37.6853	35.2645	2855	2.94	5.4	6	62.4	6	1.00	62.2	81.0	5.8
OCNG6-5	-37.7124	35.2703	2890	2.90	5.2	6	50.6	6	0.97	49.2	58.8	4.3
OCNG6-6	-37.7258	35.2729	2998	2.92	3.4	5	81.2	5	0.92	75.0	94.6	13.3
OCNG6-7	-37.7375	35.2750	3028	2.89	7.1	6	66.4	6	0.96	63.6	42.8	5.8
OCNG6-8	-37.7861	35.2840	3106	2.86	8.3	5	9.4	5	0.90	8.5	16.7	11.6
OCNG6-9	-37.8030	35.2866	3118	2.80	21.0	5	38.3	5	1.00	38.5	46.7	7.2
OCNG6-10	-37.8198	35.2903	3131	2.80	16.7	5	101.3	5	0.88	89.4	98.8	10.0
OCNG6-11	-37.8344	35.2931	3146	2.82	7.9	6	121.1	6	1.00	120.5	132.6	3.2
OCNG6-12	-37.8468	35.2955	3141	2.84	6.0	6	117.1	6	0.91	106.0	114.5	8.3
profile 25W												
OCNG6-13	-37.6979	35.3445	2872	3.01	10.5	5	51.7	5	1.01	52.4	54.7	5.5
OCNG6-14	-37.7119	35.3467	2954	2.97	14.5	4	43.1	4	1.01	43.4	44.6	17.1
profile 26E												

---

... continuing next page...

... table 2 continuing...

---

Site	long	lat	z	Tw	tilt	nT	G	nλ	λ	UHF	CTHF	$\sigma_{HF}$
KT17	-35.7259	34.8948	2643	3.22	3.5	5	35.1	6	0.82	28.8	35.8	3.0
KT16	-35.6522	34.8816	2565	3.24	2.7	5	36.5	3	0.87	31.8	39.5	1.9
KT21	-35.4110	34.8349	2710	3.18	1.7	5	127.0	5	0.88	111.6	114.4	8.0
OCNG12-8	-35.2939	34.8143	2968	3.07	4.5	5	42.2	5	1.02	42.9	44.2	4.1
OCNG12-9	-35.2784	34.8101	2966	3.06	7.0	6	65.1	6	0.89	57.9	68.5	5.1
OCNG12-10	-35.2620	34.8072	2945	3.15	6.1	6	122.4	6	0.88	107.6	112.3	5.1
OCNG12-11	-35.1897	34.7930	2770	3.15	65.5	3	59.6	3	1.04	61.8	65.4	78.2
KT26	-35.1269	34.7816	2838	3.09	4.0	5	100.8	2	0.78	78.8	103.7	1.9

profile 27E

OCNG7-1	-34.8022	34.6424	2795	3.09	17.1	5	14.3	5	0.99	14.1	20.6	17.0
OCNG7-2	-34.8199	34.6455	2753	3.08	11.7	4	11.3	5	0.96	10.8	18.9	2.3
OCNG7-3	-34.8367	34.6491	2761	3.08	16.1	6	23.4	4	0.97	22.8	27.1	5.5
OCNG7-4	-34.8523	34.6525	2742	3.10	10.5	6	27.8	5	0.98	27.2	52.2	7.4
OCNG7-5	-34.8825	34.6579	2783	3.09	8.2	5	26.4	4	1.01	26.8	34.8	4.6
OCNG8-32	-34.8996	34.6613	2792	3.11	16.9	4	22.7	3	1.03	23.3	22.1	4.7
OCNG8-31	-34.9161	34.6645	2805	3.10	11.7	5	29.9	4	0.94	28.0	34.9	6.2
OCNG8-30	-34.9330	34.6676	2812	3.10	13.2	6	82.5	5	1.04	85.6	95.5	15.4
OCNG8-29	-34.9496	34.6708	2803	3.10	12.5	4	28.2	5	0.94	26.6	37.8	4.0
OCNG8-28	-34.9654	34.6739	2785	3.10	7.6	6	109.9	6	0.96	105.6	92.0	5.5
OCNG8-27	-35.0493	34.6895	2768	3.13	4.7	5	41.5	4	1.00	41.6	54.8	10.1
OCNG8-26	-35.0651	34.6926	2761	3.13	7.8	6	27.6	6	0.98	26.9	37.4	5.8
OCNG8-25	-35.0814	34.6955	2760	3.12	8.2	5	56.2	4	1.02	57.4	73.1	5.8
OCNG8-24	-35.0973	34.6986	2710	3.15	13.6	5	105.8	4	0.95	100.0	120.2	19.7

---

... continuing next page...

... table 2 continuing...

Site	long	lat	z	Tw	tilt	nT	G	nλ	λ	UHF	CTHF	$\sigma_{HF}$
OCNG8-23	-35.1136	34.7018	2799	3.12	5.8	5	48.9	4	0.92	44.9	52.3	6.2
KT18	-35.1222	34.7034	2801	3.08	2.4	5	42.9	6	0.84	36.0	40.4	1.9
OCNG8-22	-35.1295	34.7049	2799	3.12	5.0	6	41.6	5	0.89	36.9	36.4	6.5
OCNG8-21	-35.1456	34.7079	2785	3.12	7.1	6	63.4	5	0.98	61.9	76.3	13.9
OCNG8-20	-35.1618	34.7111	2785	3.11	6.2	6	57.3	5	0.97	55.5	66.3	4.1
OCNG8-19	-35.1782	34.7141	2780	3.11	5.6	6	22.0	5	0.91	20.1	26.9	5.3
OCNG8-18	-35.1946	34.7174	2770	3.12	6.6	6	36.6	5	0.90	32.9	29.5	6.2
OCNG8-17	-35.2169	34.7213	2622	3.21	11.8	5	14.5	4	0.94	13.6	14.7	5.5
OCNG8-16	-35.2333	34.7243	2594	3.21	19.5	6	1.7	6	1.07	1.8	-3.5	6.6
OCNG8-15	-35.2494	34.7278	2546	3.24	6.7	6	-0.2	6	0.98	-0.2	10.2	6.5
OCNG8-14	-35.2659	34.7309	2553	3.28	6.7	6	2.3	5	0.91	2.1	9.4	9.3
OCNG8-13	-35.2825	34.7339	2536	3.30	10.1	6	9.1	5	0.94	8.5	17.5	8.9
OCNG8-12	-35.2990	34.7370	2513	3.34	6.3	6	21.9	6	0.97	21.3	38.9	6.3
OCNG8-11	-35.3395	34.7446	2737	3.17	8.8	6	24.9	5	0.96	23.9	34.8	5.6
OCNG8-10	-35.4094	34.7577	2577	3.27	15.7	6	43.0	6	1.02	43.6	37.9	10.0
OCNG8-9	-35.4227	34.7605	2579	3.26	10.0	6	30.1	5	0.98	29.5	43.4	13.4
OCNG8-8	-35.4394	34.7637	2568	3.24	23.4	6	36.4	4	1.23	44.8	57.8	13.9
KT19	-35.4660	34.7689	2563	3.19	1.7	2	125.1	3	0.98	122.9	143.4	5.2
OCNG8-7	-35.4820	34.7717	2681	3.20	23.6	4	139.8	3	0.93	130.2	140.8	23.8
OCNG8-7a	-35.4820	34.7717	2681	3.20	8.7	6	103.5	5	0.98	101.2	111.1	12.8
OCNG8-6	-35.4984	34.7748	2680	3.20	6.2	5	101.8	4	0.95	96.7	106.6	13.4
OCNG8-5	-35.5699	34.7881	2653	3.20	19.8	4	59.5	3	1.04	61.6	79.1	22.2
OCNG8-4	-35.6328	34.8002	2915	3.19	7.8	6	64.9	6	0.90	58.5	46.8	3.9
OCNG8-3	-35.6438	34.8023	2899	3.19	8.9	6	52.2	6	0.91	47.3	51.4	6.2
OCNG8-2	-35.6612	34.8054	2782	3.21	4.6	6	94.6	5	0.89	84.5	106.0	5.5

... continuing next page...

... table 2 continuing...

---

Site	long	lat	z	Tw	tilt	nT	G	nλ	λ	UHF	CTHF	$\sigma_{HF}$
OCNG8-1	-35.6768	34.8084	2824	3.22	5.4	5	63.7	4	0.88	56.3	54.8	7.6
profile 28E												
OCNG9-1	-35.8022	34.7552	2889	3.19	4.4	6	22.9	6	0.85	19.6	18.2	5.5
OCNG9-2a	-35.7869	34.7519	2919	3.19	4.6	6	24.8	6	0.87	21.7	28.2	8.0
OCNG9-3	-35.7712	34.7490	2928	3.19	3.7	6	22.9	6	0.88	20.0	23.5	1.1
OCNG9-4	-35.7551	34.7460	2929	3.19	5.0	6	30.2	6	0.84	25.5	30.8	2.3
OCNG9-5	-35.7382	34.7428	2931	3.19	12.4	6	34.0	6	0.88	29.8	34.5	14.1
OCNG9-6	-35.7237	34.7402	2934	3.19	8.3	6	47.8	6	0.89	42.4	51.3	5.0
OCNG9-7	-35.6787	34.7317	2896	3.19	21.9	5	50.0	5	1.01	50.7	55.3	11.2
OCNG9-8	-35.6595	34.7282	2847	3.22	11.5	5	60.1	5	0.92	55.1	53.3	13.3
OCNG9-9	-35.5300	34.7035	2749	3.20	5.3	5	66.2	5	0.87	57.7	59.5	13.8
OCNG9-10	-35.5133	34.7000	2759	3.20	18.0	5	49.1	5	0.89	43.6	35.5	10.8
OCNG9-11	-35.4967	34.6972	2735	3.19	8.7	5	55.7	4	0.93	51.9	52.4	7.3
OCNG9-12	-35.4798	34.6942	2743	3.20	7.9	6	66.6	6	0.98	65.1	63.2	9.8
OCNG9-13	-35.4628	34.6906	2591	3.22	11.4	6	56.4	6	0.99	55.9	76.9	14.0
OCNG9-14	-35.4459	34.6880	2612	3.22	19.8	5	35.9	5	1.08	38.8	48.0	4.1
OCNG9-15	-35.4288	34.6843	2564	3.22	7.8	5	45.7	5	0.95	43.3	57.8	9.2
OCNG9-16	-35.2699	34.6543	2687	3.18	5.2	5	31.1	5	0.89	27.5	28.5	6.2
OCNG9-17	-35.2530	34.6511	2723	3.16	4.9	4	116.9	4	0.91	106.0	117.8	11.6
OCNG9-18	-35.2360	34.6476	2712	3.14	4.4	4	119.9	4	0.99	118.6	130.6	9.6
OCNG9-19	-35.1813	34.6371	2702	3.14	21.5	3	41.9	2	1.10	46.1	60.9	28.3
OCNG9-20	-35.1687	34.6348	2755	3.11	8.7	6	43.0	6	0.96	41.2	59.4	4.5
OCNG9-21	-35.1557	34.6325	2766	3.10	8.7	3	77.5	3	1.15	89.4	85.2	9.9

---

... continuing next page...

... table 2 continuing...

---

Site	long	lat	z	Tw	tilt	nT	G	nλ	λ	UHF	CTHF	σHF
KT20	-34.9709	34.5974	2385	3.16	8.8	3	61.6	0	0.92	56.7	77.4	18.5

profile 23E

OCNG11-11	-34.9350	34.9766	3137	2.83	11.3	4	182.5	3	0.98	178.3	181.1	33.7
OCNG11-10a	-34.9547	34.9803	3158	2.83	6.1	4	107.8	3	0.96	102.9	140.9	31.6
OCNG11-9	-34.9841	34.9862	3476	2.80	5.9	6	225.8	6	0.87	196.4	201.0	9.1
OCNG11-8	-35.0112	34.9911	3215	2.86	24.8	5	107.2	2	0.96	102.8	109.7	15.7
OCNG11-7	-35.0615	35.0007	3281	2.83	5.9	3	121.9	3	0.98	119.0	140.4	14.1

profile 24E

KT23	-35.5915	35.0232	2224	3.73	3.9	5	134.1	4	0.83	110.7	111.4	11.3
OCNG10-1	-35.4159	34.9900	2878	3.11	11.3	3	141.8	2	1.01	143.6	141.2	125.8
KT24	-35.4159	34.9901	2879	3.01	2.8	5	141.8	3	0.93	131.2	128.4	5.1
KT25	-35.4026	34.9877	2833	3.02	6.4	5	126.5	5	0.91	115.6	118.0	33.6
OCNG11-3	-35.3692	34.9811	2586	3.09	6.7	5	92.9	4	1.08	100.3	141.9	9.0
OCNG11-4	-35.2862	34.9657	2913	2.93	4.9	5	61.8	5	0.86	53.0	71.3	5.3
OCNG11-5	-35.2272	34.9547	2946	3.08	4.9	5	23.9	4	0.93	22.1	26.6	7.4
OCNG11-6a	-35.2105	34.9515	2894	3.00	7.5	5	36.4	4	1.03	37.3	48.3	11.0
KT28	-35.0236	34.9163	2675	3.05	2.1	4	111.6	3	1.08	120.0	109.4	9.7
KT14	-34.7277	34.8601	2289	3.49	1.3	3	7.3	1	0.95	6.9	38.3	8.2

profile 25E

---

... continuing next page...

... table 2 continuing...

Site	long	lat	z	Tw	tilt	nT	G	nλ	λ	UHF	CTHF	σHF
KT15	-34.7200	34.7957	2399	3.40	3.3	3	121.7	1	1.05	127.5	124.9	34.5
KT31	-34.7201	34.7954	2400	3.45	17.9	3	171.0	0	1.00	171.0	166.2	61.3
KT27	-35.0748	34.8488	2463	3.35	4.2	3	37.9	2	0.97	36.7	48.9	12.7
OCNG12-6	-35.2429	34.8806	2960	3.06	11.6	5	60.5	5	0.91	55.0	56.9	4.6
OCNG12-5	-35.2587	34.8840	2953	3.08	9.6	6	26.0	6	0.87	22.5	31.4	2.4
OCNG12-4	-35.2386	34.9181	2957	3.08	8.1	4	30.8	3	0.91	28.1	4.1	8.1
OCNG12-3	-35.3199	34.8950	2662	3.14	20.7	4	68.1	3	0.94	63.7	64.9	16.9
OCNG12-2	-35.3329	34.8977	2691	3.10	24.4	4	59.0	3	0.99	58.5	60.6	10.5
OCNG12-1	-35.3498	34.9013	2691	3.16	8.0	6	81.2	5	1.09	88.2	76.8	8.2
KT22	-35.5261	34.9344	2370	3.48	4.4	3	33.7	3	0.84	28.3	39.1	4.5
OCNG12-7	-35.2735	34.8431	2980	3.08	8.5	6	58.5	6	0.87	51.0	53.3	3.4
KT29	-34.9880	34.9513	3219	2.91	4.6	3	177.3	0	1.00	177.3	183.0	57.0

Table 3: Table of pore water concentrations.

	Depth	Cl	SO4	Na	K	Ca	Mg	Ba	Sr	Br	Li	B	Mn	pH
	(cm)	mmol/kg	mmol/kg	mmol/kg	mmol/kg	mmol/kg	mmol/kg	μmol/kg	μmol/kg	nmol/kg	μmol/kg	μmol/kg	μmol/kg	
	KT1-1	10	559.0	27.97	479.0	10.34	10.81	53.24	5.267	79.73	816.9	25.67	443.5	0.84
	KT1-2	20	550.2	27.75	475.4	10.92	10.31	52.76						7.86
	KT1-3	30	567.7	28.48	485.2	10.89	10.52	54.10	5.199	80.90	829.3	31.13	434.6	0.80
	KT1-4	40	550.5	28.03	473.6	0.00	10.62	52.58						7.81
	KT1-5	50	549.2	27.91	468.5	10.97	10.27	52.57	5.161	83.80	802.4	23.05	438.1	5.69
28	KT1-6	60	549.6	28.11	478.0	9.58	9.22	50.84	5.172	83.85	804.6	23.13	432.6	13.92
	KT1-8	80	560.2	28.56	471.0	0.00	10.64	52.87						7.75
	KT1-10	100	552.5	27.96	471.3	10.99	10.42	52.91	5.229	85.04	806.4	22.98	438.0	33.19
	KT1-11	130	554.7	27.95	473.9	10.85	10.37	53.15	5.171	84.71	810.6	22.79	437.7	40.04
	KT1-12	170	560.9	28.24	478.8	11.31	10.44	53.55	5.178	85.92	818.8	22.96	444.1	46.93
	KT1-13	210	571.0	28.61	487.6	11.35	10.58	54.51	5.161	87.40	835.0	23.39	450.9	51.76
	KT1-14	250	557.3	27.79	475.5	10.82	10.24	53.17	5.159	86.70	811.9	23.04	445.1	56.15
	KT1-15	290	565.5	28.27	481.5	11.32	10.42	53.79	5.158	87.68	820.0	22.77	442.0	55.87
														7.68

... continuing next page...

... table 3 continuing...

		Depth (cm)	Cl mmol/kg	SO4 mmol/kg	Na mmol/kg	K mmol/kg	Ca mmol/kg	Mg mmol/kg	Ba μmol/kg	Sr μmol/kg	Br nmol/kg	Li μmol/kg	B μmol/kg	Mn μmol/kg	pH
∞	KT1-16	330	556.1	28.01	477.2	0.00	11.19	54.07	5.171	89.02	539.7	23.14	449.1	56.20	7.63
	KT1-17	370	553.0	27.50	475.3	10.48	9.47	51.61	5.161	89.10	807.9	23.31	454.3	58.94	7.70
	KT1-18	400	554.0	27.23	472.3	10.74	10.01	52.82	5.162	87.62	811.0	23.41	453.4	60.62	7.69
	KT3-1	10	553.6	27.53	474.7	10.53	10.33	53.58	0.261	95.00	887.3	28.19	506.0	0.11	
	KT3-4	40	559.9	28.13	480.2	10.68	11.11	53.95	0.253	145.40	893.2	28.11	477.3	0.13	7.38
	KT3-7	70	549.7	27.56	471.6	10.35	11.16	52.90	0.251	168.31	892.5	26.16	491.4	0.29	
	KT3-10	100	551.5	27.65	472.9	10.52	11.13	52.83	0.248	171.13	887.6	24.73	472.6	0.30	
	KT3-11	130	550.0	27.52	471.6	10.33	11.03	52.64	0.239	183.17	883.0	25.06	476.3	0.16	
	KT3-12	170	551.5	27.65	473.6	12.13	11.15	51.61	0.238	198.32	875.6	27.13	478.2	0.07	
	KT3-13	210	550.8	27.40	472.5	10.57	11.26	52.34	0.254	198.71	885.6	23.13	485.8	1.38	
	KT3-14	250	545.4	26.74	467.9	10.91	11.20	51.35	0.242	206.73	877.3	22.59	510.9	6.41	
	KT3-15	290	594.7	28.84	504.5	12.33	14.31	55.53	0.306	233.37	935.5	23.58	544.9	11.84	
	KT3-16	330	570.6	27.93	489.7	11.63	11.46	53.51	0.242	218.65	909.6	21.32	537.5	9.49	

... continuing next page...

... table 3 continuing...

68

	Depth (cm)	Cl mmol/kg	SO4 mmol/kg	Na mmol/kg	K mmol/kg	Ca mmol/kg	Mg mmol/kg	Ba μmol/kg	Sr μmol/kg	Br nmol/kg	Li μmol/kg	B μmol/kg	Mn μmol/kg	pH
	KT3-17	370	546.8	27.66	469.6	10.73	10.80	52.56	0.244	164.43	857.9	24.31	464.1	7.48
	KT3-18	410	549.6	27.52	470.9	10.77	11.20	52.48	0.257	189.64	861.0	24.67	486.9	9.97
	KT3-19	440	580.9	27.94	491.2	12.18	12.17	54.43	0.283	245.19	908.0	22.24	524.3	9.87
	KT4-1	10	550.8	27.64	468.6	10.18	10.52	52.98	5.181	87.66	798.5	25.73	450.9	0.90
	KT4-2	20	556.7	28.24	468.0	10.84		52.95						7.56
	KT4-3	30	558.7	28.06	475.8	10.74	10.73	53.59	5.162	87.92	818.6	25.35	447.9	0.82
	KT4-4	40	554.8	28.07										7.54
	KT4-5	50	549.9	27.42	469.5	10.14	10.37	52.65	5.151	86.59	806.0	25.20	441.8	0.82
	KT4-6	60	563.8	28.19	484.0	11.00	10.33	54.72	5.143	87.37	888.0	25.88	451.6	0.84
	KT4-7	70	548.7	27.57	471.0	10.70	10.06	53.30	5.145	88.18	867.3	26.30	457.8	0.82
	KT4-8	80	548.1	27.47	470.6	10.66	10.02	53.22	5.146	88.95	862.0	26.21	454.6	0.84
	KT4-9	90						5.136	93.67			28.07	471.7	0.93
	KT4-10	100	551.8	28.14	473.5	11.01	10.41	53.62	5.136	90.92	864.8	25.47	449.4	0.80

... continuing next page...

... table 3 continuing...

	Depth (cm)	Cl mmol/kg	SO4 mmol/kg	Na mmol/kg	K mmol/kg	Ca mmol/kg	Mg mmol/kg	Ba μmol/kg	Sr μmol/kg	Br nmol/kg	Li μmol/kg	B μmol/kg	Mn μmol/kg	pH
	KT4-12	170	546.3	27.28	469.0	10.61	9.98	53.08	5.131	90.10	853.3	26.37	451.9	0.83
	KT4-13	210	554.8	27.50	475.9	10.53	10.03	53.87	5.119	89.39	876.9	25.04	441.8	0.92
	KT5-1	10	560.3	28.08	481.4	11.09	10.66	53.99	0.272	88.59	895.6	27.97	479.7	0.06
	KT5-4	40	550.1	27.85	473.2	11.56	10.43	52.82	0.295	93.85	875.0	25.65	507.7	3.87
	KT5-7	70	555.9	27.92	477.3	11.33	10.52	53.47	0.292	96.96	888.6	25.53	499.2	12.21
	KT5-10	100	550.8	27.59	473.3	11.15	10.38	53.01	0.283	92.49	881.8	25.60	511.2	18.81
	KT5-11	130	544.2	27.21	467.5	10.95	10.21	52.39	0.273	93.78	868.2	24.66	506.6	26.89
	KT5-12	170	548.1	27.50	471.0	11.70	10.11	52.45	0.269	94.61	875.0	24.77	512.4	30.68
	KT5-13	210	549.9	27.34	472.1	11.04	10.17	52.59	0.254	95.88	882.3	24.39	492.4	35.67
	KT5-14	250	545.9	27.03	468.7	10.84	10.11	52.40	0.245	99.60	872.0	25.91	494.4	38.47
	KT5-15	290	549.1	27.09	471.4	10.65	10.13	52.74	0.249	102.45	880.3	25.27	493.0	39.36
	KT5-16	330	549.2	27.07	471.9	10.77	10.11	52.76	0.224	98.29	886.8	25.12	485.3	35.45
	KT5-17	370	553.7	27.53	475.5	11.90	10.12	53.03	0.230	104.94	894.2	25.68	522.5	31.77

... continuing next page...

... table 3 continuing...

91

	Depth (cm)	Cl mmol/kg	SO4 mmol/kg	Na mmol/kg	K mmol/kg	Ca mmol/kg	Mg mmol/kg	Ba μmol/kg	Sr nmol/kg	Br μmol/kg	Li μmol/kg	B μmol/kg	Mn μmol/kg	pH	
	KT5-18	400	549.3	27.27	471.8	11.47	10.14	52.51	0.243	103.00	884.0	23.88	499.1	32.46	
	KT6-1	10	544.9	27.21	468.3	10.22	9.96	52.64	0.284	94.01	862.8	29.75	528.9	0.02	
	KT6-4	40	550.2	27.53	473.2	10.78	10.27	52.73	0.276	95.19	876.2	45.56	512.5	0.01	
	KT6-7	70	537.6	27.14	462.4	11.07	10.08	51.68	0.271	94.41	850.7	31.64	494.3	0.35	7.66
	KT6-10	100	541.9	27.42	465.5	11.42	10.28	52.02	0.299	97.14	863.9	25.87	523.8	5.77	
	KT6-11	130	547.1	27.68	470.2	11.81	10.37	52.39	0.287	96.27	868.1	25.73	518.4	12.06	
	KT6-12	170	545.5	27.46	468.4	10.97	10.24	52.44	0.281	98.53	866.7	26.19	512.3	21.47	
	KT6-13	210	546.0	27.33	468.4	11.10	10.23	52.52	0.266	97.66	867.6	25.86	507.1	28.23	7.67
	KT6-14	250	546.5	27.32	469.5	11.27	10.18	52.39	0.259	99.85	869.3	25.62	514.3	33.47	
	KT6-15	290	547.7	27.41	470.8	11.14	10.20	52.55	0.260	101.46	873.4	25.78	514.4	35.88	
	KT6-16	330	547.4	26.93	470.6	10.49	10.06	52.74	0.246	105.10	868.6	25.62	505.5	38.54	
	KT6-17	370	545.9	26.94	469.2	10.72	10.04	52.45	0.246	104.55	870.6	26.44	512.3	38.34	
	KT6-18	410	547.2	26.96	470.1	10.68	10.05	52.49	0.232	105.73	869.9	26.29	500.6	36.88	

... continuing next page...

... table 3 continuing...

92

	Depth (cm)	Cl mmol/kg	SO4 mmol/kg	Na mmol/kg	K mmol/kg	Ca mmol/kg	Mg mmol/kg	Ba μmol/kg	Sr nmol/kg	Br μmol/kg	Li μmol/kg	B μmol/kg	Mn μmol/kg	pH
KT6-19	440	545.9	27.05	468.4	11.07	10.06	52.29	0.238	104.61	878.4	24.39	492.6	34.83	
KT7-2	20	552.2	27.92	473.5	11.28	10.40	53.15	0.277	92.81	845.5	29.83	477.7	0.10	
KT7-3	30						0.282	90.76			24.96	464.5	5.74	
KT7-4	40	547.5	27.67	468.7	11.05	10.41	52.79			841.8				
KT7-7	70	573.5	28.90	491.1	11.57	10.82	55.22	0.230	76.00	879.3	21.95	407.5	17.01	7.73
KT7-10	100	547.2	27.49	468.3	10.96	10.37	52.66	0.162	61.45	835.7	17.36	337.5	19.66	
KT7-11	130	549.4	27.59	470.6	10.98	10.32	53.02	0.191	80.35	840.0	21.85	427.2	29.64	
KT7-12	170	545.1	27.52	466.4	11.29	10.28	52.28	0.262	94.23	827.2	24.21	486.1	34.82	
KT7-13	210	546.2	27.08	466.8	10.50	10.07	52.43	0.263	98.08	830.9	25.81	504.7	40.03	
KT7-14	250	546.5	27.10	467.4	10.53	10.08	52.58	0.268	103.58	827.4	27.41	527.5	42.04	
KT7-15	290	540.5	26.65	461.9	10.72	10.14	51.88	0.237	92.99	815.8	25.00	491.8	37.15	
KT7-16	330	546.8	27.29	468.5	11.09	10.21	52.47	0.259	99.07	828.6	24.73	504.3	37.90	
KT7-17	370	547.8	27.35	467.9	11.33	10.26	52.33	0.254	103.02	816.9	24.29	512.1	37.13	7.6

... continuing next page...

... table 3 continuing...

93

	Depth (cm)	Cl mmol/kg	SO4 mmol/kg	Na mmol/kg	K mmol/kg	Ca mmol/kg	Mg mmol/kg	Ba μmol/kg	Sr nmol/kg	Br μmol/kg	Li μmol/kg	B μmol/kg	Mn μmol/kg	pH
KT9-1	10	555.4	27.82	474.6	10.34	10.23	53.63	0.234	74.71	830.2	23.53	434.4	0.74	
KT9-4	40	552.4	27.77	472.0	12.05	10.30	52.72	0.251	83.84	821.8	24.38	459.1	0.70	
KT9-7	70	546.4	27.21	466.9	11.09	10.22	52.30	0.247	84.30	809.3	24.30	443.9	0.58	
KT9-10	100	563.4	27.88	482.1	11.16	10.55	53.35	0.243	84.62	827.5	23.74	450.2	0.90	7.6
KT9-11	130	602.1	29.84	514.5	11.52	11.09	57.93	0.230	84.87	898.7	23.68	442.7	0.97	
KT9-12	170	549.5	27.30	469.3	10.33	10.05	52.96	0.230	91.19	816.3	23.96	471.1	3.22	
KT9-13	210	548.6	27.59	468.5	10.97	10.23	52.70	0.240	95.70	807.6	23.60	448.6	6.26	7.74
KT9-14	250	549.7	27.21	468.8	10.56	10.12	52.68	0.301	90.61	812.7	23.81	460.2	10.13	
KT9-15	290	550.2	27.38	469.4	10.59	10.31	52.80	0.234	91.27	809.2	23.08	463.6	15.31	
KT11-2	20	555.4	28.10	475.1	11.02	10.35	53.62	0.270	91.70	839.0	26.90	498.6	0.27	
KT11-4	40	549.8	27.63	469.7	10.64	10.16	53.11	0.251	84.26	825.9	25.87	461.9	0.18	
KT11-7	70	558.9	28.23	477.7	11.23	10.41	53.92	0.257	88.58	838.9	27.78	488.2	0.13	
KT11-10	100	550.0	27.46	470.6	10.89	10.06	53.01	0.250	85.33	831.2	25.82	466.2	0.24	7.74

... continuing next page...

... table 3 continuing...

94

	Depth (cm)	Cl mmol/kg	SO4 mmol/kg	Na mmol/kg	K mmol/kg	Ca mmol/kg	Mg mmol/kg	Ba μmol/kg	Sr nmol/kg	Br μmol/kg	Li μmol/kg	B μmol/kg	Mn μmol/kg	pH
KT11-11	130	549.4	27.40	469.7	10.35	10.09	53.15	0.260	88.00	832.0	26.80	475.6	0.46	
KT11-12	170	551.6	27.72	471.8	11.52	10.15	52.41	0.244	84.15	827.9	24.02	459.5	2.16	
KT11-13	210	552.6	27.91	472.2	11.11	10.23	53.26	0.247	89.17	836.6	24.21	476.7	4.47	7.7
KT11-14	250	545.8	27.36	466.4	10.58	10.08	52.77	0.246	88.17	823.1	24.25	462.8	6.35	
KT11-16	320	549.3	27.31	469.5	10.47	10.00	53.08	0.246	87.50	827.3	24.60	470.3	9.28	
KT11-17	350	731.4	36.92	628.4	14.39	13.50	70.73	0.224	83.34	1103.2	23.10	448.3	9.23	
KT11-18	380	555.3	27.38	473.9	10.73	10.03	53.42	0.217	81.30	826.3	23.24	434.5	9.57	
KT12-2	20	549.0	27.66	471.1	10.96	10.13	52.95	5.159	83.33	864.6	30.33	428.4	0.80	
KT12-6	60	545.2	27.77	468.4	11.15	10.20	52.47	5.181	85.72	857.4	22.70	440.6	4.00	
KT12-10	100	547.9	28.06	472.7	11.11	9.98	52.26	5.176	86.78	854.5	22.97	440.3	12.07	7.74
KT12-11	130	553.3	28.14	474.7	11.29	10.37	53.45	5.161	84.54	863.6	22.64	424.3	16.63	
KT12-12	170	550.7	27.86	472.5	11.13	10.27	53.18	5.166	85.48	864.3	22.80	429.8	22.83	
KT12-13	210	550.8	27.88	472.5	11.19	10.30	53.22	5.160	86.11	867.3	23.09	436.9	27.41	

... continuing next page...

... table 3 continuing...

56

	Depth (cm)	Cl mmol/kg	SO4 mmol/kg	Na mmol/kg	K mmol/kg	Ca mmol/kg	Mg mmol/kg	Ba μmol/kg	Sr nmol/kg	Br μmol/kg	Li μmol/kg	B μmol/kg	Mn μmol/kg	pH
KT12-14	250	552.8	27.83	474.6	11.03	10.44	53.41	5.143	83.60	868.1	22.22	428.0	30.41	
KT12-15	290	549.0	27.92	471.7	11.36	10.36	53.01	5.155	86.29	868.2	22.64	426.6	32.00	7.66
KT12-16	330	548.2	27.64	470.6	11.09	10.58	52.72	5.148	85.82	864.3	23.14	435.6	34.23	
KT12-17	370	547.9	27.22	470.5	10.79	10.09	52.95	5.141	86.62	865.8	23.79	437.7	35.34	
KT12-18	410	555.6	27.57	476.7	11.01	10.16	53.56	5.133	84.51	884.1	22.88	428.6	33.61	
KT12-19	430	552.7	27.54	473.3	11.14	10.36	53.08	5.131	84.62	861.3	22.74	428.7	32.88	
KT15-1	10	553.8	27.99	475.0	10.54	10.23	53.76	5.189	91.63	864.3	27.48	467.9	2.61	
KT15-3	30	558.7	27.85	481.7	10.49	9.68	53.44	5.141	86.54	859.1	27.39	454.0	0.84	
KT15-5	50	552.7	27.36	474.1	10.63	9.86	53.46	5.123	84.06	866.3	32.75	443.4	0.93	7.8
KT15-7	70	548.4	27.34	470.6	10.84	9.89	53.05	5.126	87.38	856.6	26.07	462.7	1.07	
KT15-9	90	549.1	27.06	470.8	10.62	9.79	53.13	5.115	85.24	859.7	25.78	461.2	1.30	
KT15-10	100	554.3	27.28	474.1	10.55	9.83	53.52	5.128	85.99	868.3	25.11	454.1	1.44	
KT15-11	120	552.9	27.33					5.118	84.84		24.79	439.8	0.86	7.72

... continuing next page...

... table 3 continuing...

96

	Depth (cm)	Cl mmol/kg	SO4 mmol/kg	Na mmol/kg	K mmol/kg	Ca mmol/kg	Mg mmol/kg	Ba μmol/kg	Sr μmol/kg	Br nmol/kg	Li μmol/kg	B μmol/kg	Mn μmol/kg	pH
KT15-12	170	554.3	27.44	475.6	10.59	9.92	53.74			869.8				
KT19-1	10	549.7	27.73	472.0	10.55	9.91	53.36	5.129	85.30	856.7	25.34	441.8	0.86	
KT19-2	20	550.8		472.2		9.92								7.6
KT19-3	30	567.2	28.08	486.6	11.93	10.18	54.69	5.134	83.59	883.3	25.29	442.2	0.90	
KT19-4	40	558.9	27.65		10.78									
KT19-5	50							5.123	83.56		25.07	431.1	0.81	
KT19-6	60	548.0	27.12	470.0	10.49	9.80	53.19	5.130	83.49	860.4	24.88	438.8	0.89	
KT19-7	75	550.4	27.17	472.3	10.51	9.83	53.36	5.123	82.98	864.8	24.47	439.2	0.79	
KT19-8	85	551.9	27.22	473.0				5.128	82.41		24.35	432.1	0.82	
KT19-9	95			467.8		9.81								
KT19-10	105	538.5	26.64	461.7	10.34	9.62	52.24	5.109	82.40	852.3	24.29	430.0	0.83	7.67
KT23-1	10	553.1	27.90	474.5	10.50	10.24	53.69	5.161	90.01	872.5	26.27	460.9	0.82	
KT23-2	20						53.40							

... continuing next page...

... table 3 continuing...

26

	Depth (cm)	Cl mmol/kg	SO4 mmol/kg	Na mmol/kg	K mmol/kg	Ca mmol/kg	Mg mmol/kg	Ba μmol/kg	Sr μmol/kg	Br nmol/kg	Li μmol/kg	B μmol/kg	Mn μmol/kg	pH
KT23-3	30	547.5	28.00	469.7	10.34	10.39	53.38	5.130	93.36	860.5	25.73	438.7	1.56	
KT23-6	60	545.2	27.66	467.9	10.96	10.22	52.67	5.167	92.38	858.5	25.77	449.2	0.95	
KT23-8	80							5.152	90.89		23.95	436.9	0.86	
KT23-9	90							5.168	94.38		24.69	442.0	0.81	7.81
KT23-10	100	547.6	27.67	469.7	10.82	10.18	52.79	5.154	93.46	864.3	26.26	442.2	0.84	
KT23-11	130	550.6	27.78	472.4	10.67	10.28	53.25	5.147	96.43	863.4	23.72	436.5	7.04	
KT23-12	170	549.4	27.65	471.6	11.05	10.18	52.83	5.165	97.97	868.0	24.35	443.2	12.47	
KT23-13	210	560.8	28.08	480.7	11.04	10.50	54.01	5.094	97.29	884.3	24.31	442.5	15.52	7.78
KT23-14	250	563.6	28.22	483.4	11.23	10.34	54.31	5.082	99.55	890.8	24.70	437.5	11.93	
KT31-1	10	546.7	27.36	466.4	10.32	10.09	52.84	0.221	89.49	806.2	27.46	497.4	0.13	7.53
KT31-4	40	550.9	27.24	469.9	10.09	9.86	53.30	0.224	89.81	813.4	27.87	505.4	0.11	
KT31-7	70	540.3	26.63	460.4	9.94	9.71	52.23	0.219	88.03	791.3	27.52	494.0	0.17	
KT31-10	100	547.4	27.34	466.5	10.22	10.03	52.93	0.211	89.35	802.1	26.72	496.9	0.04	7.56

... continuing next page...

... table 3 continuing...

	Depth (cm)	Cl mmol/kg	SO <sub>4</sub> mmol/kg	Na mmol/kg	K mmol/kg	Ca mmol/kg	Mg μmol/kg	Ba μmol/kg	Sr nmol/kg	Br μmol/kg	Li μmol/kg	B μmol/kg	Mn μmol/kg	pH
KT31-11	130	547.1	27.04	466.6	10.09	9.95	52.85	0.212	88.73	803.3	27.92	497.7	0.06	